U-PB GEOCHRONOLOGY AND LITHOGEOCHEMISTRY OF THE HOPE BAY GREENSTONE BELT, SLAVE STRUCTURAL PROVINCE, NORTHWEST TERRITORIES, CANADA

by

MANFRED U. HEBEL

B.Sc., Concordia University, 1995

A THESIS SUBMITTED IN PARTIAL FULFILMENT OF
THE REQUIREMENTS FOR THE DEGREE OF

MASTER OF SCIENCE

in

THE FACULTY OF GRADUATE STUDIES

(Department of Earth and Ocean Sciences)

We accept this thesis as conforming

to the required standard

THE UNIVERSITY OF BRITISH COLUMBIA

April 1999

Abstract

The Hope Bay greenstone belt (HBGB) is one of several Late Archean greenstone belts recognised within the Slave Structural Province (SSP) in the Northwest Territories, Canada. Unlike most other major greenstone belts in the SSP relatively little is known about the age and evolution of the HBGB. The main goal of this study was to construct a detailed chronostratigraphic and chemostratigraphic framework for the belt that would constrain the temporal and tectonic evolution and thus permit the HBGB to be placed in the regional geological context of the Slave Structural Province.

A regional geochronological and lithogeochemical program was carried out in conjunction with geological mapping by BHP Minerals Canada Ltd. personnel. A total of 21 U-Pb age determinations, 174 major and trace element analyses, and 19 rare earth element analyses resulted from the study. U-Pb geochronology was selected as the critical tool for constraining the stratigraphic and temporal evolution of the belt because of its high blocking temperature and the precise ages that can be obtained using this method. Major, trace, and rare earth element data were employed to characterise the geochemistry of various igneous units and investigate the possible paleotectonic settings in which individual units were generated.

The HBGB is characterised by a basal series of mafic dominated tholeiitic volcanic flows (Young Group), overlain by a sequence of calc-alkaline volcanic rocks (Westerberg Group), that are in turn overlain by sedimentary rocks of the Tweedy and Farrar group. These sequences were deposited over a period of at least 116 m.y. from ca. 2716 to ca. 2600 Ma. Chemical compositions of volcanic rocks are typified by low abundance of HFSE and depletions in Nb, Ti, Eu, and P relative to REE. The striking similarity between the overall lithologic assemblage and the geochemical signature of volcanic rocks in the HBGB with

modern arc and back-arc systems (e.g. Mariana and Tonga-Kermadec regions) suggest the HBGB evolved in an arc-backarc geodynamic setting.

Table of Contents

List of Tables

List of Figures

Acknowledgments

This body of work has benefited from the assistance of numerous individuals. First and foremost, I wish to thank my supervisor Jim Mortensen whose guidance in the field and laboratory allowed this effort to come to fruition. A huge debt of gratitude is owed to Richard Friedman whose endless patience and steady hand spared the author much grief in the U-Pb chemistry lab. James Gebert is thanked for sharing his wealth of knowledge on the Hope Bay greenstone belt and who's wry wit provided endless hours of amusement. This work would not be possible without the generous funding provided by BHP Minerals Canada Ltd. Thanks to Greg MacMaster of BHP Minerals Canada Ltd. for his ideas and insights into this project and the mining industry.

Thanks are extended to Anna, Darren, Jamie, Tod, Dinger, Scotty, Rob, Terri, Chris, and Steve and all the geologists I've worked and played with. Chris, thanks for allowing me to tap into that huge database of knowledge you possess. Steve thanks for shedding a ray of light into the black box of lithogeochemistry. A special debt of gratitude is extended to Dr. Evil whose perceptions of life and answer to the "meaning of life the universe and everything" proved the Hitchhikers Guide to the Galaxy wrong.

Finally, My family: Mom, Dad, Erica, Andrea, Oma, and Opa are thanked for their unwavering support throughout my life. Thanks for the emails Kidz! To my close friends, Dave and George, thanks for everything! Last but not least, thanks A.H! There are no words to describe the amount of support and inspiration you've provided over the years, except, what took you so long?

Chapter 1

Introduction

The Hope Bay greenstone belt (HBGB) lies in the northern portion of the Bathhurst Block in the northeastern part of the Slave Structural Province (Figure 1.1). A regional geochronological and lithogeochemical program was undertaken in conjunction with regional geological mapping of the HBGB in June 1996. The program is entirely funded by BHP Minerals Canada Ltd. and resulted in 21 U-Pb age determinations, 174 major and trace element analyses, and 19 rare earth element analyses. The main thrust of the study was to construct a detailed chronostratigraphic framework for the belt that would constrain its temporal evolution and thus permit the HBGB to be placed in the regional geological context of the SSP. In light of the resulting temporal framework, lithogeochemical results were used to investigate rock compositions and tectonomagmatic affinity of the igneous rock units in the HBGB within this chronostratigraphy.

Methods

U-Pb geochronology

U-Pb geochronology was selected as the main dating tool for this study. High precision age determinations were achieved primarily on zircon ($ZrSiO_2$) and to a lesser extent on titanite ($CaTiOSiO_5$) crystals. The robust nature of this method coupled with high blocking temperatures (~ 900°C) of zircon crystals (Lee et al., 1991) results in a powerful method for testing stratigraphic relationships throughout the HBGB. Analyses were carried out by the author at the Geochronology Laboratory of the University of British Columbia.

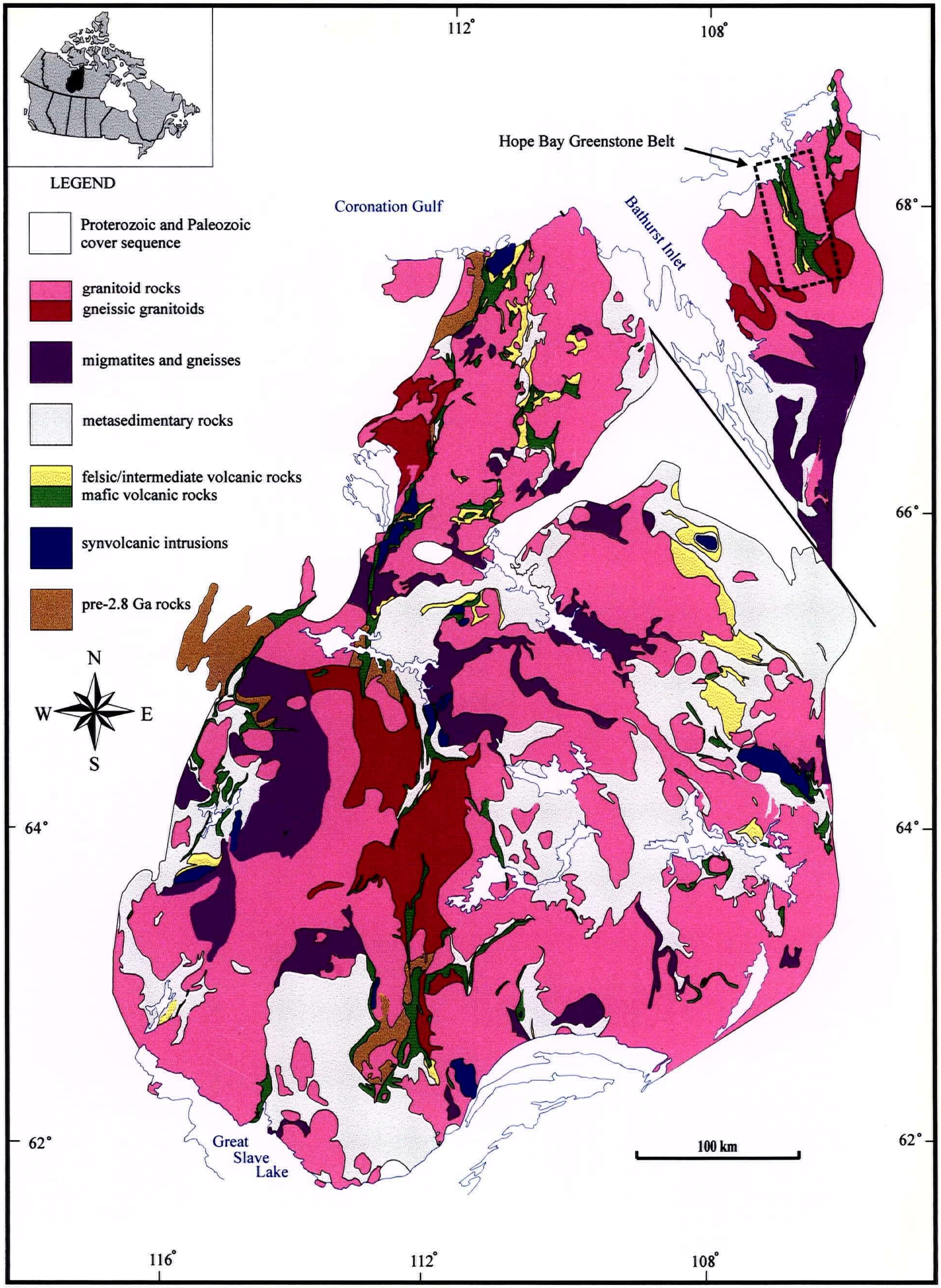

Figure 1.1. Location of the Hope Bay greenstone belt within the Slave Structural Province (modified from Fyson 1997-13).

Lithogeochemistry

Major and trace element geochemistry were determined for volcanic and plutonic rocks of the HBGB using X-ray fluorescence at Chemex Labs in North Vancouver, British Columbia, using glass beads for majors and pressed pellets for trace elements. A subset of samples were selected for rare earth element analyses using inductive coupled plasma mass spectrometry at Activation Laboratories in Ancaster, Ontario. Resulting data are integrated into the chronostratigraphy, derived from isotopic dating, and used to establish the chemostratigraphy and possible tectonomagmatic affinity of the supracrustal sequences within the HBGB.

Presentation

This thesis is presented as two research papers (Chapter 2 and 3), to be submitted for publication in refereed journals. These are preceded by introductory comments (Chapter 1) and followed by concluding remarks (Chapter 4). Some care was taken to eliminate redundancies in such topics as regional geology and introductory comments. However, to benefit readers' clarity and continuity a certain amount of repetition is unavoidable.

Chapter 2 discusses the geology and U-Pb geochronology of the HBGB. Twenty-one age determinations provide a temporal framework for the evolution of supracrustal secessions. Chapter 3 explores the lithogeochemistry and possible tectonomagmatic setting of igneous units in the HBGB within the chronostratigraphy established in chapter two. Immobile-incompatible trace element ratios are used to characterise individual igneous rock suites and rare earth element abundances are used to suggest potential geodynamic settings.

References

Lee, J.W., Williams, I.S., and Ellis, D.J. (1997). Pb, U, and Th diffusion in natural zircon. Nature, v. 390 p 159-162.

Chapter 2

U-Pb geochronology of the Hope Bay Greenstone Belt, Slave Structural Province, Northwest Territories, Canada

Introduction

The Hope Bay greenstone belt (HBGB) lies in the northeastern portion of the Slave Structural Province (SSP) (Figure 2.1). This mafic dominated greenstone belt is one of several Archean volcanic successions belonging to the Yellowknife Supergroup (YkSG) (Henderson, 1970). The use of high precision U-Pb geochronology in conjunction with geological mapping has provided a temporal framework for the evolution of the YkSG and surrounding plutonic suites (Mortensen et al., 1988; Isachsen et al., 1991. van Breemen et al., 1992). Age determinations indicate the YkSG was deposited between 2715-2655 Ma. However, the preponderance of this data is from the western and central greenstone belts with scant ages from belts in the east. Despite this bias, all dates fall within the temporal framework established from the type section at Yellowknife.

The work on the Yellowknife greenstone belt (YkGB) (Mortensen et al, 1988; Isachsen et al, 1991) serves as an excellent example of the level of geochronology needed to unravel the complex history of Archean volcanic successions in the SSP. In an effort to address the dearth of data from eastern belts a detailed geochronolocal study of the HBGB was initiated. The main thrust of this work is to constrain the evolutionary history of supracrustal rocks within the HBGB and in turn place the findings in context of the Yellowknife Supergroup and overall evolution of the SSP.

Regional Geology of the Slave Structural Province

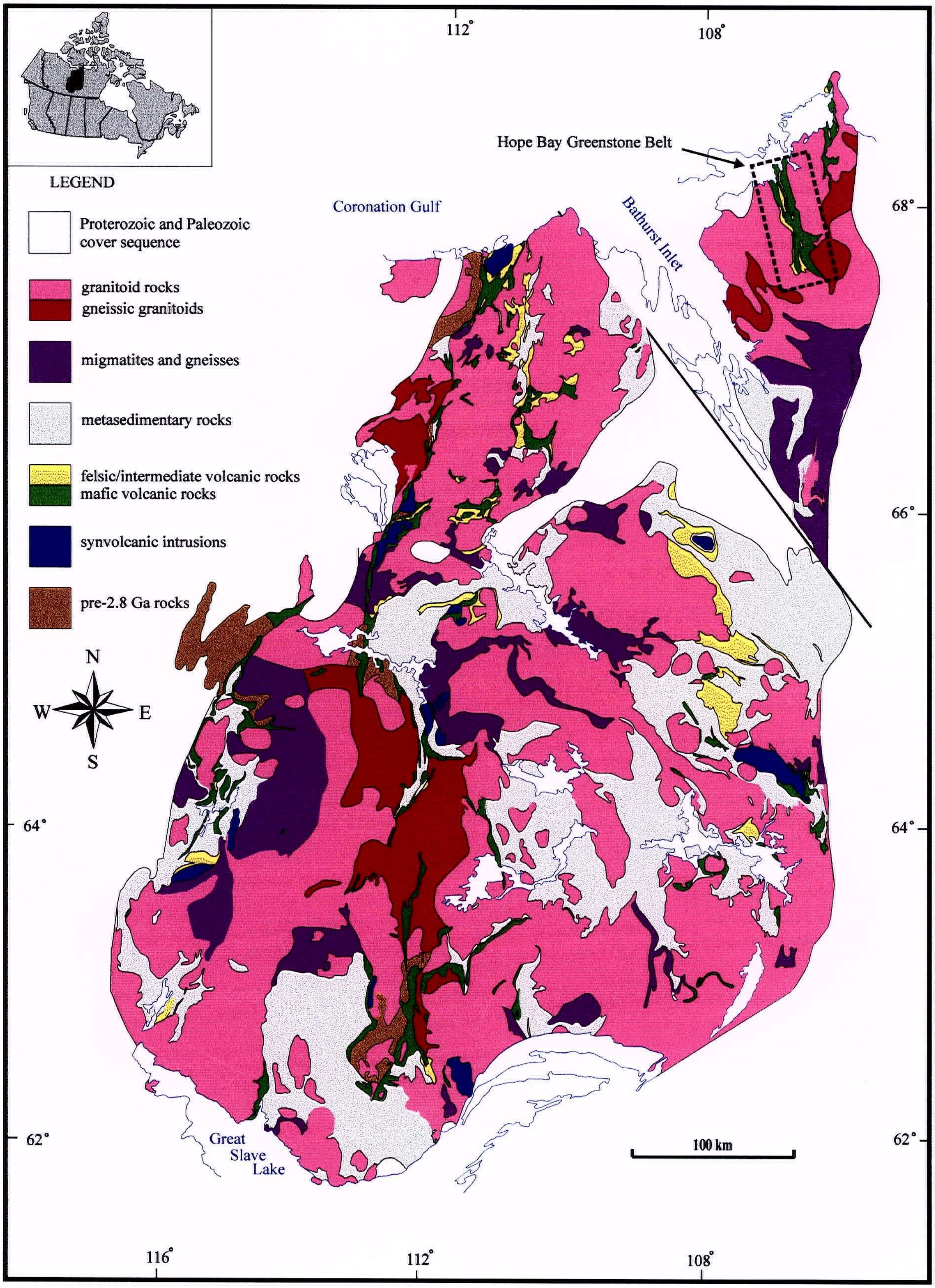

Figure 2.1. Generalized geology of the Slave Structural Province (modified from Fyson 1997 -13).

The following geological overview is drawn largely from prior excellent synopses by: Padgham (1985, 1991), Fyson and Helmstaedt (1988), Hoffman (1989), Padgham and Fyson (1992), Isachsen and Bowering (1994), and King and Helmstaedt (1997).

The Slave Structural Province (SSP) located in the northwestern Canadian Shield (Figure 2.1) is a well exposed (≅ 210 000 km^2), dominantly ~2715-2655 Ma granite-greenstone-turbidite terrane with subordinate inliers of ~4030-2900 Ma gneiss-granite basement rocks, >2800 Ma continental shelf sedimentary rocks, and <2605 Ma polymictic conglomerate-sandstone rocks. The craton is bounded to the west by the ~1910-1800 Ma Wopmay orogen and to the east by the ~2020-1910 Ma Thelon orogen. To the south, southwest, and northeast the SSP is onlapped by Proterozoic strata. Henderson (1970) initially assigned all supracrustal rocks within the SSP to the Yellowknife Supergroup (YkSG). Workers have since resolved the YkSG into three sequences 1) pre-YkSG: a basal orthoquartzite assemblage, 2) the main greenstone supracrustal sequence (metavolcanic and metasedimentary rocks) and 3) post-YkSG: an upper polymictic conglomerate assemblage.

Basement rocks have thus far only been recognised in the western part of the SSP and include a heterogeneous assemblage of orthogneiss, migmatitic gneiss, tonalite, and granodiorite. These rocks are typically strongly metamorphosed, deformed and intruded by amphibolite dykes. The apparent restriction of basement rocks to the western SSP is supported by isotopic boundaries established from sulphide Pb isotopic compositions and whole rock Nd analyses (Thorpe et al.. 1992; Davis and Hegnar 1992; Yamashita et al.. 1995). These data are interpreted to reflect the presence of old sialic basement in the west and an absence of such basement in the east.

Pre-YkSG supracrustal rocks are also apparently restricted to the western SSP, where they form a thin discontinuous veneer over crystalline basement rocks. The pre-YKSG units are commonly deformed and comprise mature orthoquartzite with local quartz pebble conglomerate, rhyolitic volcanic rock, chert-magnetite iron formation, siltstone, and calc-silicate rocks locally intruded by ultramafic sills and dykes.

Approximately 26 separate granite-greenstone belts are included within the YkSG. These greenstone belts have been further subdivided into mafic-dominated "Yellowknife-type" and a felsic-dominated "Hackett River-type" (Padgham, 1985). Yellowknife-type belts are typically comprised of voluminous massive to pillowed tholeiitic basalt flows (locally variolitic), interleaved with calc-alkaline felsic volcanic and volcaniclastic rocks, turbidites, and local synvolcanic conglomerate and carbonate units. Hackett River-type belts are comprised of calc-alkaline felsic and intermediate rocks intercalated with turbidites in the upper portions of the section. Geochronological age determinations bracket YkSG volcanism between 2715 Ma and 2655 Ma (Mortensen et al., 1988; Isachsen et al., 1991). Volcanic belts are typically isoclinally folded, well-foliated, and cut by belt-parallel shear zones. Metamorphism within the SSP is predominately at greenschist facies although, it locally reaches lower to middle amphibolite facies.

A late (<2.6 Ga) sedimentary assemblage consisting of conglomerate and sandstone unconformably overlies the main greenstone sequence. Polymictic conglomerates within this package are typically clast supported, include many lithologies from the volcanic hinterland, and bear a striking similarity with the Timiskaming Group found in the Superior Province (Fyson and Helmstaedt, 1988).

Late Archean plutonic rocks in the SSP were intruded between 2.70 and 2.58 Ga (van Breemen et al., 1992; Villeneuve et al., 1997). Villeneuve et al. (1997) further subdivide the intrusive rocks into 2.70-2.64 Ga predeformational tonalite and diorite, 2.62-2.59 Ga K-feldspar megacrystic granite, and postdeformational 2.60-2.58 Ga two-mica granite. Plutonic age determinations thus far indicate a magmatic hiatus from 2.640-2.625 Ga.

The SSP shows evidence of three distinct episodes of deformation: 1) >2.8 Ga structures are recorded within the Acasta terrain in the western Slave, but are poorly understood; 2) a pan-SSP deformational event is recorded between 2.7 and 2.6 Ga and characterised by regional compression, local plutonic deformation, and late extension (ca. <2.583 Ga); and 3) 1.84-1.74 Ga brittle to ductile faulting related to the Wopmay and Thelon orogenic belts affect the eastern and western SSP.

Geology of the Hope Bay Greenstone Belt

The Hope Bay greenstone belt (HBGB) lies in the northern portion of the Bathhurst Block in the northeastern part of the SSP (Figure 2.1). Fraser (1964) first mapped the belt as an Archean volcanic terrane belonging to the YkSG. Gibbons (1986) and Gebert (1990, 1993) classified the supracrustal sequence as a Yellowknife-type belt containing a series of north-south trending linear fractures. The belt is composed primarily of mafic and felsic metavolcanic and subvolcanic rocks, local ultramafic sills and with subordinate metasedimentary rocks. The volcanic belt is surrounded by synvolcanic to postvolcanic granitoid rocks. Metamorphic grade within the HBGB ranges from predominately lower greenschist to amphibolite facies near belt margins.

The entire HBGB has been remapped from 1996-1997 by the geological staff of BHP Minerals Canada Ltd. (primarily J. S. Gebert and M.U. Hebel) (Figure 2.2). The revised geological interpretation of supracrustal sequences within the HBGB based on this mapping form the stratigraphic and structural framework for the present study. Informal formation and group names have been assigned by the author to supracrustal rocks within the HBGB to facilitate clarity and continuity for the reader.

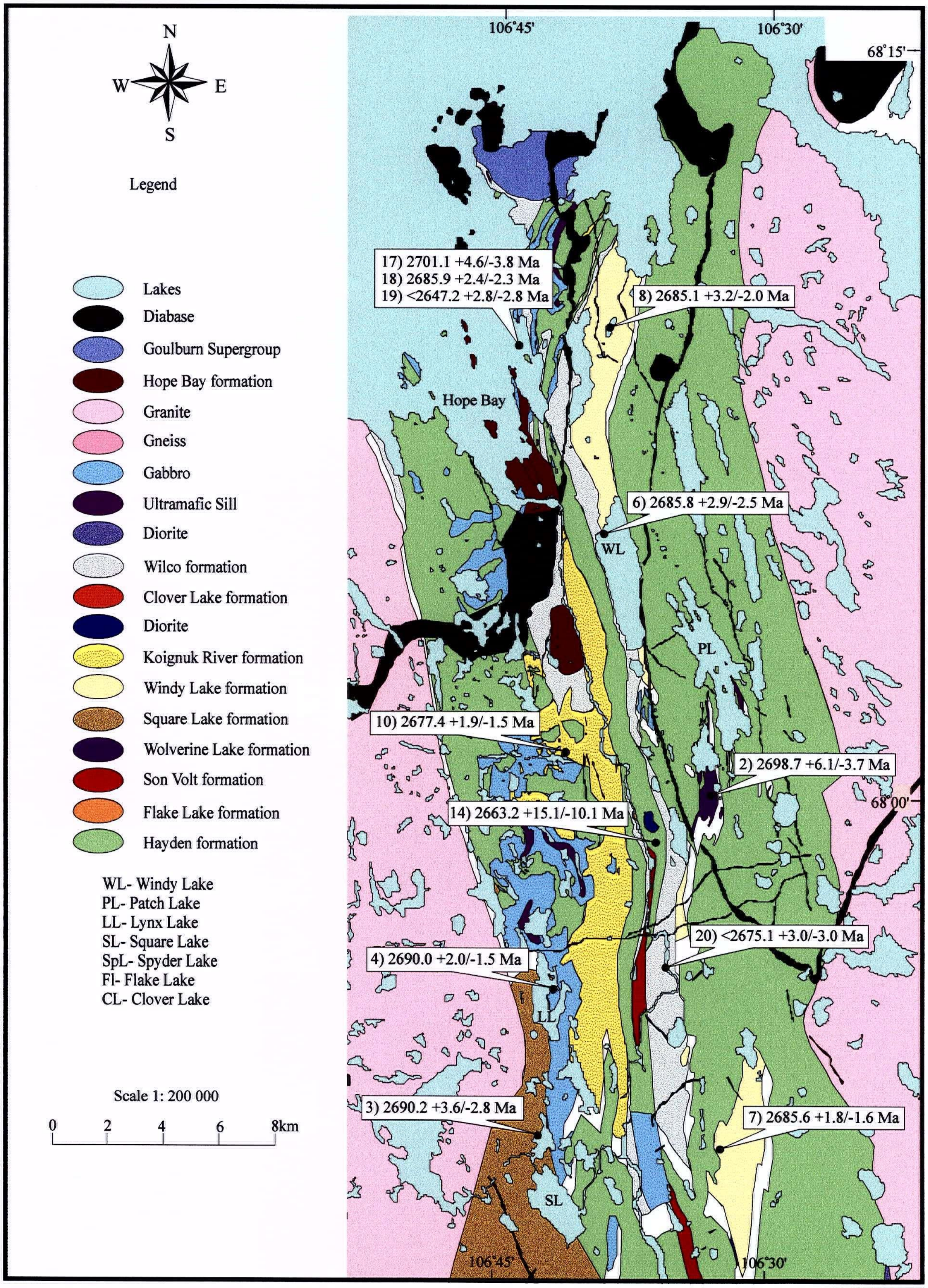

Figure 2.2a. Generalised geology for the northern portion of the HBGB.

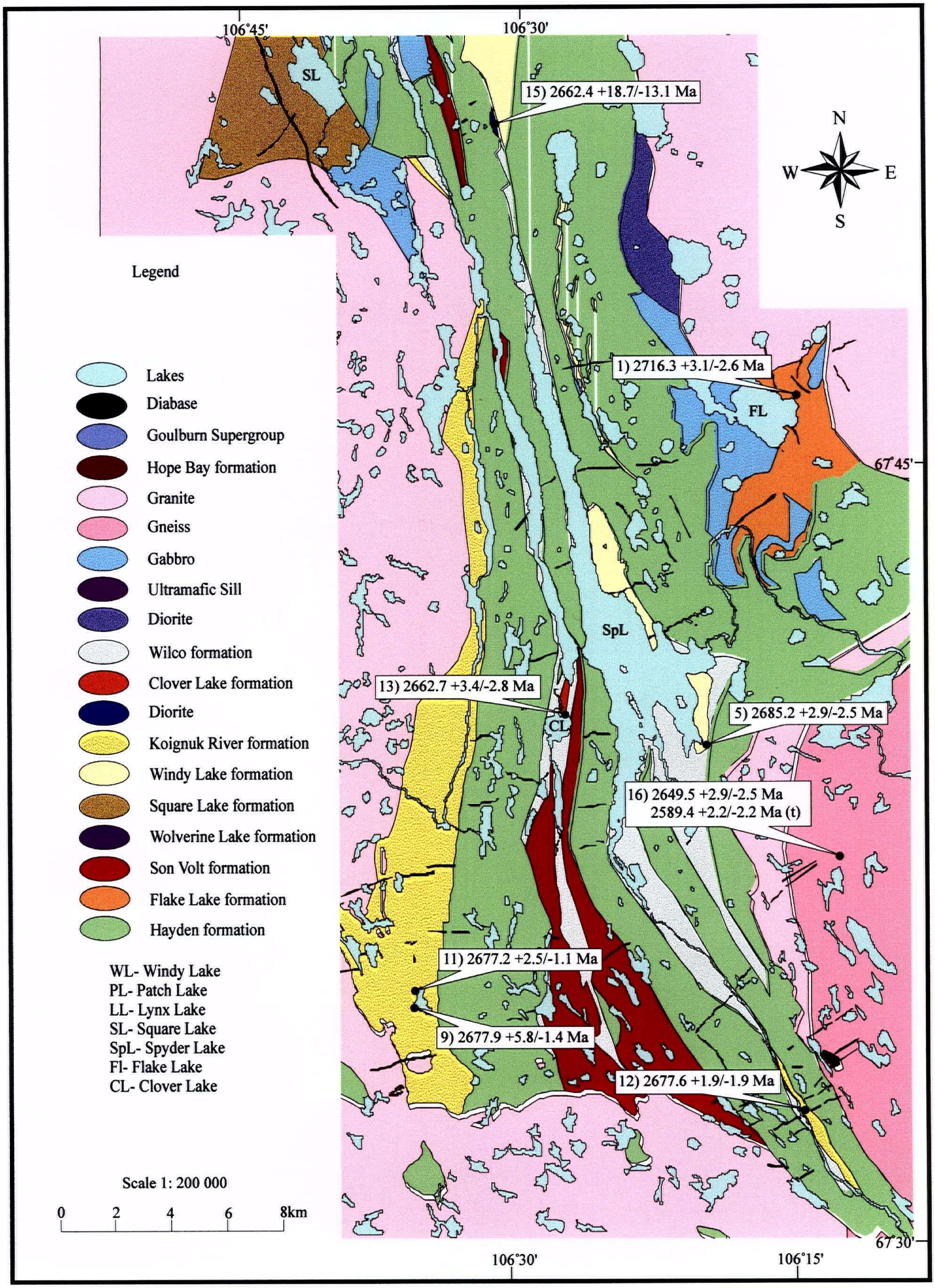

Figure 2.2b. Generalised geology for the southern portion of the HBGB.

Mafic rocks are collectively assigned to the Hayden formation (Figure 2.2) and consist of massive and pillowed metabasalt flows and metagabbros. Pillows are commonly variolitic and elongate with length to width ratios ranging from 2:1 up to 10-15:1. Geochemically most mafic rocks are typical Archean tholeiitic basalts although minor magnesium-rich basaltic komatiites have recently been recognised (Lindsey, 1998). Gabbro sills with pod-like geometry are ubiquitous throughout the volcanic sequences, with larger coarse-grained bodies up to 100 metres restricted to the northern portion of the belt. Thick sills commonly grade into more leucocratic differentiates. Ultramafic sills are also found throughout the belt. These sills typically form thin discontinuous intrusive bodies but can reach thicknesses of up to 200 metres in the northern portion of the belt. The HBGB is a mafic dominated volcanic sequence and thus is an exception to the typical felsic dominated greenstone belts found in the eastern SSP.

Unlike many Archean greenstone belts, the HBGB also contains a significant component of intermediate rocks. Intermediate units are assigned to the Son Volt formation (Figure 2.2) and were erupted primarily as fragmental rocks although flows occur locally. Felsic volcanic rocks (Flake Lake, Wolverine Lake, Square Lake, Windy Lake, Koignuk River, and Clover Lake formations; Figure 2.2) are dominantly composed of dacitic feldspar-phyric ash and lapilli tuffs with subordinate rhyolitic compositions. Many felsic rocks exhibit volcaniclastic textures suggesting they have been reworked by sedimentary processes. Volcaniclastic rocks are intercalated with flows and felsic epiclastic rocks with rapid facies changes common. Metasedimentary rocks (Wilco and Hope Bay formations; Figure 2.2), including sandstone, siltstone, greywacke, shale, and conglomerate units are interleaved with both mafic and felsic volcanic rocks.

Previous Geochronology Studies

Bevier and Gebert (1991) reported five U-Pb age determinations from the HBGB prior to this study. These data indicated a minimum age range for felsic volcanism within the belt of 8 (±5) million years (2685^{+4}_{-2} Ma to 2677^{+3}_{-1} Ma). Synvolcanic and postvolcanic plutons were dated at 2672 Ma and 2608 Ma respectively. The 2608 Ma zircon age was derived from a granite pluton that contained a foliated mafic xenolith; thus providing a minimum age for regional metamorphism.

Analytical Methods

All U-Pb age determinations reported here were derived from zircons with the exception of a single sample for which an age was obtained from titanite. Most zircon and titanite concentrates were extracted from 20-25 kg samples. Mineral extraction and U-Pb analytical procedures are similar to those described by Mortensen et al. (1995). In order to minimise the effects of surface-correlated Pb loss, all zircon and titanite fractions were strongly abraded prior to analysis (Krogh 1982). Both multigrain and single grain analyses were done. Procedural blanks were 2 to 10 picograms for Pb and 1 to 2 picograms for U. Errors for individual analyses were calculated using the error propagation method of Roddick (1987). The decay constants recommended by Steiger and Jäger (1977) were used in age calculations and initial common Pb compositions were estimated using the model of Cumming and Richards (1975). Concordia intercept ages were calculated using either the regression models of Davis (1982) or York (1969) and the algorithm of Ludwig (1980). All age errors are expressed at the 2σ level. U-Pb analytical data is given in Table 2.1, and regression parameters are listed in Table 2.2.

Table 2.1. U-Pb analytical data for the HBGB.

Fraction[1]	Wt	U[2]	Pb[3]	^{206}Pb[4]/^{204}Pb	Pb[5]	^{208}Pb[6]	Isotopic ratios (1σ,%)[7]			^{207}Pb/^{206}Pb
	μg	ppm	ppm		pg	%	^{206}Pb/^{238}U	^{207}Pb/^{235}U	^{207}Pb/^{206}Pb	age[7]
Sample 1 (97PGMC101, Flake Lake rhyolite, 67°46.3'N, 106°16.3'W)										
A f,N1,st,3	5	17	10	793	3	13.1	0.5168 (0.17)	13.310 (0.23)	0.18679 (0.17)	2714.1 (5.6)
B f,N1,st,3	7	17	10	1861	2	12.8	0.5083 (0.16)	13.078 (0.21)	0.18661 (0.12)	2712.5 (3.8)
C f,N1,st,2	2	11	7	487	2	17.0	0.5217 (0.40)	13.607 (0.45)	0.18916 (0.17)	2734.8 (5.6)
D f,N1,st,4	10	56	34	1416	12	13.3	0.5038 (0.08)	12.940 (0.16)	0.18626 (0.09)	2709.4 (3.1)
E f,N1,st,4	9	12	7	674	5	13.7	0.5112 (0.20)	13.160 (0.28)	0.18672 (0.17)	2713.5 (5.6)
F f,N1,st,4	11	41	25	6226	2	13.3	0.5232 (0.12)	13.490 (0.17)	0.18698 (0.08)	2715.8 (2.8)
Sample 2 (96PTMC119, Wolverine Lake quartz feldspar porphyry, 68°00.7'N, 106°33.7'W)										
A c,N2,p,1	5	123	70	2148	9	7.2	0.5140 (0.11)	13.075 (0.17)	0.18447 (0.09)	2693.5 (3.0)
B c,N2,e,p,1	5	61	35	1422	7	8.5	0.5071 (0.21)	13.009 (0.25)	0.18604 (0.10)	2707.5 (3.4)
C c,N2,p,1	3	72	41	1642	4	8.3	0.5125 (0.12)	13.096 (0.17)	0.18535 (0.12)	2701.3 (3.8)
D m,N2,p,1	18	131	73	7235	10	6.6	0.5124 (0.09)	13.026 (0.15)	0.18435 (0.07)	2692.4 (2.4)
E c,N2,p,1	9	83	46	1976	11	6.8	0.5097 (0.12)	12.980 (0.18)	0.18468 (0.09)	2695.3 (2.9)
F c,N2,p,t,1	7	93	52	1067	18	7.0	0.5154 (0.09)	13.127 (0.17)	0.18472 (0.10)	2695.7 (3.5)
G m,N2,p,t,1	6	123	69	2218	10	8.0	0.5099 (0.11)	12.948 (0.17)	0.18418 (0.08)	2690.9 (2.7)
H c,N2,p,1	5	124	70	1117	16	6.9	0.5114 (0.10)	13.029 (0.18)	0.18476 (0.10)	2696.1 (3.3)
I c,N2,p,1	7	129	75	8817	3	10.9	0.5100 (0.09)	12.940 (0.15)	0.18403 (0.07)	2689.6 (2.4)
J c,N2,p,1	9	91	51	2621	10	7.0	0.5079 (0.09)	12.913 (0.16)	0.18438 (0.08)	2692.7 (2.7)
K c,N2,p,1	6	89	50	3463	5	7.8	0.5047 (0.11)	12.781 (0.17)	0.18366 (0.08)	2686.2 (2.6)
Sample 3 (96PQMC113, Square Lake tuff, 67°54.1'N, 106°42.1'W)										
A m,N1,st,5	23	34	20	2541	10	12.5	0.5037 (0.09)	12.783 (0.16)	0.18405 (0.09)	2689.7 (2.8)
B m,N1,st,5	45	46	28	7379	9	12.7	0.5112 (0.10)	12.981 (0.16)	0.18416 (0.08)	2690.7 (2.5)
C m,N1,st,3	7	25	15	1842	3	14.9	0.5067 (0.09)	12.860 (0.11)	0.18408 (0.06)	2690.0 (2.0)
D f,N1,e,p,3	5	24	15	1274	3	14.4	0.5026 (0.14)	12.735 (0.22)	0.18378 (0.14)	2687.3 (4.6)
E f,N1,e,p,3	7	38	23	4424	2	13.7	0.5148 (0.16)	13.063 (0.19)	0.18403 (0.11)	2689.6 (3.8)
F f,N1,e,p,3	7	37	22	1826	4	13.6	0.5107 (0.11)	12.946 (0.18)	0.18385 (0.09)	2687.9 (3.1)
Sample 4 (97PQMC109, Square Lake flow, 67 57.2'N, 106°41.6'W)										
A m,N1,p,3	8	75	46	2975	6	14.7	0.5089 (0.12)	12.913 (0.18)	0.18403 (0.08)	2689.6 (2.7)
B m,N1,p,4	8	53	32	3633	4	15.1	0.5075 (0.09)	12.869 (0.16)	0.18391 (0.08)	2688.5 (2.6)
C m,N1,p,3	5	51	31	3455	2	14.2	0.5177 (0.14)	13.140 (0.19)	0.18408 (0.09)	2690.0 (2.8)
D m,N1,p,2	6	86	53	6375	3	14.7	0.5153 (0.11)	13.075 (0.17)	0.18402 (0.08)	2689.5 (2.6)
E m,N1,p,4	10	44	26	4407	3	14.6	0.4976 (0.11)	12.611 (0.17)	0.18381 (0.09)	2687.6 (2.9)
Sample 5 (97PBMC104, Windy Lake tuff, 67°39.7'N, 106°20.5'W)										
A c,N1,e,t,5	39	367	195	390	968	10.3	0.4681 (0.15)	11.781 (0.32)	0.18252 (0.22)	2675.9 (7.3)
B m,N1,e,t,3	4	227	134	691	37	11.7	0.5098 (0.12)	12.899 (0.22)	0.18353 (0.14)	2685.0 (4.6)
C m,N1,e,t,3	12	352	179	397	267	10.9	0.4465 (0.12)	11.267 (0.29)	0.18300 (0.22)	2680.2 (7.1)
D m,N1,e,t,3	7	232	128	357	123	12.5	0.4742 (0.12)	11.940 (0.32)	0.18261 (0.24)	2676.7 (7.8)
E m,N1,e,t,3	7	190	100	413	8	13.9	0.4436 (0.19)	11.175 (0.31)	0.18272 (0.21)	2677.7 (6.9)
F m,N1,e,t,3	6	150	87	919	28	10.8	0.5066 (0.10)	12.818 (0.19)	0.18350 (0.12)	2684.7 (3.9)
Sample 6 (96PTMC123, Windy Lake lapilli, 68°06.3'N, 106°39.3W)										
A c,N2,e,t,1	23	82	45	8177	7	9.4	0.4956 (0.09)	12.535 (0.15)	0.18345 (0.08)	2684.3 (2.6)
B c,N2,e,t,1	8	34	22	2046	4	18.0	0.5143 (0.10)	13.132 (0.17)	0.18520 (0.09)	2700.0 (2.8)
C c,N2,e,t,1	4	58	34	1653	4	12.0	0.5124 (0.11)	12.969 (0.17)	0.18357 (0.10)	2685.4 (3.2)
D c,N2,e,t,1	7	73	42	3437	4	11.2	0.5090 (0.10)	12.890 (0.16)	0.18366 (0.08)	2686.2 (2.7)
E c,N2,e,t,1	11	74	43	1030	23	10.9	0.5076 (0.10)	12.832 (0.18)	0.18334 (0.10)	2683.3 (3.4)
Sample 7 (97PAMC106, Son Volt lapilli, 67°54.1'N, 106°32.9'W)										
A m,N2,st,p,1	7	73	42	3939	4	14.9	0.4865 (0.10)	12.301 (0.16)	0.18338 (0.08)	2683.7 (2.6)
B m,N2,st,p,1	4	42	25	3112	2	11.7	0.5160 (0.12)	13.059 (0.18)	0.18357 (0.08)	2685.4 (2.8)
C m,N2,st,p,1	5	139	85	9531	2	14.1	0.5159 (0.09)	13.062 (0.15)	0.18362 (0.07)	2685.8 (2.5)
Sample 8 (97PTMC111, Windy Lake quartz-feldspar porphyry, 68°09.5'N, 106°39.4'W)										
A c,N1,st,p,3	16	86	49	18512	2	9.9	0.5072 (0.25)	12.812 (0.28)	0.18322 (0.07)	2682.2 (2.4)
B c,N1,st,p,3	27	71	41	15741	4	9.9	0.5126 (0.15)	12.958 (0.19)	0.18334 (0.07)	2683.3 (2.4)
C c,N1,st,p,3	20	71	41	19679	2	10.0	0.5161 (0.10)	13.061 (0.15)	0.18355 (0.07)	2685.2 (2.3)
Sample 9 (96PCMC108, Koignuk River quartz-feldspar porphyry, 67°34.5'N, 106°35.0'W)										
A c,N2,e,t,2	18	37	22	2910	7	10.3	0.5089 (0.10)	12.850 (0.16)	0.18314 (0.09)	2681.5 (2.9)
B c,N2,e,t,1	9	52	30	1374	10	9.4	0.5115 (0.11)	12.885 (0.18)	0.18269 (0.10)	2677.5 (3.3)

Table2.1 (continued) U-Pb analytical data for the HBGB.

Fraction[1]		Wt	U^2	Pb^3	$^{206}Pb^4$ / ^{204}Pb	Pb^5	$^{208}Pb^6$	Isotopic ratios (1σ,%) [7]			$^{207}Pb/^{206}Pb$
		μg	ppm	ppm		pg	%	$^{206}Pb/^{238}U$	$^{207}Pb/^{235}U$	$^{207}Pb/^{206}Pb$	age[7]
C	c,N2,e,t,1	9	50	29	773	17	10.2	0.5111 (0.12)	12.910 (0.20)	0.18321 (0.12)	2682.1 (4.0)
D	c,N2,e,t,2	16	43	25	2106	10	11.5	0.5105 (0.08)	12.856 (0.16)	0.18265 (0.08)	2677.1 (2.7)
E	c,N2,e,t,1	10	54	32	1466	11	11.1	0.5138 (0.09)	12.940 (0.17)	0.18266 (0.09)	2677.1 (3.1)
F	c,N2,e,t,2	12	71	41	5836	5	11.0	0.5093 (0.09)	12.832 (0.15)	0.18275 (0.08)	2678.0 (2.6)
G	c,N2,e,t,2	11	43	25	2851	5	10.7	0.5088 (0.10)	12.802 (0.16)	0.18250 (0.09)	2675.8 (2.8)
H	c,N2,e,t,4	11	26	15	3357	3	10.9	0.5085 (0.14)	12.799 (0.19)	0.18255 (0.08)	2676.2 (2.7)
Sample 10 (96PTMC118, Koignuk River flow, 68°01.3'N, 106°41.3'W)											
A	c,N1,e,p,3	18	54	32	13147	2	12.6	0.5139 (0.10)	12.949 (0.15)	0.18274 (0.08)	2677.9 (2.7)
B	c,N1,e,p,3	35	52	31	7525	8	12.7	0.5087 (0.11)	12.804 (0.16)	0.18256 (0.08)	2676.3 (2.5)
C	c,N1,e,p,3	30	48	28	21174	2	11.7	0.5141 (0.09)	12.946 (0.15)	0.18263 (0.08)	2676.9 (2.5)
D	m,N1,e,p,2	6	29	17	1758	3	11.6	0.5041 (0.15)	12.684 (0.20)	0.18248 (0.10)	2675.6 (3.3)
E	m,N1,e,p,2	7	16	10	1293	3	11.4	0.5153 (0.12)	12.979 (0.19)	0.18266 (0.11)	2677.2 (3.5)
Sample 11 (96PCMC107, Koignuk River flow, 67°34.8'N 106°34.7W)											
A	c,N2,e,t,1	13	57	32	1950	12	10.4	0.4980 (0.10)	12.532 (0.17)	0.18252 (0.09)	2675.9 (2.8)
B	f,N2,e,t,3	50	39	23	4317	14	11.7	0.5025 (0.08)	12.638 (0.15)	0.18241 (0.08)	2674.9 (2.5)
C	f,N2,e,t,3	50	40	24	4628	13	11.6	0.5078 (0.10)	12.789 (0.16)	0.18266 (0.08)	2677.2 (2.5)
D	c,N2,e,t,1	14	42	24	4422	9	11.1	0.5002 (0.11)	12.602 (0.17)	0.18273 (0.08)	2677.8 (2.6)
E	f,N2,e,t,4	28	38	22	3300	10	11.0	0.5098 (0.12)	12.839 (0.18)	0.18265 (0.08)	2677.1 (2.7)
F	f,N2,e,t,1	9	30	18	1232	7	11.9	0.5064 (0.10)	12.815 (0.12)	0.18353 (0.07)	2685.0 (2.4)
G	f,N2,e,t,1	5	567	328	1405	57	11.0	0.5062 (0.08)	12.742 (0.12)	0.18255 (0.09)	2676.2 (2.9)
I	f,N2,e,t,1	4	54	32	808	8	12.4	0.5039 (0.13)	12.687 (0.16)	0.18262 (0.10)	2676.9 (3.2)
J	f,N2,e,t,1	3	52	30	1040	5	10.5	0.5028 (0.12)	12.702 (0.14)	0.18323 (0.10)	2682.3 (3.2)
H	f,N2,e,t,1	4	59	35	1076	7	12.2	0.5145 (0.21)	12.955 (0.22)	0.18264 (0.12)	2677.0 (3.9)
Sample 12 (96PBMC104, Koignuk River tuff, 67°32.4'N, 106°15.0'W)											
A	c,N2,e,p,1	5	111	65	2813	6	11.5	0.5089 (0.09)	12.828 (0.15)	0.18284 (0.08)	2678.8 (2.6)
B	m,N2,e,p,1	3	68	39	538	11	10.9	0.5101 (0.11)	12.833 (0.22)	0.18246 (0.15)	2675.4 (4.9)
C	m,N2,e,p,1	3	62	36	1143	5	11.1	0.5110 (0.12)	12.842 (0.20)	0.18226 (0.12)	2673.5 (3.8)
D	m,N2,e,p,1	5	63	37	3012	3	11.6	0.5120 (0.17)	12.892 (0.20)	0.18262 (0.13)	2676.9 (4.3)
E	m,N2,e,p,1	5	33	19	770	7	11.6	0.5016 (0.17)	12.664 (0.24)	0.18313 (0.15)	2681.4 (5.0)
F	c,N2,e,p,1	7	90	52	6103	3	12.5	0.5006 (0.10)	12.616 (0.16)	0.18277 (0.08)	2678.2 (2.6)
Sample 13 (97PBMC103, Clover Lake rhyolite, 67°40.1'N, 106°27.5'W)											
A	f,N2,e,p,3	20	469	271	625	418	12.0	0.5003 (0.10)	12.473 (0.22)	0.18081 (0.15)	2660.3 (5.1)
B	f,N2,e,p,1	5	140	66	2054	8	15.9	0.3913 (0.09)	9.640 (0.16)	0.17866 (0.09)	2640.5 (3.1)
C	f,N2,e,s,1	6	307	181	626	81	15.3	0.4908 (0.10)	12.237 (0.22)	0.18082 (0.15)	2660.5 (5.0)
D	f,N2,e,p,3	12	97	47	1816	14	17.8	0.3943 (0.11)	9.667 (0.18)	0.17784 (0.09)	2632.8 (3.1)
E	f,N2,e,p,5	22	263	159	1985	82	14.4	0.5093 (0.09)	12.715 (0.17)	0.18106 (0.09)	2662.6 (2.9)
Sample 14 (97PTMC108, Sandusky diorite, 67°59.9'N, 106°36.2'W)											
A	f,N2,e,7	32	423	258	14262	26	19.2	0.4839 (0.12)	12.033 (0.17)	0.18035 (0.08)	2656.1 (2.6)
B	f,N2,e,8	40	374	229	11235	36	19.3	0.4862 (0.15)	12.107 (0.19)	0.18060 (0.09)	2658.4 (2.8)
C	f,N2,e,5	20	425	254	10449	21	18.9	0.4783 (0.10)	11.891 (0.16)	0.18033 (0.07)	2655.9 (2.4)
Sample 15 (96PUMC101, Sandusky diorite, 67°54.5'N, 106°31.7'W)											
A	f,N2,e,5	11	350	196	7813	13	14.1	0.4745 (0.09)	11.812 (0.15)	0.18056 (0.07)	2658.1 (2.5)
B	f,N2,e,9	18	246	133	6334	19	11.8	0.4688 (0.08)	11.660 (0.15)	0.18040 (0.07)	2656.6 (2.4)
C	f,N2,e,14	22	160	85	7416	13	11.1	0.4661 (0.08)	11.586 (0.15)	0.18030 (0.07)	2655.6 (2.4)
D	f,N2,e,10	25	314	184	2443	84	18.4	0.4715 (0.08)	11.741 (0.16)	0.18062 (0.08)	2658.5 (2.7)
E	f,N2,e,5	16	430	246	7253	25	17.2	0.4667 (0.11)	11.623 (0.16)	0.18063 (0.07)	2658.7 (2.4)
F	f,N2,e,6	18	585	343	6038	46	18.7	0.4689 (0.13)	11.681 (0.18)	0.18066 (0.08)	2659.0 (2.5)
Sample 16 (T961-43b, foliated granite, 67°38.0'N, 106°13.5'W)											
A	cc,N2,e,1	22	50	28	5650	6	7.3	0.5058 (0.10)	12.511 (0.16)	0.17939 (0.08)	2647.2 (2.5)
B	m,N2,e,p,1	5	124	68	3128	6	7.8	0.5020 (0.09)	12.416 (0.16)	0.17937 (0.08)	2647.1 (2.6)
C	m,N2,e,p,1	4	111	66	799	15	15.5	0.4936 (0.28)	12.147 (0.33)	0.17847 (0.13)	2638.7 (4.3)
D	cc,N2,e,p,1	7	500	256	2552	38	3.4	0.4878 (0.14)	12.003 (0.19)	0.17847 (0.10)	2638.7 (3.3)
E	c,N2,e,p,1	7	328	171	8260	8	6.2	0.4835 (0.08)	11.867 (0.15)	0.17799 (0.07)	2634.2 (2.5)
F	c,N2,e,p,1	7	349	185	11778	6	6.0	0.4904 (0.08)	12.156 (0.15)	0.17979 (0.07)	2651.0 (2.4)
G	ti,m,M20,10	36	124	65	2168	57	5.0	0.4938 (0.11)	11.801 (0.17)	0.17332 (0.09)	2589.9 (2.8)
H	ti,m,M20,10	81	159	88	1524	231	10.3	0.4940 (0.17)	11.796 (0.22)	0.17317 (0.11)	2588.5 (3.6)
Sample 17 (96PDMC126, Hope Bay Conglomerate granitoid clast, 68°09.2'N, 106°44.0'W)											
A	m,st,eq,5	13	60	36	8489	3	14.2	0.4980 (0.09)	12.656 (0.15)	0.18432 (0.08)	2692.1 (2.5)

Table2.1 (concluded) U-Pb analytical data for the HBGB.

Fraction[1]	Wt	U^2	Pb^3	$^{206}Pb^4$	Pb^5	$^{208}Pb^6$	Isotopic ratios (1σ,%) [7]			$^{207}Pb/^{206}Pb$
	µg	ppm	ppm	^{204}Pb	pg	%	$^{206}Pb/^{238}U$	$^{207}Pb/^{235}U$	$^{207}Pb/^{206}Pb$	age[7]
B m,st,eq,3	9	64	37	8877	2	13.7	0.4899 (0.14)	12.440 (0.18)	0.18416 (0.09)	2690.7 (3.0)
C m,e,p,4	7	18	11	1489	3	17.3	0.5169 (0.24)	13.201 (0.27)	0.18524 (0.10)	2700.3 (3.5)
Sample 18 (96PDMC125, Hope Bay conglomerate granitoid clast, 68°09.2'N, 106°44.0'W)										
A f,N5,eq,1	9	16	9	1049	4	9.9	0.5140 (0.13)	13.007 (0.20)	0.18352 (0.12)	2684.9 (3.9)
B f,N5,eq,1	6	33	19	1404	4	11.6	0.4976 (0.11)	12.656 (0.18)	0.18444 (0.10)	2693.2 (3.1)
C f,N5,eq,1	4	48	29	889	7	12.6	0.5123 (0.14)	13.001 (0.21)	0.18408 (0.12)	2689.9 (3.9)
D f,N5,eq,1	7	87	50	3628	5	11.1	0.5042 (0.09)	12.729 (0.15)	0.18310 (0.08)	2681.2 (2.5)
E f,N5,eq,1	8	108	57	5293	4	12.1	0.4604 (0.09)	11.515 (0.15)	0.18140 (0.07)	2665.7 (2.5)
F f,N5,eq,1	7	65	38	1571	9	14.8	0.4979 (0.09)	12.569 (0.17)	0.18308 (0.09)	2680.9 (3.0)
Sample 19 (96PDMC128, Hope Bay Conglomerate sandstone, 68°09.2'N, 106°44.0'W)										
A f,N1,st,e,1	5	183	103	2777	6	8.5	0.5060 (0.11)	12.514 (0.17)	0.17939 (0.08)	2647.2 (2.8)
B f,N1,st,e,1	5	112	67	406	9	12.5	0.5152 (0.13)	12.980 (0.28)	0.18273 (0.20)	2677.8 (6.5)
C mN1,st,e,1	26	71	40	5126	11	10.7	0.4912 (0.13)	12.289 (0.18)	0.18144 (0.08)	2666.0 (2.5)
D c,N1,st,p,1	20	139	76	6294	13	8.1	0.4978 (0.09)	12.335 (0.15)	0.17972 (0.07)	2650.3 (2.5)
E c,N1,st,e,1	10	187	100	12066	5	6.6	0.4919 (0.08)	12.245 (0.15)	0.18055 (0.07)	2657.9 (2.4)
F f,N1,st,e,1	8	199	109	10004	5	7.3	0.4990 (0.08)	12.487 (0.14)	0.18150 (0.07)	2666.6 (2.4)
G F,N1,st,e,1	7	96	55	3839	5	11.3	0.4969 (0.10)	12.474 (0.16)	0.18207 (0.08)	2671.8 (2.6)
Sample 20 (96PKMC121, Wilco sediments, 67°57.5'N, 106°35.6'W)										
A c,N2,t,p,1	4	135	88	2072	8	14.1	0.5417 (0.10)	14.739 (0.17)	0.19733 (0.08)	2804.3 (2.6)
B m,N2,t,1	14	50	30	1265	16	10.7	0.5150 (0.09)	13.328 (0.17)	0.18768 (0.09)	2722.0 (3.1)
C m,N2,e,t,1	8	77	63	2603	9	12.1	0.6553 (0.12)	24.013 (0.17)	0.26577 (0.08)	3281.3 (2.6)
D m,N2,e,t,1	8	66	40	1622	10	14.7	0.5114 (0.12)	12.864 (0.18)	0.18243 (0.09)	2675.1 (3.0)
E m,N2,st,e,1	10	58	34	1939	9	10.8	0.5136 (0.09)	13.034 (0.16)	0.18408 (0.09)	2689.9 (2.9)

Notes: Analytical techniques are listed in Mortensen et al. (1995).

1 Upper case letter = fraction identifier; All fractions air abraded; Grain size, intermediate dimension: cc=>180µm, c= <180µm to >134µm, m=<134µm and >104µm, f=<104µm; Magnetic codes:Franz magnetic separator sideslope at which grains are nonmagnetic (N) or Magnetic (M); e.g., N1=nonmagnetic at 1°; Field strength for all fractions =1.8A; Front slope for all fractions=20°; Grain character codes: ti=titanite, e=elongate, eq=equant, p=prismatic, st=stubby, t=tabular, ;Numeral=number of grains analysed.

2 U blank correction of 1-3pg ± 20%; U fractionation corrections were measured for each run with a double ^{233}U-^{235}U spike (about 0.005/amu).

3 Radiogenic Pb

4 Measured ratio corrected for spike and Pb fractionation of 0.0043/amu ± 20% (Daly collector) and 0.0012/amu ± 7% and laboratory blank Pb of 10pg ± 20%. Laboratory blank Pb concentrations and isotopic compositions based on total procedural blanks analysed throughout the duration of this study.

5 Total common Pb in analysis based on blank isotopic composition

6 Radiogenic Pb

7 Corrected for blank Pb, U, and common Pb. Common Pb corrections based on Cumming and Richards (1975) at the age of the rock or the $^{207}Pb/^{206}Pb$ age of the fraction (errors are 2σ in Ma)

Table 2.2. Regression parameters.

Sample No.	Fractions	Upper Intercept (Ma)	Lower Intercept (Ma)	Probability of fit (% or MSWD)		Regression method
1 (97PGMC101)	A,B,D,E,F	$2716.3^{+3.1}_{-2.6}$	381^{+222}_{-227}	91		Davis
2 (96PTMC119)	A,D,F,G,I,K	$2698.7^{+6.1}_{-3.7}$	909^{+342}_{-314}	96		Davis
3 (96PQMC113)	A,B,C,D,E,F,G	$2690.2^{+3.6}_{-2.8}$	89^{+72}_{-73}	70		Davis
4 (97PQMC109)	A,B,C,D,E	$2690.0^{+2.0}_{-1.5}$	166^{+205}_{-212}	96		Davis
5 (97PBMC104)	A,B,C,D,E,F	$2685.2^{+2.9}_{-2.5}$	133^{+90}_{-91}	56		Davis
6-(96PTMC123)	A,C,D,E	$2685.8^{+2.9}_{-1.5}$	101^{+243}_{-258}	44		Davis
7-(97PAMC106)	A,B,C	$2685.6^{+1.8}_{-1.6}$	85^{+122}_{-126}	82		Davis
8 (97PTMC111)	A,B,C	$2685.1^{+3.2}_{-2.0}$	397^{+500}_{-426}	65		Davis
9 (96PCMC108)	B,D,E,F,G,H	$2677.9^{+5.8}_{-1.4}$	260^{+796}_{-920}	83		Davis
10 (96PTMC118)	A,B,C,D,E	$2677.4^{+1.9}_{-1.5}$	226^{+388}_{-373}	97		Davis
11 (96PCMC107)	A,B,C,D,E,G,H,I	$2677.2^{+2.5}_{-1.1}$	81^{+253}_{-269}	81		Davis
12 (97PBMC103)	A,C,E	$2662.7^{+3.4}_{-2.8}$	167^{+332}_{-359}	67		Davis
14 (97PTMC108)	A,B,C	$2663.2^{+15.1}_{-10.1}$	269^{+141}_{-136}		0.96	Modified York II
15 (96PUMC101)	A,B,C,D,E,F	$2662.4^{+18.7}_{-13.1}$	135^{+413}_{-419}		1.39	Modified York II
16 (T961-43B)	A,B,C,D,E	$2649.5^{+2.9}_{-2.5}$	651^{+133}_{-132}	49		Davis
17 (96PDMC126)	A,B,C	$2701.1^{+4.6}_{-3.8}$	438^{+179}_{-176}	41		Davis
18-(96PDMC125)	A,D,E,F	$2685.9^{+2.4}_{-2.3}$	397^{+65}_{-65}	68		Davis

Geochronology of the Hope Bay Greenstone Belt

U-Pb analytical data are presented for 20 samples from the HBGB. Sample locations with age determinations are shown in Figure 2.3. Zircon morphologies are generally similar in all dated samples and range from equant grains to slender acicular grains with length to width (l:w) ratio of 5:1. Short stubby prisms were the dominant morphology observed. Low U (<100 ppm) content zircons were the norm with few elevated U levels encountered (100-567 ppm).

Volcanic and hypabyssal rocks

Sample 1 (97PGMC101, Flake Lake fm) – quartz-eye rhyolite

A massive quartz-eye rhyolite flow cross cut by gabbroic dykes, bounded by gabbro on the west, basalt on the south, and granite on the north and eastern flank was sampled from a glacially striated outcrop on the eastern shore of Flake Lake in the southern portion of the HBGB (Figure 2.3b). Zircons separated from this sample are relatively non-magnetic and form a homogeneous population consisting of colourless, pale pink, subhedral, stubby grains, 80-120 microns in length with a length to width ratio of ~2:1. Most zircon grains were broken, probably during the mineral separation process. There were no visible cores or igneous zoning and rare bubble-shaped inclusions were present. Measured U concentrations were low (<57 ppm, Table 2.1). Five strongly abraded multigrain fractions range from 0.1 to 3.6 % discordant and define a chord with upper and lower concordia intercepts of $2716.3^{+3.1}_{-2.6}$ Ma and 381 Ma (Figure 2.4a) respectively. The upper intercept is interpreted as the crystallisation age of the rhyolite with the relatively young lower intercept indicating a recent Pb loss event. Fraction C lies to the right of the discordia curve with a $^{207}Pb/^{206}Pb$ age of 2734.8 ±5.6 Ma and is

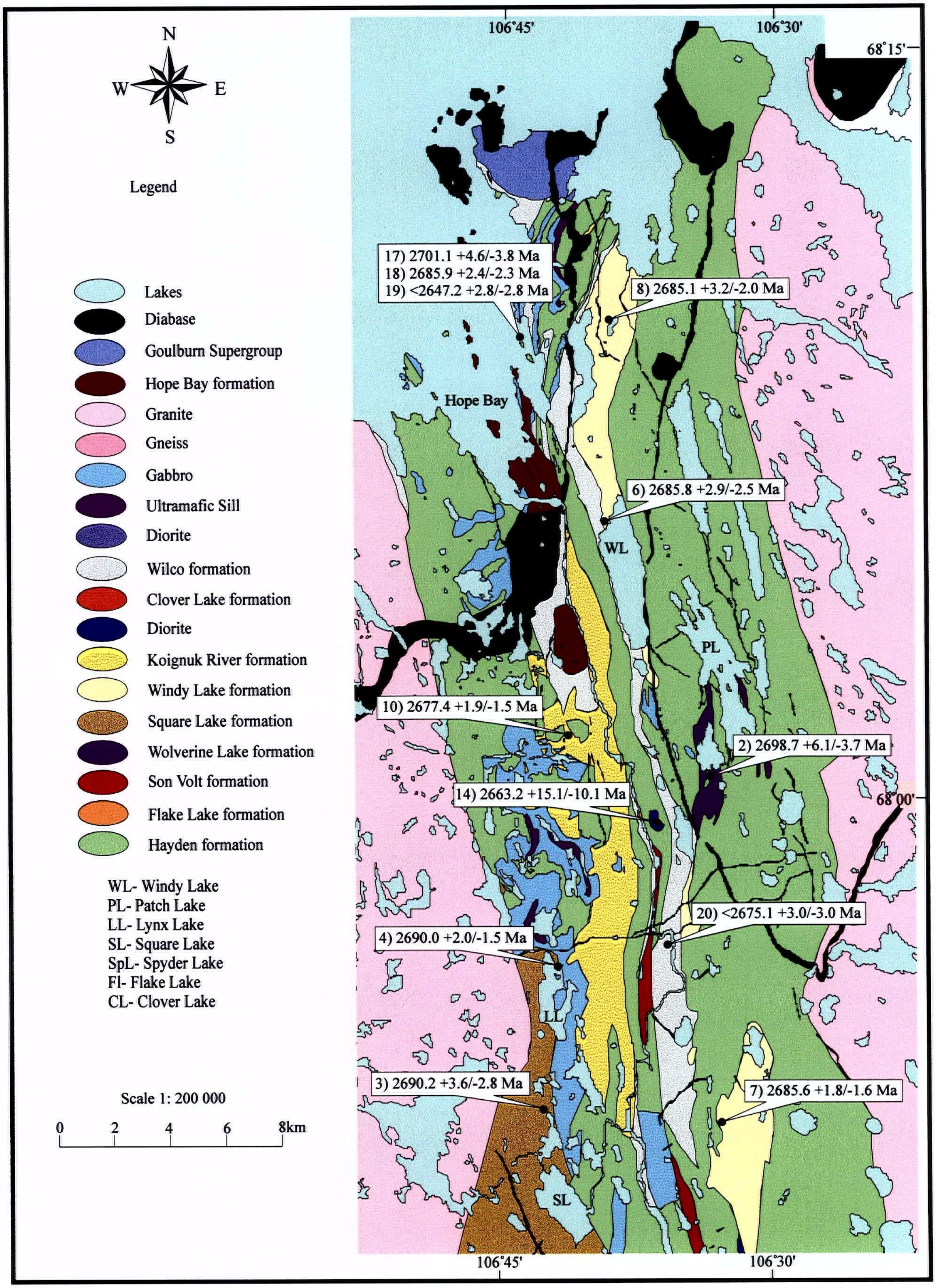

Figure 2.3a. Age determinations for the Northern portion of the HBGB. All ages derived from zircon crystals.

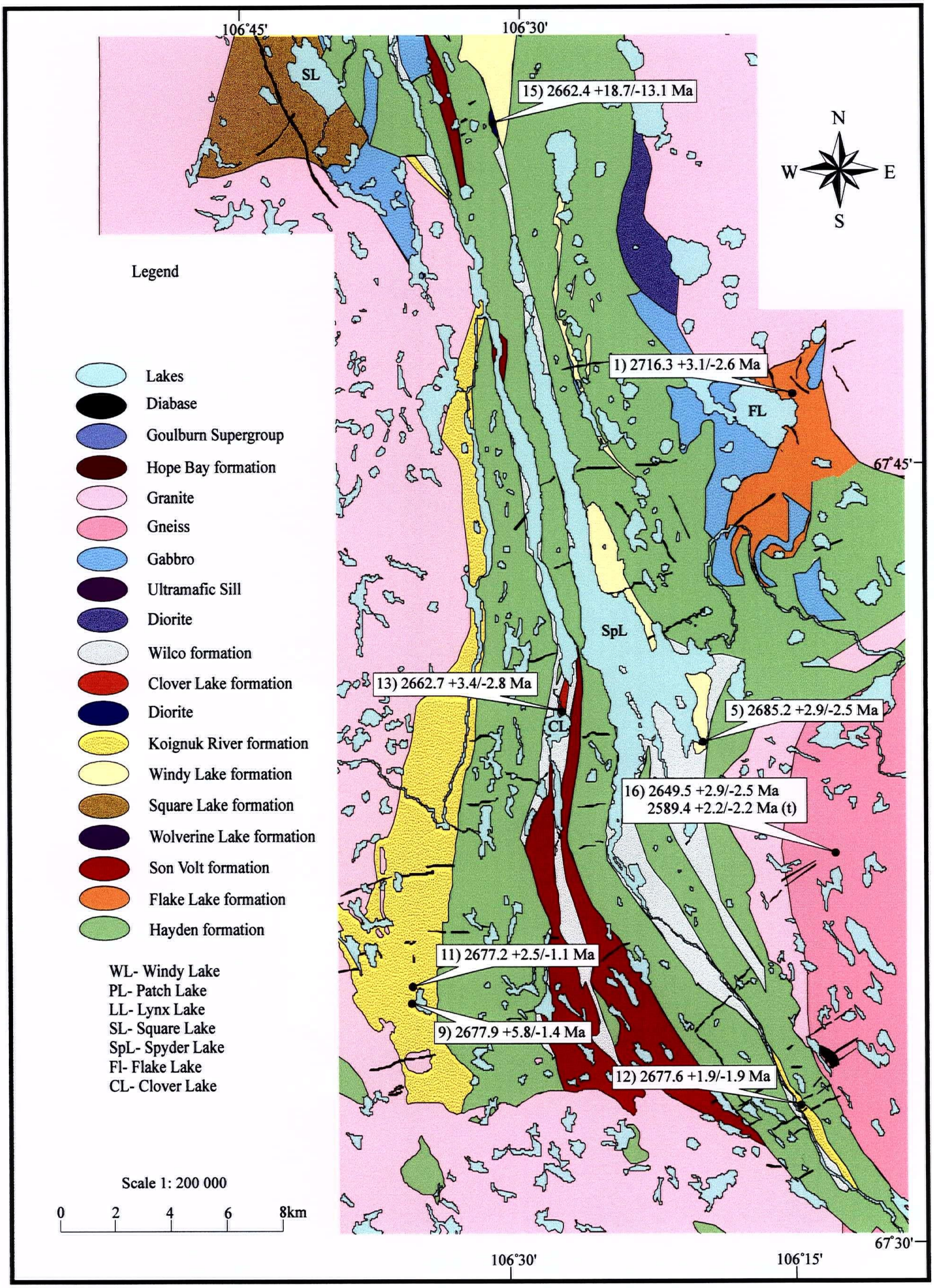

Figure 2.3b. Age determinations for the Southern portion of the HBGB. All ages derived from zircon crystals with the exception of one age derived from titanite (t).

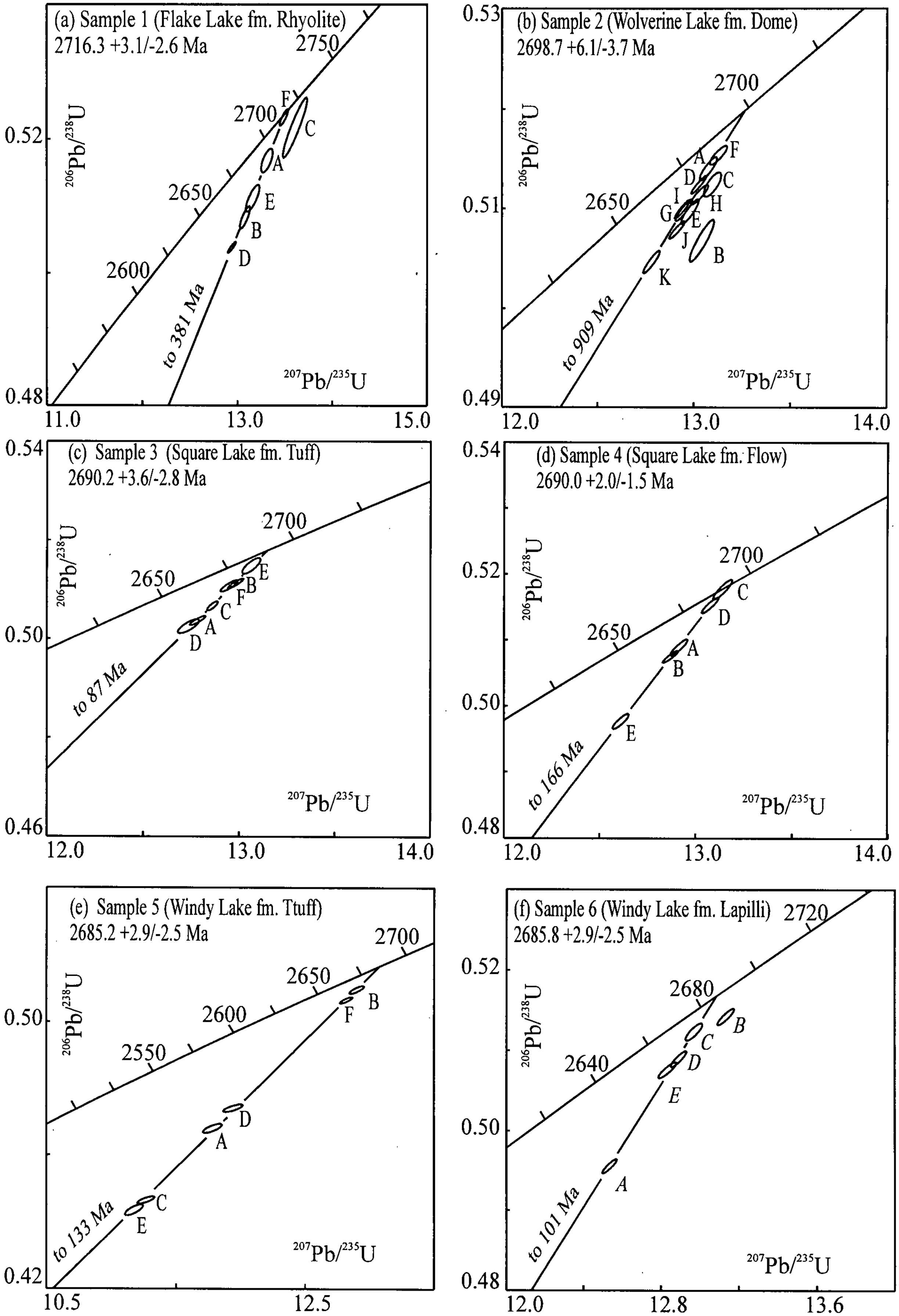

Figure 2.4. U-Pb concordia plots for rocks of the HBGB (samples 1-6).

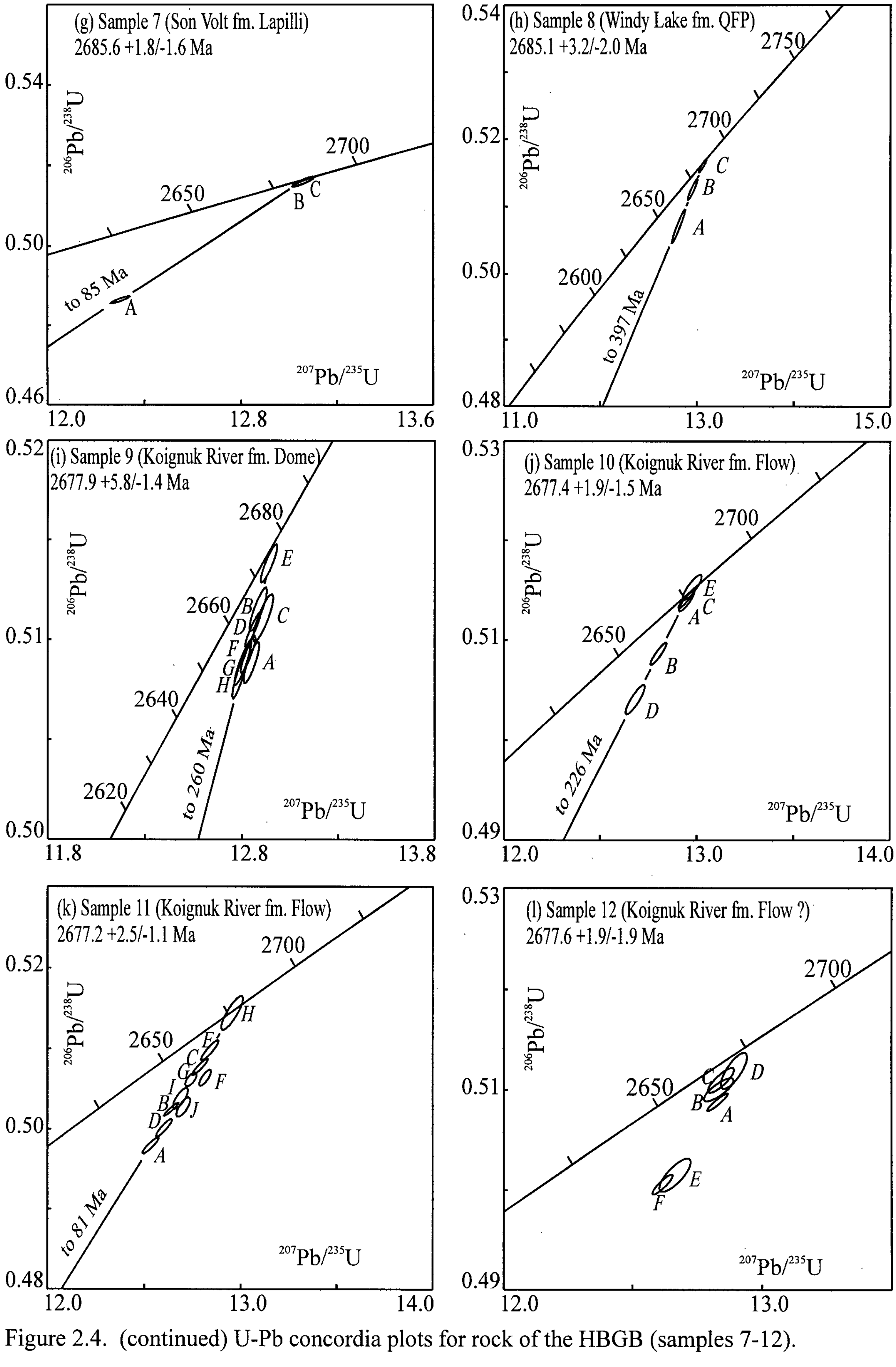

Figure 2.4. (continued) U-Pb concordia plots for rock of the HBGB (samples 7-12).

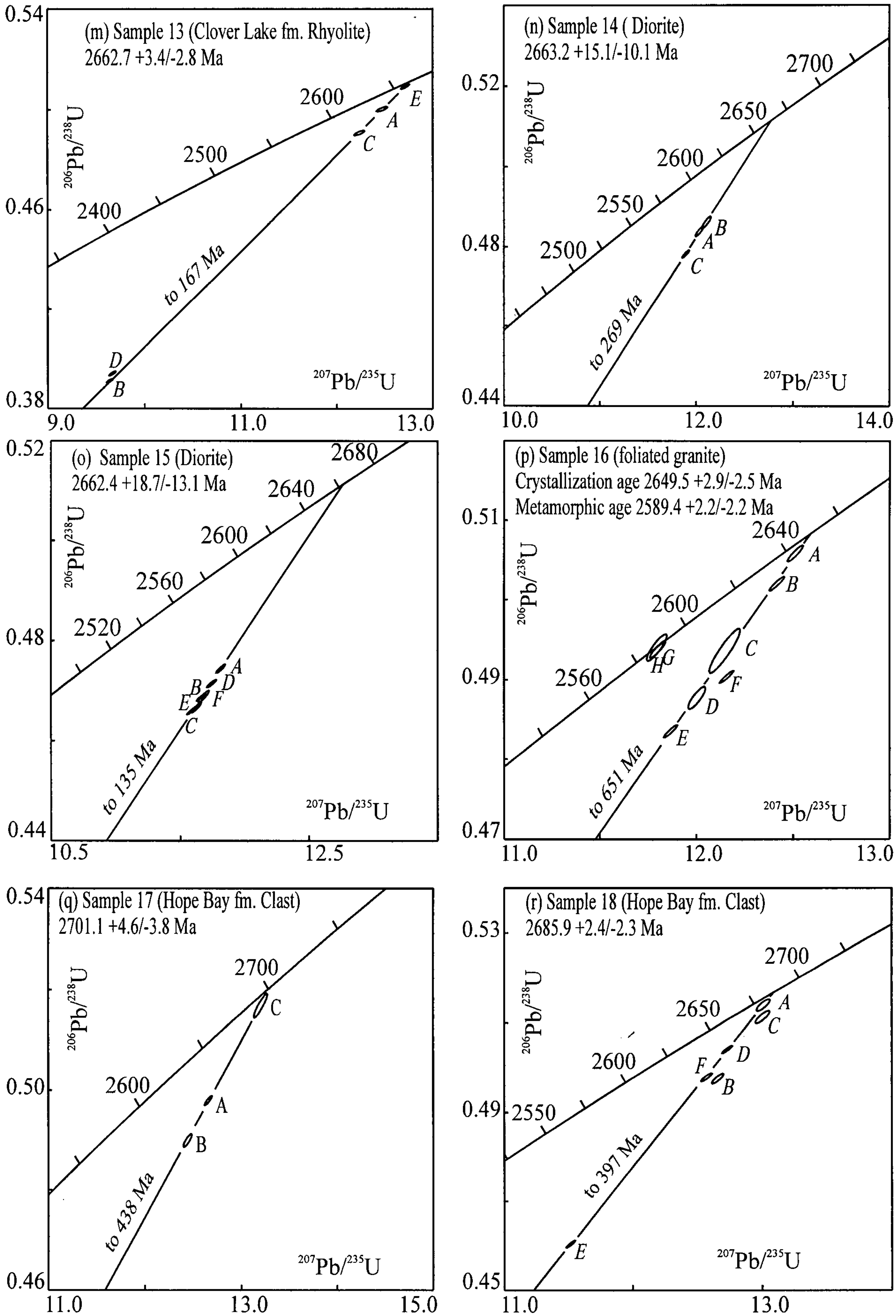

Figure 2.4. (continued) U-Pb concordia plots for rocks of the HBGB (samples 13-18).

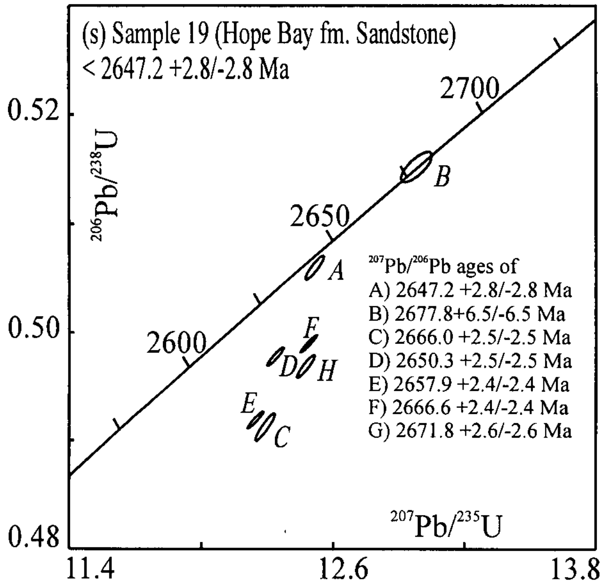

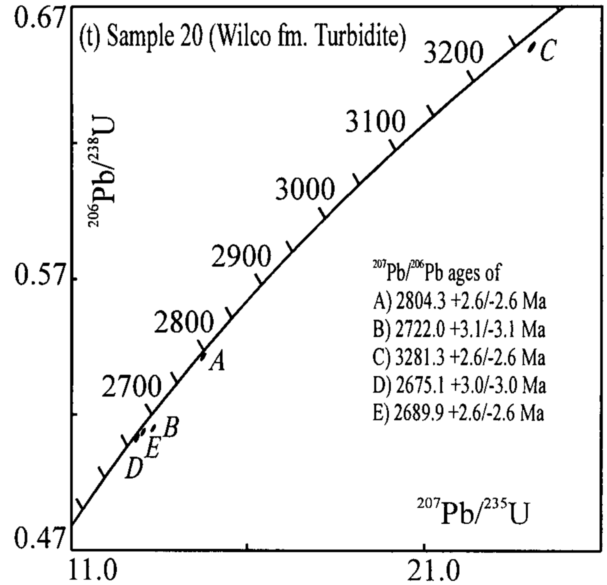

Figure 2.4. (concluded) U-Pb concordia plots for rocks of the HBGB (samples 19-20).

interpreted to have included an older inherited component. This interpretation is supported by the anomalously high proportion of ^{208}Pb in the analysis (17 % ^{208}Pb vs. 12.8-13.7 % ^{208}Pb in the other four fractions; Table 2.1).

Sample 2 (96PTMC119, Wolverine Lake fm) – quartz-feldspar porphyry

This unit crops out in the northern portion of the HBGB south of Patch Lake (Figure 2.3a) where it intrudes a volumous sequence of basaltic flows. Zircons recovered from this sample show a uniform morphology, comprising subhedral to euhedral, clear to somewhat turbid, moderately fractured, pale coppery pink prismatic crystals with ubiquitous broken terminations. Minor bubble and rod-like inclusions were present and no visible cores or zoning are apparent. Eleven single grains of similar morphology and size were analysed (Table 2.1) with degrees of discordance ranging from 0.7-2.8 %. The data show considerable scatter (Figure 2.4b) that is thought to reflect the effects of an older inherited zircon component in at least some of the grains. Six analyses define a linear array that bound the left side of the data array, resulting in upper and lower intercepts of $2698.7^{+6.1}_{-3.7}$ Ma and 908 Ma respectively. The upper intercept age gives a maximum crystallisation age for the quartz-feldspar porphyry.

Sample 3 (96PQMC113, Square Lake fm) – feldspar phyric felsic tuff

The feldspar phyric tuff sample was collected from a small glacially polished outcrop north of Square Lake and 1000 meters east of the western bordering granites (Figure 2.3a). Extensive lichen cover precludes conclusive interpretation of lithological relationships between adjacent units. Tuffaceous fragments exclusively comprise quartz phyric porphyry. Heavy mineral separates contained abundant gem quality equant, multi-faceted zircons with few rod and bubble shaped fluid inclusions. Zircons formed a bimodal size distribution predominately consisting of 100-134 micron and subordinate 134-160 micron grains with no visible zoning or inherited cores. Three fractions from each population were analysed (Table 2.1) and range from slightly to moderately discordant (0.6-2.8%). A linear regression through all fractions yields an upper intercept, interpreted as the crystallisation age for the tuff, of $2690.2^{+3.6}_{-2.8}$ Ma and a relatively young lower intercept age of 89 Ma suggesting a recent Pb-loss event (Figure 2.4c).

Sample 4 (97PQMC109, Square Lake fm) – quartz-feldspar phyric dacite flow

The sample was collected near the western margin of the belt on the northeastern shore of Lynx Lake (Figure 2.3a) from a dacitic flow interbedded with volcaniclastic rocks and intruded by a gabbro pod. Zircon separates formed a homogenous population of gem quality, 100-134 micron, pale pink, euhedral, and sharply faceted translucent prisms with a length to width aspect of 2:1. No visible cores or igneous zoning were noted. Five low U fractions were analysed (Table 2.1) and results included one concordant and four variably discordant (0.5-3.8%) analyses. The concordant zircon yielded a $^{207}Pb/^{206}Pb$ age of $2690.0^{+2.8}_{-2.8}$ Ma and a linear regression through all grains gives upper and lower intercept ages of $2690.0^{+2.0}_{-1.5}$ Ma and 166 Ma respectively (Figure 2.4d). The upper intercept age is interpreted as the best estimate for the crystallisation of the flow.

Sample 5 (97PBMC104, Windy Lake fm) – dacitic tuff?

This sample was collected along the eastern shore of Spyder Lake (Figure 2.3b) from an area of rubbley frost-heaved rock. This unit has been strongly carbonate altered, and the intensity of the metasomatism precludes assigning a definite rock type, although the abundant feldspar laths in a fine-grained matrix are similar to a dacitic tuff unit found further north along strike. The sample yielded abundant ~180 micron, euhedral, moderately fractured cloudy pale brown zircons. The grains form a single zircon population comprised of multifaceted grains with no visible apparent cores or igneous zoning. Measured U contents of six analysed grains (Table 2.1) are relatively high (~150-367 ppm), and the analyses form a discordant linear array (1.3-13.9 %) (Figure 2.4e). Calculated upper and lower concordant intercepts are $2685.2^{+2.9}_{-2.5}$ Ma and 133 Ma respectively. The upper intercept age is interpreted as the crystallisation age of the feldspar phyric flow.

Sample 6 (96PTMC123, Windy Lake fm) – dacitic volcaniclastic lapilli

This sample located north of Windy Lake from the northern portion of the HBGB (Figure 2.3a) consists of a volcaniclastic lapilli unit intercalated with suspected turbidite sediments. The sample matrix is weakly carbonate altered and strongly feldspar phyric, and consists largely of angular monolithic lapilli sized quartz phyric felsic fragments. Recovered zircon prisms form a homogenous population of pale pink, translucent, stubby, sharply faceted prisms. No apparent igneous zoning or inherited cores were detected. Five single zircon analyses (Table 2.1) range from 0.9-4.9 % discordant. If fraction B is omitted from the data array the remaining fractions yield a regressed interpreted crystallisation age determination of $2685.8^{+2.9}_{-2.5}$ Ma (Figure 2.4f). Fraction B is interpreted as an inherited xenocrystic zircon with a $^{207}Pb/^{206}Pb$ age of $2700.0^{+2.8}_{-2.8}$ Ma.

Sample 7 (97PAMC106, Windy Lake fm) – dacitic lapilli

This sample was collected from a volcaniclastic unit 6 km southeast of Lynx Lake in the central portion of the HBGB (Figure 2.3a). Fragments are monolithic and comprise lapilli sized angular quartz-feldspar porphyry clasts hosted in a felsic fine-grained crystalline matrix. Prior to sample processing, the matrix and contained fragments were separated in an attempt to determine ages of fragments and matrix separately; however only a small number of poor quality, highly fractured zircons unsuitable for analysis were recovered from the matrix. A small quantity of gem quality zircons was recovered from the fragments. The translucent pale pink grains are characterised by slightly elongate (l:w of 2.5:1) stubby prisms with abundant fractures and minute bubble-shaped fluid inclusions. Three single grains were selected for analyses (Table 2.1). One analysis is 5.6% discordant whereas two fractions (B and C) are nearly concordant (0.2 %) with $^{207}Pb/^{206}Pb$ ages of $2685.4^{+2.8}_{-2.8}$ Ma and $2685.8^{+2.5}_{-2.5}$ Ma (Figure 2.4g) respectively. A linear regression through all analyses results in an upper concordia intercept of $2685.6^{+1.8}_{-1.6}$ Ma and a lower concordia intercept of and 85 Ma. The upper intercept age is interpreted as the crystalline age for the quartz-feldspar porphyry component of this unit and provides a minimum crystallisation age for the volcaniclastic unit.

Sample 8 (97PTMC111, Windy Lake fm) – quartz-feldspar porphyry

Sample 8 located east of Hope Bay (Figure 2.3a) is from a massive quartz-feldspar phyric rhyodacite porphyry body that is overlain and flanked by abundant felsic volcaniclastic rocks. Zircons recovered comprise a single population of ~150 micron, multifaceted stubby prisms with few bubble-shaped inclusions. The gem quality grains showed no evidence of igneous zoning or inherited cores. One concordant and two slightly discordant (0.7-1.7%) fractions were analysed (Table 2.1) and define a linear array with calculated upper and lower concordia intercepts of $2685.1^{+3.2}_{-2.0}$ Ma and 397 Ma respectively (Figure 2.4h). Fraction C is nearly concordant (0.1 %) with a $^{207}Pb/^{206}Pb$ age of $2685.2^{+2.3}_{-2.4}$ Ma. The former upper intercept age is interpreted as the age of crystallisation.

Sample 9 (96PCMC108, Koignuk River fm) – quartz feldspar dome

A subvolcanic feeder to a rhyodacite flow (sample 11) is located along the western margin of the southern portion of the greenstone belt (Figure 2.3b). Heavy mineral separates contained abundant clear, gem quality zircons forming two size populations. The dominant group is comprised of 74-105 micron (l:w of 2:1), slender, pale pink, euhdral, sharply faceted, tabular prisms with minute rod and bubble-shaped fluid inclusions. Grains from the subordinate population were 134-160 microns in diameter, translucent, stubby (l:w of 2:1), pale pink, and generally free of inclusions. No visibly apparent igneous zoning or inherited cores were recognised in either group. Eight fractions, including three single grain fractions, were analysed (Table 2.1). The analyses $^{207}Pb/^{206}Pb$ ages ranged from 0.2- 1.2 % discordant. Fractions A and C yield slightly older $^{207}Pb/^{206}Pb$ ages (Table 2.1) then the remaining six analyses and are thought to have incorporated a minor inherited component. A regression through the remaining six analyses yields with and lower concordia intercepts of $2677.9^{+5.8}_{-1.4}$ Ma and 260 Ma respectively (Figure 2.4i). The upper concordia intercept is considered the crystallisation age of the porphyry stock.

Sample 10 (96PTMC118, Koignuk River fm) – dacitic flow

This sample was collected west of Patch Lake (Figure 2.3a) where it forms a spatially restricted lava flow that is intercalated with abundant volcaniclastics and intruded by a quartz feldspar porphyry stock. The sample contains parallel oriented feldspar laths hosted in a massive fine-grained matrix. Heavy mineral concentrates yielded abundant gem quality zircons. Two main size populations are present; the main population consists of ~250 micron (l:w of 3:1), multifaceted, euhedral translucent pale pink grains, whereas the subordinate group is characterised by ~100-134 micron (l:w of 2:1), multifaceted, translucent pale pink prisms. Both groups include a small number of bubble-shaped inclusions with no visible cores or igneous zoning. Five fractions were selected representing both populations (Table 2.1). Three analyses are concordant with the remaining two 1.2 % and 2.0 % discordant. The concordant fractions $^{207}Pb/^{206}Pb$ ages are $2677.9^{+2.7}_{-2.7}$ Ma (fraction A), $2676.9^{+2.5}_{-2.5}$ Ma (fraction C), and $2677.2^{+3.5}_{-3.5}$ Ma (fraction E) yielding an average $^{207}Pb/^{206}Pb$ age of $2677.3^{+2.9}_{-2.9}$ Ma. A linear regression through all data points results in upper and lower corcordia intercepts of $2677.4^{+1.9}_{-1.5}$ Ma and 226 Ma respectively (Figure 2.4j). The upper intercept is interpreted as the best estimate of the crystallisation age for the dacitic flow.

Sample 11 (96PCMC107, Koignuk River fm) – rhyodacidic flow

This sample was collected from a quartz-feldspar phyric flow located along the southwestern margin of the HBGB (Figure 2.3b). The unit flanks a larger intrusive felsic porphyry dome (sample 9) and is intercalated with flow breccia and fine-grained sediments. Zircons similar in appearance to those recovered in sample 9 were recovered from the felsic flow. Ten fractions representing both grain size populations, including seven single grain fractions, were analysed (Table 2.1). One single grain (fraction H) yielded a concordant analysis with a $^{207}Pb/^{206}Pb$ age of $2677.0^{+3.9}_{-3.9}$ Ma. The remaining grains were variably discordant (1.0-3.2 %). Fractions F and J yield marginally older $^{207}Pb/^{206}Pb$ ages (Table 2.1) then the remaining eight analyses and are thought to have incorporated a minor inherited component. A linear regression omitting fractions F and J constrain an age of $2677.2^{+2.5}_{-1.1}$ Ma (Figure 2.4k).

Sample 12 (96PBMC104, Koignuk River fm) – felsic tuff?

A fine to medium-grained unit tentatively interpreted to be a felsic tuff occurs in the southern portion of the belt (Figure 2.3b) where it is intercalated with sediments. A moderate amount of zircon was extracted from this sample. Two distinct size populations were recovered. Both size populations were multifaceted, tabular, pale pinkish brown crystals with no visible zoning or cores. Minute bubble and rod-shaped inclusions were noted. Populations were divided based on their grain sizes; 100-134 microns (l:w 0f 2:1) and 180-200 microns (l:w of 3:1) respectively. Six single grain fractions were analysed (Table 2.1). Individual analyses were 0.5-2.8 % discordant with $^{207}Pb/^{206}Pb$ ages ranging from 2673.5-2681.4 Ma (Figure 2.4l). Despite the apparent variation in ages all fractions are within analytical error and thus a weighted average of the $^{207}Pb/^{206}Pb$ ages of 2677.6 ± 1.9 Ma is interpreted as the age of deposition of this unit.

Sample 13 (97PBMC103, Clover Lake fm) – massive rhyolite

This sample, located on the northern shore of Clover Lake (Figure 2.3b), is from a small isolated outcrop bordered by turbidites along the eastern and western flanks. The rhyolite consists of rare quartz eyes hosted within a black massive matrix. A single zircon population of ~100 micron tabular pale pink prisms with commonly broken terminations was recovered from the sample. Minute rare elliptical clear inclusions are present and grains are of moderate clarity. Five analyses (Table 2.1) range from 0.4-22.7% discordant. A regression (excluding the two highly discordant fractions) gives upper and lower intercepts ages of $2662.7^{+3.4}_{-2.8}$ Ma and 167 Ma respectively (Figure 2.4m). The upper intercept age is interpreted as the crystallisation age for the rhyolite.

Plutonic rocks

Sample 14 (97PTMC108, Diorite) – coarse grained diorite

A small outcrop of megacrystic diorite occurs in the northern portion of the HBGB east of Lynx Lake (Figure 2.3a). Copious quantities of high U (Table 2.1) acicular prismatic monocrystalline zircons were recovered from this sample. Reddish pink tabular zircons are elongate (l:w of 5:1) and of moderate quality with highly fractured terminations. No apparent igneous zoning or inherited cores were noted. Three fractions (Table 2.1) representing the highest quality material available were moderately discordant (4.7-6.2 %). The data define a discordia array with imprecise upper and lower concordia intercept ages of $2663.2^{+15.1}_{-10.1}$ Ma and 135 Ma respectively (Figure 2.4n). The $^{207}Pb/^{206}Pb$ ages are within analytical error of each other, hence the weighted average $^{207}Pb/^{206}Pb$ age of 2656.7 ± 1.5 Ma for the three fractions should represent the minimum crystallisation age of this rock. The upper intercept age is considered the best estimate for the age this unit.

Sample 15 (96PUMC101, Diorite) – coarse grained diorite

A diorite intrusion similar to sample 14 crops out in the centre of the supracrustal rock package and is crosscut by granite dykes (Figure 2.3b). Sample 15 is a medium-grained sheared diorite from this locality. . Zircons in this sample are identical in appearance to those from sample 14. Six fractions representing the best material were selected for analyses (Table 2.1). The data are strongly discordant (7.0-8.6 %) resulting in a discordia array (Figure 2.4o) with upper and lower intercept ages of $2662.4^{+18.7}_{-13.1}$ Ma and 269 Ma respectively. The individual $^{207}Pb/^{206}Pb$ ages for the six fractions (2655.6-2659.0 Ma) are within analytical error of each other, thus the weighted average for all $^{207}Pb/^{206}Pb$ ages (2657.7 ± 1.9 Ma) should represent the minimum crystalline age for this unit. The upper intercept age is imprecise but is considered to be the best estimate for the crystallisation age of the rock.

Sample 16 (T961-43b) – foliated migmatitic granite

Sample 16, collected by P.H. Thompsen, is from a foliated migmatitized granite extracted from the large area of plutonic rocks that bounds the HBGB in the southeast (Figure 2.3b). Heavy mineral separates yielded abundant zircon and titanite. Zircons comprise dominantly ~150 micron pale pink translucent prisms and subordinate ~300 micron elongate (l:w of 3:1) tabular grains. The grains were of excellent quality, and no apparent zoning or cores were detected. Pale brown wedge-shaped titanites of moderately good quality formed a homogenous population. Six single zircon grains were analysed (Table 2.1) and are variably discordant (0.4-4.2 %) (Figure 2.4p). Fraction F yields anomalously old $^{207}Pb/^{206}Pb$ age and is thought to contain a minor inherited component; omitting this fraction from a linear regression gives upper and lower concordia intercepts of $2649.5^{+2.9}_{-2.5}$ Ma and 651 Ma respectively. The upper intercept age is considered the crystallisation age for the granite. Multigrain titanite fractions are concordant with overlapping $^{207}Pb/^{206}Pb$ ages of $2589.9^{+2.8}_{-2.8}$ Ma and $2588.5^{+3.6}_{-3.6}$ Ma. The weighted average of the $^{207}Pb/^{206}Pb$ age of $2589.4^{+2.2}_{-2.2}$ Ma for the two titanite analyses gives the best estimate for the timing of peak metamorphism that affected this section of the HBGB.

Sedimentary rocks

Sample 17 (96PDMC126, Hope Bay fm) – granitoid clast

This rounded cobble was collected from a clast supported polymictic conglomerate with coarse-grained sandstone interbeds found on an island within Hope Bay located in the northern tip of the HBGB (Figure 2.3a). Heavy mineral separates yielded a minute amount of homogenous, pristine, euhedral, multifaceted, stubby zircon with few rod-like inclusions. Three low U (<65 ppm) fractions with no apparent cores or zoning were analysed (Table 2.1) and define a discordant (0.8-9.1 %) linear array with upper and lower intercept ages of $2701.1^{+4.6}_{-3.8}$ Ma and 438 Ma (Figure 2.4q) respectively. The upper intercept is considered the crystallisation age of the granitoid clast.

Sample 18 (96PDMC125, Hope Bay fm) – granitoid clast

Sample 18 is from the same polymictic conglomerate unit as sample 17 (Figure 2.3a). The rounded granitoid cobble yielded a small quantity of stubby, monocrystalline, equant, and multifaceted zircons. Facets are slightly rounded, no zoning or inherited cores were detected, and small rod-shaped fluid inclusions were present in a few grains. Six single grains were analysed (Table 2.1) and are variably discordant (0.5-10.1%). A regression through four of six analyses gives upper and lower intercepts of $2685.9^{+2.4}_{-2.3}$ Ma and 397 Ma (Figure 2.4r). The upper intercept is interpreted to be the crystallisation age of the rock. Two other analyses, fractions B and C give anomalously old $^{207}Pb/^{206}Pb$ ages of $2691.4^{+3.1}_{-3.1}$ Ma and $2689.9^{+3.9}_{-3.9}$ Ma, respectively and are considered to represent an older inherited zircon component.

Sample 19 (96PDMC128, Hope Bay fm) – coarse-grained sandstone

This sample is from a coarse-grained sandstone interbedded within a polymictic conglomerate (hosts sample 17 and 18) sequence on a small island located in Hope Bay (Figure 2.3a). A heterogeneous collection of stubby to prismatic grains of moderate to excellent clarity was recovered from heavy mineral concentrates. Seven single, high quality grains were selected to represent the various grain morphologies present. Analyses (Table 2.1) ranged from concordant to 4.1 % discordant with $^{207}Pb/^{206}Pb$ ages ranging from $2677.8^{+6.5}_{-6.5}$ Ma to $2647.2^{+2.8}_{-2.8}$ Ma (Figure 2.4s). The youngest age is considered to represent the maximum depositional age for this sequence.

Sample 20 (96PKMC121, Wilco fm) – quartz-feldspar rich greywacke

The sample is from a small isolated outcrop of greywacke found in the central portion of the volcanic sequence east of Lynx Lake (Figure 2.3a). Grain morphologies recovered from heavy mineral concentrates are diverse ranging from slender acicular prisms to short, stubby, and rounded grains. Zircons selected for single grain analyses (Table 2.1) were of excellent quality with rare rod and/or bubble-shaped inclusions present and no visible cores or igneous zoning was noted. Slightly discordant analyses (0.6-2.0 %) with $^{207}Pb/^{206}Pb$ ages (Figure 2.4t) of 2675.1 ± 3.0 Ma, 2689.9 ± 2.9 Ma 2722.0 ± 3.1 Ma, 2804.3 ± 2.6 Ma, and 3281.3 ± 2.6 Ma indicate a highly diverse sediment source and a maximum depositional age for the unit of 2675.1 ± 3.0 Ma.

Stratigraphic Reconstruction of the HBGB

Twenty-one U-Pb ages reported here, together with results of U-Pb dating studies by other workers, provide a relatively complete temporal and stratigraphic framework for the HBGB (Figure 2.5 and 2.6). Data indicate felsic volcanism spanned a period of at least 53 millions years (2716-2663 Ma) suggesting that the bulk of supracrustal rocks in the HBGB was deposited over that period. This is strikingly similar to the depositional time frame for rocks of the YkGB (2715-2655 Ma). The apparent clustering of ages (Figure 2.5) may indicate that the magmatism was episodic; however, the age differences between the magmatic events are too

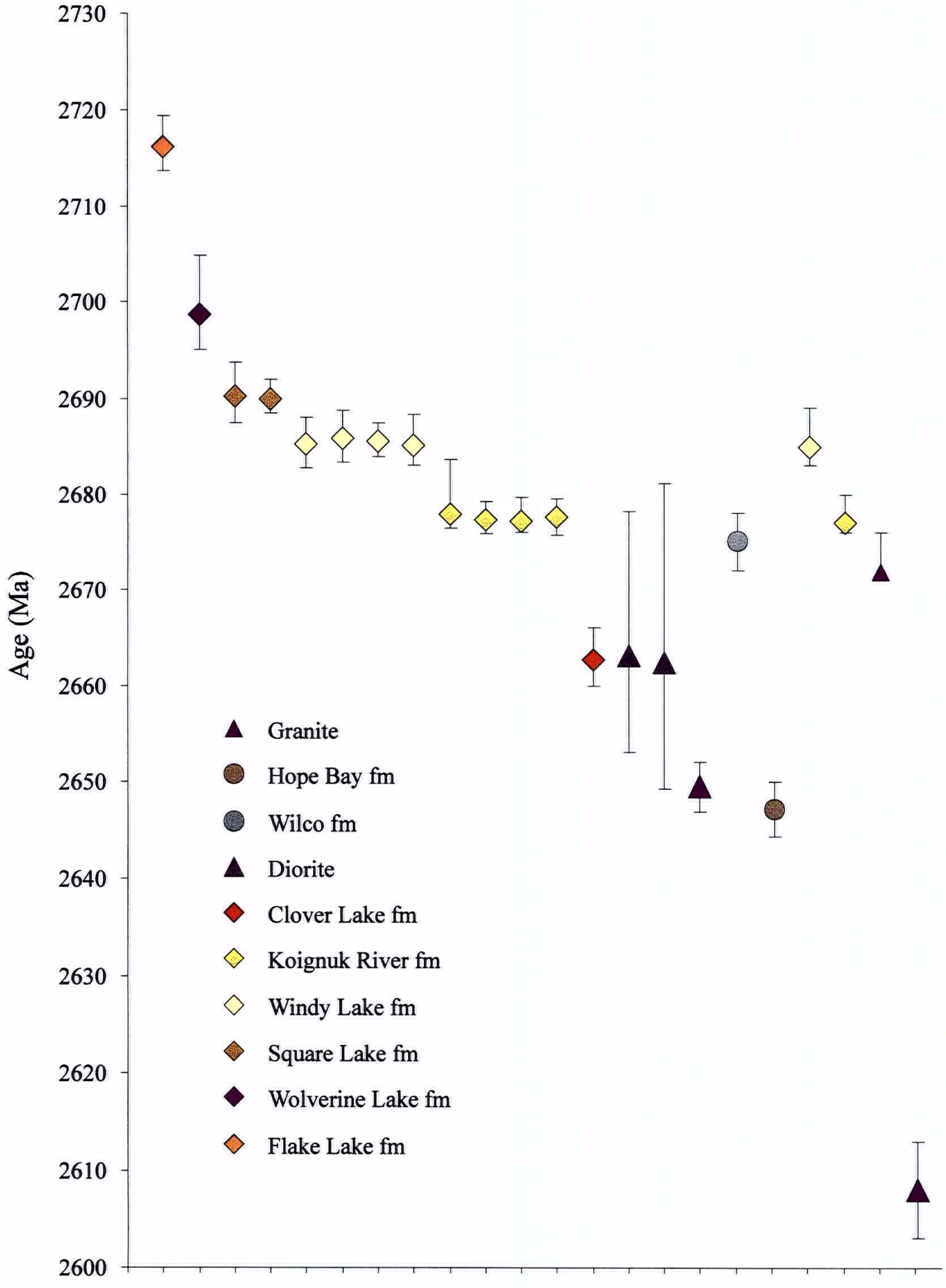

Figure 2.5. Plot of age determinations with associated errors for volcanic (◇), plutonic (△), and sedimentary rocks (○) within the HBGB.

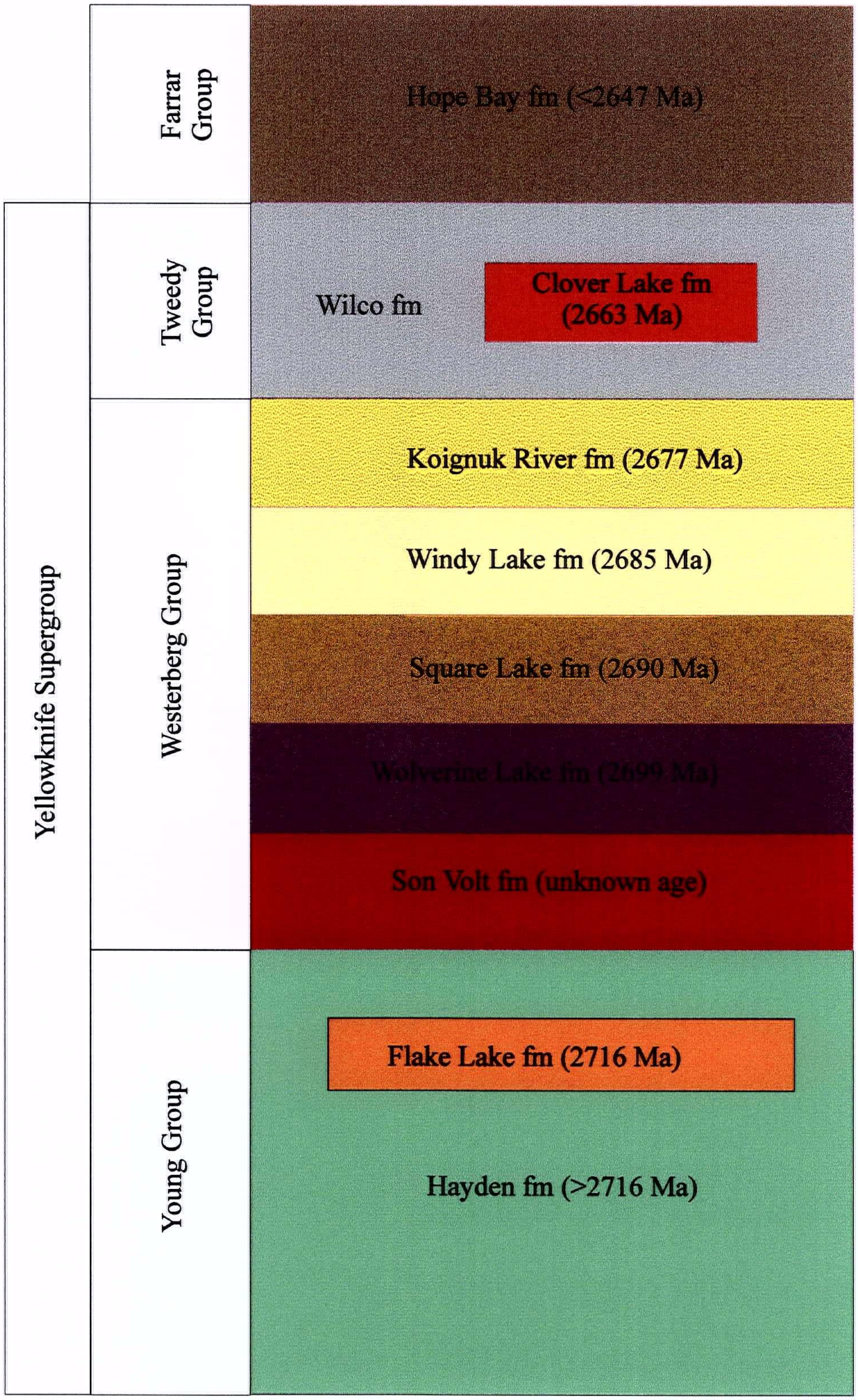

Figure 2.6. Generalized stratigraphic column for the HBGB.

small to preclude essentially continuous magmatism over the 53 million years in the HBGB. If the ages of the sedimentary units are considered, the temporal framework of the HBGB supracrustal sequences span a period of at least 69 m.y. (>2716 Ma to < 2647 Ma).

Although the exact number of mafic cycles in the HBGB remains uncertain (Chapter 3), mafic volcanics within the HBGB have been collectively assigned to the Hayden formation. Directly determining the age of mafic volcanics is difficult. Lack of suitable material to date within sequences requires the use of indirect age information to constrain the depositional age of these units. However, two age determinations provide some preliminary temporal constraints for this formation. To the southwest of Patch Lake (Figure 2.3a), the 2699 Ma Wolverine Lake formation clearly crosscuts mafic volcanic rocks and west of Flake Lake (Figure 2.3b) pillow tops face toward the 2716 Ma Flake Lake formation suggesting the bulk of the Hayden formation is pre-2716 Ma.

The oldest felsic unit discovered thus far, the 2716 Ma Flake Lake formation is a poorly exposed rock suite spatially restricted to an area around Flake Lake (Figure 2.3b). The stratigraphic position of the formation within the upper portion of the Hayden formation suggests it was deposited during the waning stages of mafic volcanism, and possibly represents the differentiated product of a high level Hayden formation mafic magma or the partial melting of mafic or felsic rocks. This age is similar to other units across the SSP that define the onset of volcanism in the YkSG. The chemical signature (Chapter 3) of the suite may be of economic significance, as it is known to host VMS occurrences in the Superior Structural Province (Barrie et al. 1993;Thurston 1981; Lesher et al. 1986). The Hayden and Flake formations together comprise the Young Group, which is analogous to the Kam Group in the Yellowknife greenstone belt.

The Son Volt formation, a thick unit of intermediate volcanic rocks outcrops southwest of Spyder Lake (Figure 2.3b) with thin discontinuous lenses extending north up to the central portion of the belt. The precise age of this formation is uncertain as geochronological sampling of intermediate rocks failed to yield zircons. However, the Son Volt formation appears to lie stratigraphically above the mafic volcanic rocks and locally contains rare flows of variolitic pillow basalt. This relationship suggests that the Son Volt formation was erupted at the end of the main period of mafic volcanism ca. 2.7 Ga.

Deposition of the Son Volt formation was followed by an apparent period of magmatic quiescence which lasted ~ 17 m.y. and culminated in the emplacement of the 2699 Ma Wolverine Lake formation, a series of quartz- and plagioclase-phyric high level intrusions and domes. This formation appears to be spatially restricted to an area along the south western flank of Patch Lake (Figure 2.3a). However, zircon xenocrysts found in the younger Windy Lake formation north of Windy Lake (Table 2.1, Sample 6,) and on the eastern shore of Spyder Lake (Bevier and Gebert, 1991) yield $^{207}Pb/^{206}Pb$ ages of 2700 and 2701 Ma, respectively, suggesting that rocks comparable in age to the Wolverine Lake formation may be present along the length of the HBGB. Another apparent period of magmatic quiescence which lasted ~9 m.y followed emplacement of the Wolverine formation. This was in turn followed deposition of the aerially restricted Square Lake formation at 2690 Ma in west-central HBGB (Figure 2.3a). The Square Lake formation is intruded to the west by granites, to the northeast by gabbro, and fault bounded by mafics along its northeastern flank. A further apparent volcanic hiatus (~5 m.y.) was followed by deposition of the 2685 Ma Windy Lake formation, one of two dominant felsic suites found throughout the eastern HBGB. The formation is bordered by turbidites on the west, by west facing mafic volcanic rocks along the northeastern flank, and east facing mafics along the southeastern flank. The 2685 Ma volcanic event was followed by another short apparent hiatus (~7 m.y.) in magmatism, which culminated in deposition of the other regionally extensive felsic suite, the 2677 Ma Koignik River Formation found throughout the western HBGB. The unit locally (at sample site 10) crosscuts west facing mafic pillow volcanic flows and is intruded by local gabbro bodies. A final apparent hiatus (14 m.y.) between felsic volcanism events culminated in the extrusion of the Clover Lake formation at 2663 Ma, bordered on either side by turbidites. The Son Volt, Wolverine Lake, Square Lake, Windy Lake, and Koignuk River comprise the Westerberg group, which is correlative to the Banting formation of the YkGB.

Typical SSP turbidites (greywacke-mudstone units) are found throughout the HBGB and commonly underlie lakes and valleys due to the recessive weathering of these units. Sedimentary rocks interpreted to be turbidites are collectively assigned to the Wilco formation. Detrital U-Pb work on a sample of turbidite from the central HBGB resulted in a span of $^{207}Pb/^{206}Pb$ ages of: 3281 Ma, 2804 Ma, 2722 Ma, 2690 Ma, and 2675 Ma. These dates provide a maximum depositional age of 2675 Ma for this unit. More interesting are two pre-YkSG ages (2804 and 3281 Ma) derived from single zircon grains that showed no morphological evidence of prolonged transport (i.e. rounding or frosting). These ages are, however, common in other parts of the SSP. Although current models of the SSP suggest rocks of this age are restricted to the western SSP, old zircons within the Hope Bay turbidites could have been derived from a source that lay further east or these zircons may also suggest a more proximal source concealed somewhere within the Bathurst Block. Further support for the presence of basement within the Bathurst block comes from the geochemical signatures of selected Hayden formation mafics (chapter 3). Rare earth element depletions (Nb, P, and Ti) on a primitive mantle normalised diagram indicate these melts may have assimilated sialic crust (Chapter 3) (Kerrich and Wyman, 1997; Barley, 1986).

A more refined age constraint for the Wilco formation may be provided by the 2663 Ma Clover Lake formation. The position of this suite, which is bounded by turbidites on either side, suggests it was erupted shortly before or possibly during the deposition of the sedimentary rocks. The age of this unit indicates the depositional age of the Wilco formation may be ca. 2660 Ma, which is very similar to the 2661 Ma for the Burwash Formation (Bleeker and Villeneuve, 1995) of the YkSG. The Wilco and Clover Lake formations together comprise the Tweedy group.

The upper sequence in the HBGB also contains a variety of coarse-grained clastic rocks collectively assigned to the Hope Bay formation. A polymictic conglomeratic unit located in the northern portion of the HBGB (Figure 2.3a) unconformably overlies the greenstone belt and is considered to be the youngest member of the supracrustal package. Prior workers (Padgham, 1996) dated a single clast from this unit and reported an age of 2715 Ma for the cobble. Two granitic cobbles extracted from this unit and dated in this study yield ages of 2701 Ma and 2686 Ma, respectively. The 2686 Ma age suggests plutonism was occurring at the same time as volcanism during the deposition of the Windy Lake Formation. Detrital U-Pb work from a sandstone interbed found within this unit suggest a maximum age of deposition for this unit was 2647 Ma. However, this conglomerate texturally resembles the <2.6 Ga "Jackson Lake" type conglomerate, and therefore may be of similar age. Despite the homogenous age for this formation, units comprising this formation demonstrate dramatic internal facies changes along strike and it is uncertain whether this represents facies variations of a single unit or if they represent separate units of different ages.

Relatively few U-Pb age determinations for plutonic rocks are available from the Bathurst block of the SSP. U-Pb dates for three plutonic rocks in the HBGB reported in this study, together with two prior age determinations (Bevier and Gebert, 1991) indicate that most and perhaps all of the plutonic rocks within the Bathurst Block are either coeval with or younger than the supracrustal rocks of the HBGB. Age data for plutonic rocks within the Bathurst Block is still too limited to preclude the possibility of older crystalline basement in this region. The few dates have shown the existence of synvolcanic (2672 Ma, ca 2663 Ma, and 2650 Ma) and sydeformational (2608 Ma) plutonism. In addition, if granitic cobbles hosted within the Hope Bay formation are locally derived then synvolcanic plutonism extends from 2701-2650 Ma.

A foliated orthogneiss unit borders the southeastern contact of the belt. Titanite interpreted to be metamorphic in origin was extracted from this unit, and dated at 2589 Ma. This is believed to represent the time of peak of regional metamorphism in this area. However, a granite intrusion dated on the northwest side of the HBGB which contains foliated mafic xenoliths suggests the lower age limit for the peak of regional metamorphism and deformation of the HBGB is 2608 (Bevier and Gebert, 1993). A similar paradox is observed by Villeneuve et al. (1997) with the relatively undeformed 2602 Ma Chin Lake stock of the Anialik River greenstone belt and the nearby <2600 Ma String Lake conglomerate which displays a strong penetrative foliation. Villeneuve et al. (1997) suggest this apparent contradiction may result from differing local strain rates within the regional deformation events or suggests the terminal deformation event was episodic.

Evolution of the HBGB

Archean greenstone belts have commonly been considered to contain numerous volcanic cycles, exhibiting a regular progression from mafic to felsic compositions. Cyclical volcanism is repeated to produce stacked sequences commonly in excess of ten kilometres in thickness. This process was believed to occur over a relatively short timeframe and in close proximity to the present distribution of the volcanic sequences. The volcanic successions are thought to result from three main processes: 1) tapping and differentiating from subvolcanic magma chambers, 2) interleaving of distal deposits of one volcano with the proximal deposits of another volcano, and 3) tectonic thrusting and interleaving of volcanic strata (Sylvester et al., 1997).

The HBGB appears to be typical of such sequences; geochronological, geochemical (Chapter 3), and structural data suggest mafic-felsic sequences likely resulted from all three mechanisms.

The HBGB appears to contain a simple stratigraphy (Figure 2.2 and 2.6) with an older unit of dominantly mafic volcanic rocks (Young group), a middle unit of dominantly felsic rocks (Westerberg group) of various ages, and a younger unit of sedimentary rocks (Tweedy and Farrar group) derived from the erosion of mafic, felsic and plutonic rocks. However, age determinations in concert with local younging directions suggest structural complexity. Within the HBGB there are several areas where older units overly younger lithologies: 1) In the northern HBGB, west younging mafics are bordered to the east by younger turbidites underlying Windy Lake (Figure 2.2a) and in the southern portion of the belt turbidites underlying and along strike of Spyder Lake may define a major thrust fault spanning the entire length of the belt. 2) On the northeast side of Spyder Lake a thrust fault appears to have placed older mafic volcanic rocks upon 2685 Ma felsic volcanic rocks (Figure 2.2b), 3) Mafic volcanics are also suspected to be thrusted upon turbidites to the west of Clover Lake (Figure 2.2b). Hence, the occurrence of turbidites within the HBGB may be used to infer the top of the volcanic pile.

Volcanism within the HBGB spanned a period in excess of 53 m.y. and if the Hope Bay formation is synchronous to the Jackson Lake Formation of the YkSG then the age framework for supracrustal rocks of the HBGB exceeds 100 m.y. In light of the complex structural relationships present and protracted evolutionary history for the belt, assigning a definitive depositional history for the belt is fraught with numerous pitfalls. Despite the complexities, the prolonged temporal framework, evidence of thrust faults, and contrasting geochemical sugnatures of the mafic (MORB and ocean island signatures) and felsic volcanic rocks (arc signature) can be reconciled in an island arc/back-arc geodynamic setting. With the tholeiitic Hayden and Flake Lake formations deposited in a back-arc basin, respectively preceding the deposition of the overlying Son Volt and calc-alkaline Wolverine Lake, Square Lake, Windy

Lake, Koignuk River, and Clover Lake formations were deposited in the fore-arc (chapter 3). The overlying sedimentary successions were then deposited after the mafic and felsic rocks were brought together during formation of the SSP.

The back-arc/island arc system proposed for the HBGB is consistent with the one proposed for the YkGB by Helmstaedt and Padgham (1986) and given our present level of knowledge of these granite-volcanic-turbidite terranes appears to best explain the formation of the main phase of the YkSG in the SSP.

Placing the findings of this study into the context of the overall evolution of the SSP is a precarious task. At our present level of understanding; with key elements necessary to formulate a tectonic model likely removed during the Thelon and Wopmay orogens and dubious lithological relationship, models explaining the evolution of the SSP fall tentatively under two main doctrines: collisional and extension tectonics. However, proponents of any one model are hard pressed to reconcile the protracted history of the SSP (4.0-2.6 Ga) coupled with the inherent diversity of rocks that comprise the SSP. Hence, workers are increasingly gravitating to a multi-stage tectonic model invoking a hybrid of the two end member beliefs (Isachsen and Bowering, 1994; Bleeker et al., 1997; Bleeker and Ketchum; 1998).

Conclusions

Twenty-one U-Pb age determinations for rocks of the HBGB help constrain volcanism, plutonism, sedimentation, and deformation within the belt. Volcanism occurred over an interval of at least 53 million years, beginning with the deposition of mafic rocks, the bulk of which are thought to have been deposited in a back-arc basin prior to circa 2716 Ma. Calc-alkaline felsic volcanism deposited in an island arc setting occurred from 2716 Ma to 2663 Ma and is separated by suspected volcanic hiatuses. Sedimentation of turbidites ensued volcanic activity at ca. 2663

Ma and was in turn followed by a protracted depositional hiatus of ca 60 m.y. culminating with the deposition of the Hope Bay formation at ca. 2600 Ma thus marking the top of the supracrustal sequence. Plutonic activity is marked by synvolcanic (2699 Ma, 2672 Ma, 2663 Ma, and 2650 Ma) and syndeformation (2608 Ma) intrusive rocks. Titanite cooling ages from a gneiss bordering the southeastern margin of the HBGB suggest the peak of regional metamorphism occurred at ca. 2589 Ma.

The temporal framework for the HBGB is strikingly similar to the YkGB, as both supracrustal sequences appear to have been deposited from >2716 Ma to <2600 Ma. This serves to reinforce the dominance of the YkSG throughout the entire SSP as originally proposed by Henderson (1970). Geochronological constraints indicate supracrustal successions in the HBGB are complicated by thrust faults and considering their protracted evolutionary history (>>100 m.y) support workers claim that greenstone belts are not the result of a single magmatic or tectonic event but rather represent episodic volcanism and sedimentation (Isachsen and Bowering, 1994; Sylvester et al, 1997; Bleeker et al., 1997; Bleeker and Ketchum; 1998).

References

Barley, M.E. (1986). Incompatible-element enrichment in Archean basalts: A consequence of contamination by older sialic crust rather than mantle heterogeneity. Geology v. 14, p 947-950.

Barrie, C.T., Ludden, J.N., and Green, T.H. (1993). Geochemistry of volcanic rocks associated with Cu-Zn and Ni-Cu deposits in the Abitibi subprovince. Economic Geology v.88, p 1341-1358.

Bevier, M.L., and Gebert, J.S. (1991) U-Pb geochronology of the Hope Bay-Elu Inlet area, Bathurst Block, Northeastern Slave Structural Province, N.W.T. Canadian Journal of Earth Sciences, v 28, p 1925-1930.

Bleeker, W. and Villeneuve, M. E. (1995). Structural studies along the Slave portion of the SNORCLE transect. In Slave-Northern Cordillera Lithospheric Evolution (SNORCLE), Transect meeting (April 8-9, 1995), University of Calgary, (comp) F. Cook and P Erdmer; Lithoprobe Report No 44, p 8-13.

Bleeker, W., Davis, W.J., and Villeneuve, M. E. (1997). The Slave Province: Evidence for contrasting crustal domains and a complex, multistage tectonic evolution. In Slave-Northern Cordillera Lithospheric Experiment (SNORCLE), Transect and Cordilleran tectonics Workshop Meeting (March 7-9, 1997), University of Calgary, (comp) F. Cook and P Erdmer; Lithoprobe Report No 56, p 36-37.

Bleeker, W., and Ketchum, J. (1998). Central Slave basement complex, Northwest Territories: it's autochthonous cover, decollement, and structural topology. In Current Research 1998-C; Geological Survey of Canada, p 9-19.

Cumming, G.L., and Richards, J.R. (1975). Ore lead ratios in continually changing earth. Earth and Planetary Science Letters, v. 28, p 155-171.

Davis, D.W. (1982). Optimum linear regression and error estimation applied to U-Pb data. Canadian Journal of Earth Sciences, v. 19, p 2141-2149.

Davis, W.J., and Hegner, E. (1992). Neodymium isotopic evidence for the tectonic assembly of Late Archean crust in the Slave Province, Northwest Canada. Contributions to Mineralogy and Petrology, 111, p 493-504.

Fyson, W.K. (1997). Chronological charts and Archean Stratigraphy of the Slave Province. Northwest Territories Geology Division EGS paper 1997-13, p 18.

Fyson, W.K., and Helmstaedt, H. (1988). Structural patterns and tectonic evolution of supracrustal domains in the Archean Slave Province, Canada. Canadian Journal of Earth Sciences v. 25, p 301-315.

Fraser, J.A. (1964). Geological notes on the northeastern District of Mackenzie, Northwest Territories; Geological Survey of Canada, Paper 63-40 (Map 45-1963, Scale 1:506 800) 20 p.

Gebert, J.S. 1990. Geology of the Hope Bay and Elu Inlet metavolcanic belts, Bathurst Block, northwestern Slave Province, N.W.T. Abstracts in Exploration Overview 1990, N.W.T., 26 p.

Gebert, J.S., 1993. Geology and mineral potential of the Archean Hope Bay and Elu Inlet volcanic belts, Northeastern Slave Structural Province, District of Mackenzie, NWT. Northern affairs program Northwest Territories Geology Division EGS paper 1993-1, 103 p

Gibbons, W.A., (1987). Preliminary geology of the central Hope Bay volcanic Belt, northern portions of NTS 77 A/3,6 (map with marginal notes, 1:50 000 scale) DIAND, EGS 1987-12.

Helmstaedt, H. and Padgham, W.A. (1986). A new look at the stratigraphy of the Yellowknife Supergroup at Yellowknife, NWT- Implications for the age of gold-bearing shear zones and Archean basin evolution. Canadian Journal of Earth Sciences v. 25, p 454-475.

Henderson. J.B. (1970). Stratigraphy of the Yellowknife Supergroup, Yellowknife Bay-Prosperous Lake area, District of Mackenzie, Geological Survey of Canada, Paper 70-26.

Hoffman, P.F. (1989). Precambrian geology and tectonic history of North America. In A.W. Bally and Palmer, A.R. (eds), The Geology of North America-An Overview. Geological Society of America, Boulder, Colorado, p 447-512.

Isachsen, C.E., Bowring, S.A., and Padgham, W.A. (1991). U-Pb zircon geochronology of the Yellowknife Volcanic Belt, NWT, Canada: new constraints on the timing and duration of greenstone belts magmatism. Journal of Geology v. 99, p 55-67.

Isachsen, C.E., and Bowring, S.A. 1994. Evolution of the Slave: Geology, v.22, p 917-920.

King, J.E., and Helmstaedt, H. (1997). The Slave Province, North-West Territories, Canada. In M.J. De Wit, and L.D. Ashwal. (eds), Greenstone Belts. Oxford Monographs on Geology and Geophysics; no. 35. p 459-479.

Kerrich, R. and Wyman, D.A. (1997). Review of developments in trace-element fingerprinting of geodynamic settings and their implications for mineral exploration. Australian Journal of Earth Sciences, v. 44, p 465-487.

Krogh, T.E. (1982). Improved accuracy of U-Pb zircon ages by creation of more concordant systems using an air abrasion technique. Geochimica et Cosmochimica Acta, v. 46, p 637-649.

Lesher, C.M., Goodwin, A.M., Campbell, I.H., and Gorton M.P. (1986). Trace element geochemistry of ore-associated and barren, felsic metavolcanic rocks in the Superior Province, Canada. Can. J. Earth Sci. v. 23, p 222-237.

Ludwig, K.R. (1980). Calculations of uncertainties of U-Pb isotope data. Earth and Planetary Science Letters, v. 46, p 212-220.

Lindsey, D. (1998) Geochemical and Petrographic Study of the Mafic-Ultramafic Suite in the Hope Bay Volcanic Belt, Slave Structural Province, NWT. B.Sc. thesis, University of British Columbia 55 p.

Mortensen, J.K., Thorpe, R.I., Padgham, W.A., King, J.E., and Davis, W.J. (1988). U-Pb zircon ages for felsic volcanism in the Slave, N.W.T. Radiogenic Ages and Isotopic Studies: Report 2, Geological Survey of Canada, Paper 88-2 p 85-95.

Mortensen, J.K., Ghosh, D.K., and Ferri, F. (1995). U-Pb geochronology of intrusive rocks associated with copper-gold porphyry deposits in the Canadian cordillera. In Porphyry deposits in the Northwestern Cordillera of North America. Edited by T.G. Schroter, G-2, p 491-531.

Padgham, W.A. (1985). Observations and speculations on supracrustal successions in the Slave Structural Province. In L.D. Ayres, P.C Thurston, K.D. Card, and W. Weber (eds), Evolution of Archaean Sequences. Geological Association of Canada. Special Paper 28, p 133-151.

Padgham, W.A. (1991). The Slave Province, an overview; Geological Survey of Canada, Open File 2168, p 1-40.

Padgham, W.A., and Fyson, W.K. (1992). The Slave Province: a distinct Archean craton. Canadian Journal of Earth Sciences, v.29, p 2072-2086.

Padgham, W.A. (1996). Slave conglomerate dating. Northern affairs program Northwest Territories Geology Division EGS paper 1996-12, 85 p.

Roddick, J.C. (1987). Generalised numerical error analysis with applications to geochronology and thermodynamics. Geochemica et Cosmochimica Acta, v.51, p 2129-2135.

Steiger, R.H., and Jäger, E. (1977). Subcommission on geochronology: convention on the use of decay constants in geo- and cosmochronology. Earth and Planetary Science letters, v.36, p 359-362.

Sylvester, P.J., Harper, G.D., Byverly, G.R., and Thurston, P.C. (1997). Volcanic aspects. In M.J. De Wit, and L.D. Ashwal. (eds), Greenstone Belts. Oxford Monographs on Geology and Geophysics; no. 35. p 55-90.

Thorpe, R.I., Cumming, G.I., and Mortensen, J.K. (1992). A significant Pb isotope boundary in the Slave Province and its probable relation to ancient basement in the western Slave Province. In Project summaries: Canada-Northwest Territories Mineral Development Subsidiary Agreement Geological Survey of Canada, Open File 2484, p 179-164.

Thurston, P.C. (1981). Economic evaluation of Archean felsic volcanic rocks using REE geochemistry. In Archean geology (ed J.E Glover and D.I. Groves), Special publication No.7, Geological Society of Australia, p 439-450.

van Breemen, O., Davis, W.J., and King, J.E. (1992). Temporal distribution of granitoid plutonic rocks in the Slave Province, Northwest Canadian Shield, Canadian Journal of Earth Sciences v.29, p 2186-2199.

Villeneuve, M.E., Henderson, J.R., Hrabi, R.B., Jackson, V.A., and Relf, C., (1997). 2.70-2.58 Ga plutonism and volcanism in the Slave Province, District of Mackenzie, Northwest Territories: in Radiogenic Age and Isotopic Studies: Report 10; Geological Survey of Canada, Current Research 1997-F, p 37-60.

Yamashita, K., Jensen, J.E., Creaser, R.A., and Gebert, J.S. (1995). Geology, geochemistry, and Nd isotopic study of the Hanikahimajuk Lake area (NTS 86 I/2, 86 H/14,15), northern Point lake belt, Slave Stuctural Province, NWT; Geological Association of Canada, Program with Abstracts, v.20, p A-112.

York, D. (1969). Least squares fitting of a straight line with correlated errors; Earth and Planetary Science Letters, v. 5, p 320-324.

Chapter 3

Regional lithogeochemistry of Archean volcanic successions in the Hope Bay Greenstone Belt, Slave Structural Province, N.W.T., Canada

Introduction

The Hope Bay greenstone belt (HBGB) is one of several Late Archean greenstone belts recognised within the Slave Structural Province (SSP) (Figure 3.1). Unlike most other major greenstone belts in the SSP relatively little is known about the age and evolution of the HBGB. The preponderance of data from these granite-turbidite-volcanic sequences come from studies focussing on belts from the western and central portion of the SSP. However, in light of recent research, the nature and character of the HBGB is rapidly developing. Geological mapping (Gebert, 1993) and high precision U-Pb geochronology (Chapter 2) provided key constraints and allowed supracrustal sequences to be placed into a preliminary stratigraphic sequence.

This paper examines the lithogeochemical evolution of the HBGB in the context of the chronostratigraphy established in Chapter 2. Major, trace, and rare earth element data are employed to characterise the geochemistry of various igneous units and explore the possible paleotectonic settings in which individual units were generated.

Regional Geology of the SSP

The Slave Structural Province (SSP) in the northwestern Canadian Shield (Figure 3.1) has a long and complex history, and contains rocks that record approximately half the history of

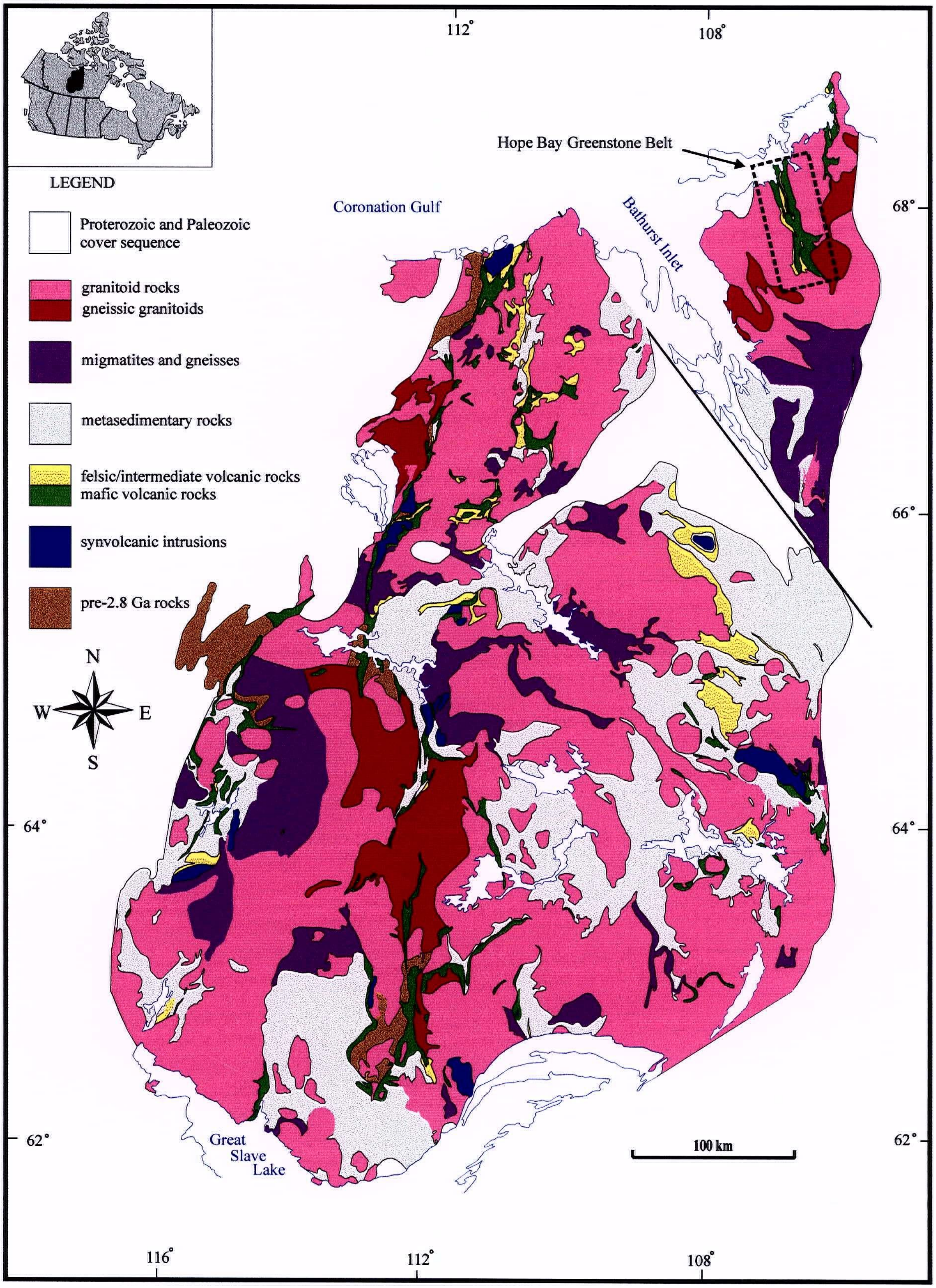

Figure 3.1. Generalized geology of the Slave Structural Province (modified from Fyson 1997-13).

the Earth (King and Helmstaedt, 1997). Henderson (1970) originally assigned all supracrustal rocks of the SSP to the Yellowknife Supergroup (YkSG). Recent geochronology studies have shown the YkSG can be further sub-divided (i.e., pre and post-YkSG), although the stratigraphy has not yet been formally revised (King and Helmstaedt, 1997).

The oldest rocks in the SSP (4.0-2.8 Ga) are gneisses, granitoids and minor supracrustal rocks (pre-YkSG) that are recognised thus far only in the western half of the province (Padgham, 1985, 1991). These rocks are thought to represent an older cratonic basement which is referred to as the Acasta terrane after the 4.02 Ga Acasta gneiss (Bowering et al., 1990; Stern and Bleeker, 1997). Younger granitoid intrusions in the western SSP have Sm-Nd-Pb isotopic signatures that indicate they were contaminated by this older terrane (Thorpe et al., 1992; Davis and Hegner 1992; Yamashita et al., 1995). In contrast, younger granitoids of the eastern SSP have isotopic signatures that indicate they have not interacted with older basement rocks. This observation is generally interpreted to indicate that older basement rocks are absent from the eastern SSP.

With minor exceptions, the bulk of the volcanic rocks of the SSP were deposited in a 60 m.y. period between 2715 and 2655 Ma (YkSG) (Isachsen and Bowering, 1994; Mortensen et al., 1992). Greenstone belts have been subdivided into mafic-dominated Yellowknife-type belts, and intermediate to felsic dominated Hackett River-type belts (Padgham, 1985, 1991). Some belts also contain minor synvolcanic conglomerate and carbonate units (e.g., Lambert et al., 1990). Voluminous turbidites were deposited throughout the SSP at the end of volcanism. In many greenstone belts turbidite deposition began during the waning stages of volcanism, and felsic volcanic rocks interfinger with the turbidites. Geochemical studies of the turbidites suggest they were derived from both felsic volcanic rocks and continental crust of granodioritic composition (McLennan and Taylor, 1984). This indicates that early synvolcanic intrusions and pre-existing basement rocks were uplifted and eroded to provide detritus.

After cessation of volcanism and deposition of the turbidites, the craton experienced a period of apparent magmatic quiescence (2640 to 2625 Ma) (van Breemen et al., 1992). Magmatic activity resumed at approximately 2625 Ma and continued until the peak of regional metamorphism and deformation at ca. 2590 Ma. A series of young conglomerates ("Jackson Lake-type") containing abundant granitoid clasts was deposited after ca. 2600 Ma. These young conglomerates record late uplift along reactivated faults and are similar to the Timiskaming Group of the Superior Province.

Geology of the Hope Bay Greenstone belt

The Late Archean HBGB (Figure 3.1) lies entirely within the fault-bounded Bathurst Block that forms the northeast portion of the SSP. The HBGB comprises a north-trending supracrustal package approximately 90 kilometres long and 15 to 20 kilometres wide. Fraser (1964) first mapped the belt in a 1:506,880 project known as *Operation Bathurst*. Gibbins (1987) mapped the northern portion of the HBGB (NTS 77 A/3, 6) and a team led by Gebert (1993) mapped the remainder of the belt (NTS 76 0/8, 10, 15, 16 and 77 A/2, 3, 6, 7, 10). Reconnaissance U-Pb geochronology studies by Bevier and Gebert (1991) constrained the timing of felsic volcanism between 2685-2677 Ma and plutonism from 2672-2608 Ma.

The entire HBGB has been remapped from 1996-1997 by the geological staff of BHP Minerals Canada Ltd. (primarily J. S. Gebert and M.U. Hebel) (Figure 3.2). The revised geological interpretation of supracrustal sequences within the HBGB based on this mapping form the stratigraphic and structural framework for the present study. Informal formation and group names, assigned by the author, have been assigned to supracrustal rock in the HBGB (Chapter 2) to facilitate clarity and continuity for the reader.

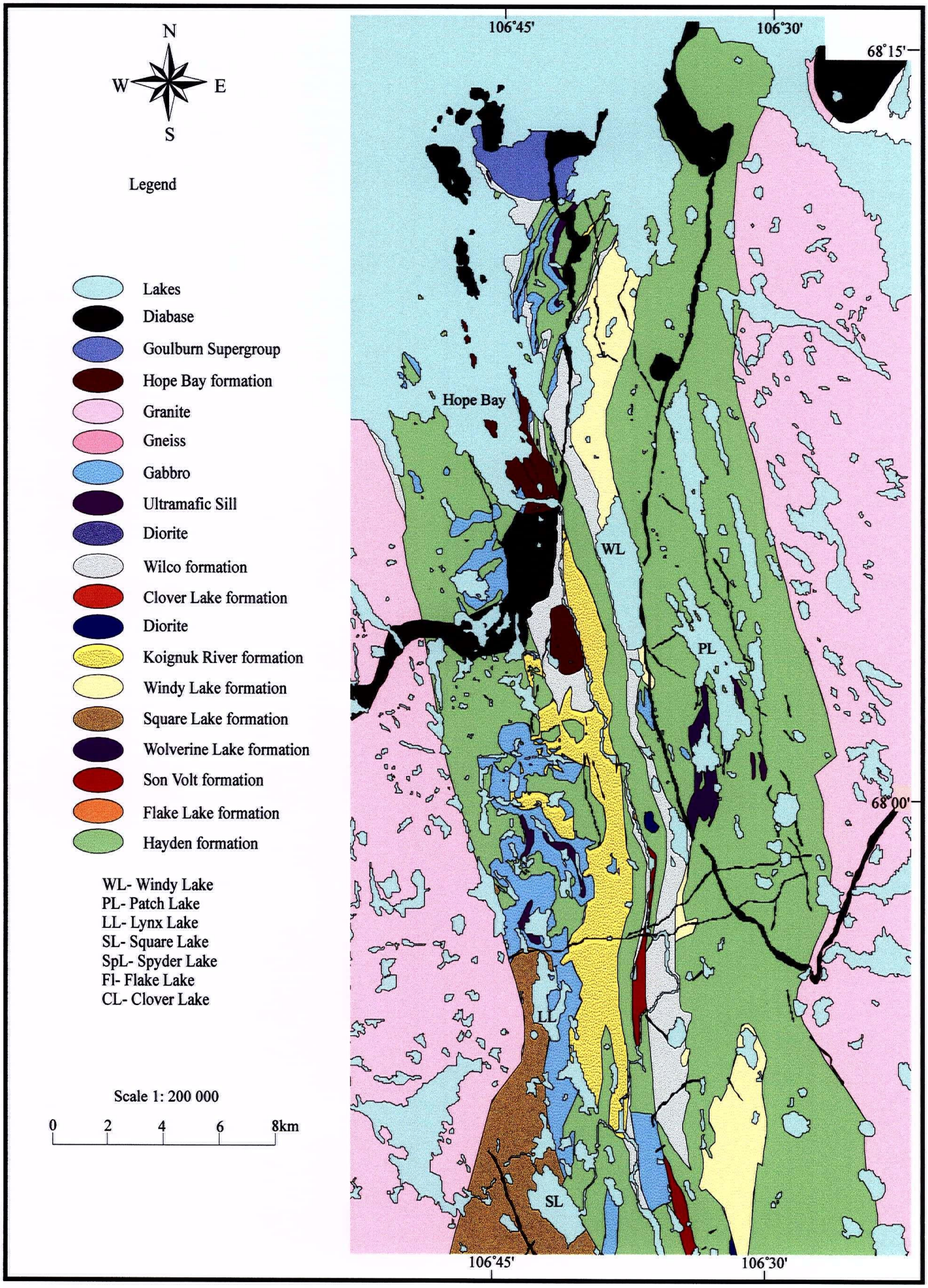

Figure 3.2a. Generalised geology for the northern portion of the HBGB.

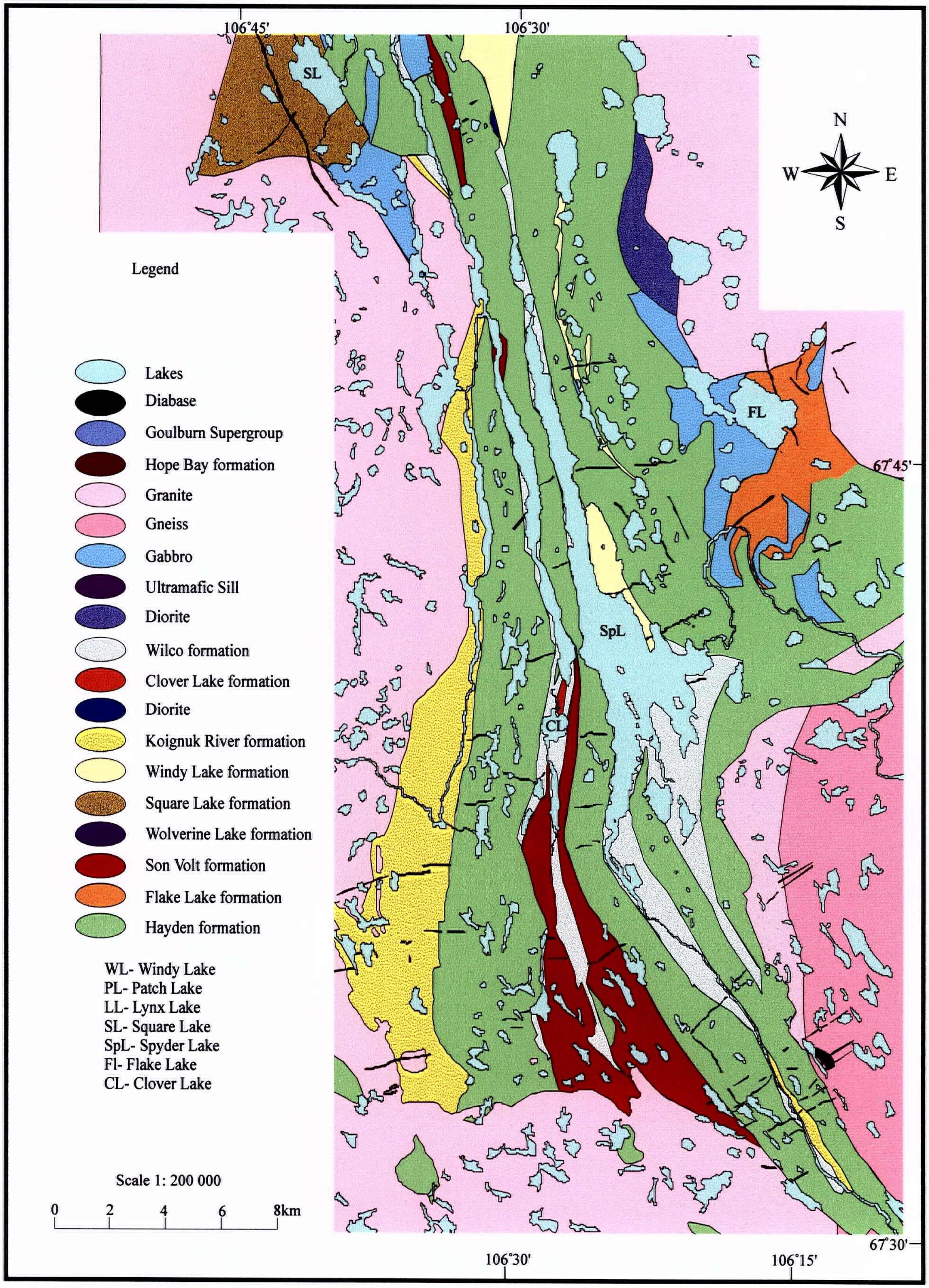

Figure 3.2b. Generalised geology for the southern portion of the HBGB.

The stratigraphy of the HBGB (Figure 3.3) is composed of the basal mafic dominated Young group, comprised of the Hayden and Flake Lake formations, respectively. Felsic volcanic and hypabyssal rocks of the Westerberg group overlie the Young group, which is in turn overlain by sedimentary rocks of the Wilco and Tweedy groups, respectively.

Deposition of supracrustal sequences (Figure 3.2 and 3.3) within the HBGB appears to have occurred over a period in excess of 100 m.y. (>2716 - <2600 Ma) (Chapter 2). Volcanism spanned an interval of at least 53 million years, beginning with the deposition of the mafic Hayden formation, the bulk of which was likely deposited prior to ca. 2716 Ma. Mafic volcanic rocks are commonly pillowed and are interlayered with massive flows and associated gabbroic sills. Variolitic textures are common in pillowed flows of the northern portion of the belt. Most mafic rocks are typical Archean tholeiitic basalts although magnesium-rich basaltic komatiites have recently been recognised (Lindsey, 1998). The Hayden formation is cut by ultramafic intrusions that form sills up to 200 metres in thickness. The 2716 Ma Flake Lake formation, dominantly consisting of rhyolitic volcanic flows occurs near the top of the Hayden mafic pile.

Unlike many Archean greenstone belts, the HBGB also contains a significant component of intermediate rocks. Intermediate units, collectively assigned to the Son Volt formation, were erupted primarily as fragmental rocks (tuff and lapilli tuff) although rare flows occur locally.

Felsic volcanism (Flake Lake, Wolverine Lake, Square Lake, Windy Lake, Koignuk River, and Clover Lake formations; Figure 3.2 and 3.3), separated by several volcanic hiatuses, occurred from 2716 Ma to 2663 Ma. Ash and lapilli tuffs of dacitic and rhyolitic composition make up the majority of the felsic volcanic rocks. Many felsic rocks exhibit volcaniclastic textures suggesting they have been reworked by sedimentary processes.

Sedimentation of turbidites (Wilco formation) followed volcanic activity at ca. 2663 Ma and was followed by a protracted depositional hiatus of ca. 60 m.y., culminating with the deposition of the fluvial sediments (Hope Bay formation) at ca. 2600 Ma. Sedimentary rocks

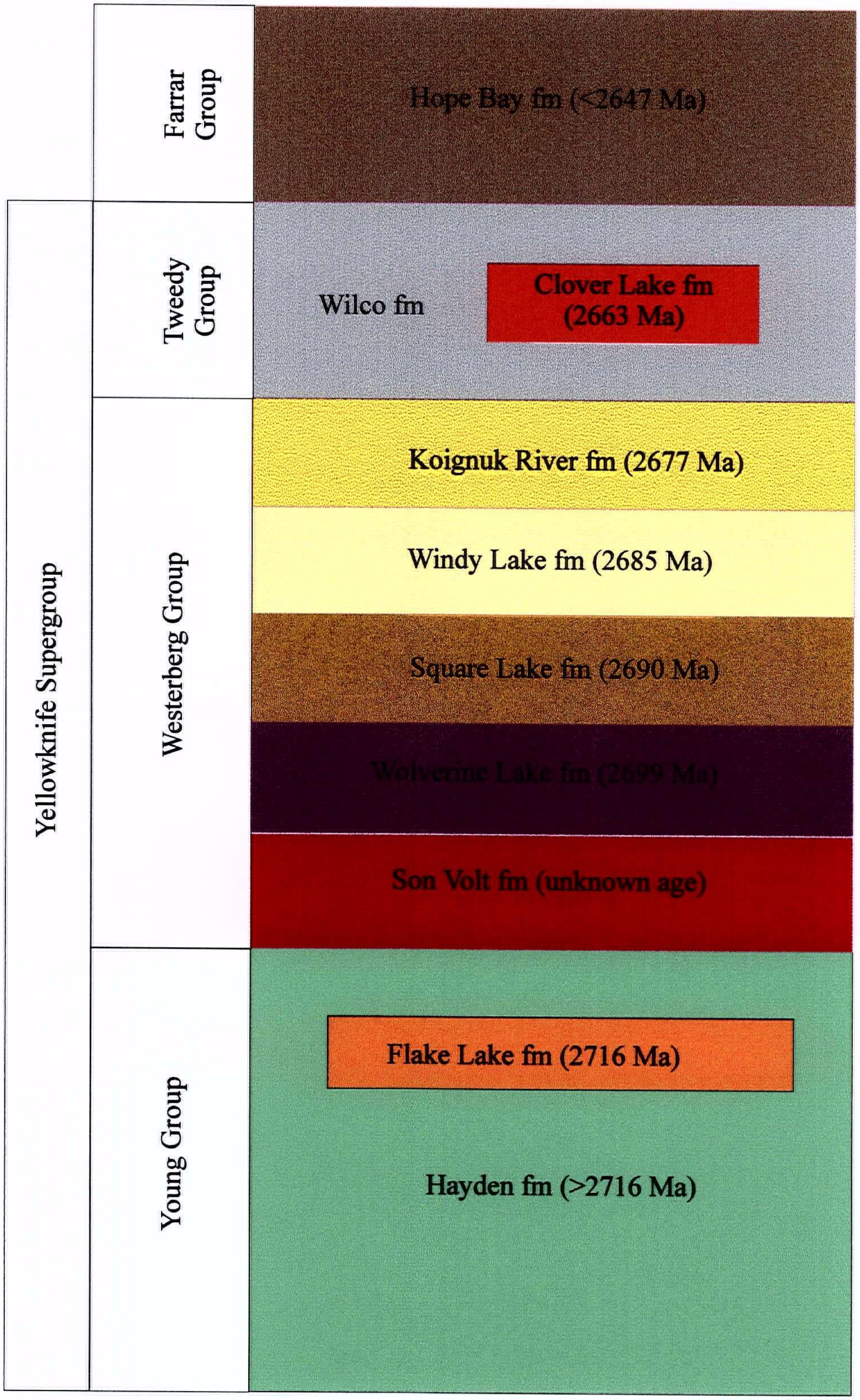

Figure 3.3. Generalized stratigraphic column for the HBGB.

are poorly exposed and underlie many of the valleys within the belt. The upper stratigraphy of the HBGB includes a series of conglomeratic units, some of which are suspected to record late uplift and erosion of the belt along fault scarps. Geochronological constraints locally demonstrate older over younger relationships and indicate supracrustal successions in the HBGB are complicated by thrust faults (Chapter 2).

The HBGB is bordered on the east by plutonic rocks, which include granodiorite, tonalite and gabbro. A granodiorite to the northeast of the HBGB has given a U-Pb zircon age of 2672 +4/-1 Ma (Bevier and Gebert, 1991), indicating these rocks are part of an early, synvolcanic intrusive suite (van Breemen et al., 1992), possibly analogous to tonalite-trondjhemite-granodiorite (TTG) suite in the Superior Province. The southeastern contact of the belt is bordered by a heterogeneous gneiss terrane that includes both migmatised turbidites and numerous granitoid intrusions. Zircons from a granitic orthogneiss within this unit yield a U-Pb age of 2649.5 +2.5/-2.5 Ma and a U-Pb titanite age (thought to record the age of metamorphism and deformation of this unit) of 2589.4 +2.2/-2.2 Ma (Chapter 2). As in other areas of the Slave, it therefore appears that the peak of regional metamorphism was approximately 2.6 Ga.

The HBGB is bordered to the west by plutonic rocks of granodioritic to granitic composition. A granite to the northwest of the HBGB yielded a U-Pb zircon age of 2608 +/- 5 Ma (Bevier and Gebert, 1991), suggesting it correlates with the syn-D2 suite of SSP granitoids (van Breemen et al., 1992).

Geochemistry

Introduction

Samples analysed in this study are dominantly of lower greenschist facies assemblages with rare exceptions that experienced upper greenschist grade metamorphism. Areas of high strain and alteration (predominantly carbonate) were avoided if possible when sampling. Although an attempt was made to sample only primary felsic strata (flows and pyroclastic deposits), a small proportion of epiclastic samples was included. However, epiclastic units invariably contained suspected primary volcanic clasts and where possible the clasts from the epiclastic units were selectively sampled. Most felsic flows and pyroclastic rock samples were feldspar- +\- quartz-phyric. Sampling of the mafic lithologies proved far less problematic with sampling of the pillowed flows restricted to the cores of pillows to minimise the effects of spilitisation.

Representative samples collected at surface exposures were in excess of one kilogram for fine-grained rocks and two kilograms for coarse grained or porphyritic rocks. All weathered surfaces were removed prior to processing. One hundred and seventy-eight samples from the HBGB were analysed by X-ray fluorescence (XRF) for ten major and six trace elements (Table 3.1) at Chemex Labs Ltd. in Vancouver, British Columbia. Major elements were determined on fusion discs and trace elements on pressed powder pellets. Nineteen samples from the data set were further analysed for rare earth elements (REE) (Table 3.2) using inductively coupled plasma emission mass spectrometry (ICP-MS) at Activation Laboratories Ltd. in Ancaster, Ontario. Quality control consisted of blind duplicates and in-house standards and documented excellent reproducibility for analyses of major and trace elements when analytical levels were well above the detection limits (Appendix 1). However, the reproducibility of Nb near detection limits (mainly with the XRF data) in two cases was poor, therefore limiting its usefulness for low Nb concentration samples. Concentrations of elements reported in Table 3.1 and 3.2 are on a volatile-free basis.

Table 3.1. Major and trace element data for rocks of the HBGB.

Sample	Rock Type	Litho unit	SiO_2	Al_2O_3	CaO	Fe_2O_3	K_2O	MgO	MnO	Na_2O	P_2O_5	TiO_2	LOI	TOTAL	Zr	Y	Nb	Ba	Sr	Rb
96PQMW027	D	K.R.	66.73	15.38	5.24	4.55	3.93	1.78	0.09	1.63	0.12	0.55	6.15	98.63	152	17	9	622	106	89
96PCMW107	D	K.R.	69.49	14.64	0.76	3.93	3.40	2.63	0.14	4.49	0.10	0.43	1.46	99.43	119	9	6	930	126	70
96PCMW108	D	K.R.	68.61	15.47	3.18	4.93	0.97	2.17	0.07	3.88	0.13	0.44	1.62	99.31	119	10	7	198	190	21
96PCJW009	R	K.R.	74.86	12.92	1.43	3.70	1.89	1.43	0.07	3.24	0.11	0.35	1.51	100.95	133	12	8	412	125	36
96PCJW007	R	K.R.	70.81	15.52	1.97	3.37	1.83	1.14	0.07	4.74	0.11	0.43	1.27	98.35	145	10	8	412	179	33
97PBMW105	R	K.R.	70.02	15.80	3.55	3.20	1.50	0.68	0.07	4.61	0.11	0.45	1.21	98.94	129	6	4	353	301	29
97PBMW205	R	K.R.	70.01	15.59	3.63	3.15	1.15	1.05	0.06	4.81	0.13	0.43	0.93	99.38	131	6	4	315	366	22
96PCJW006	R	K.R.	69.96	14.65	1.80	4.96	1.64	2.45	0.11	3.88	0.10	0.45	2.30	99.59	145	16	10	452	148	33
96PCJW005	R	K.R.	69.94	14.87	1.76	4.90	1.71	2.45	0.11	3.71	0.10	0.45	2.34	100.18	147	14	8	485	145	33
96PGJW006	R	K.R.	69.79	14.88	3.94	3.84	0.19	1.04	0.06	5.62	0.12	0.51	1.07	100.29	169	12	10	50	139	6
96PCJW008	R	K.R.	69.72	16.48	1.42	2.97	0.54	1.07	0.06	7.08	0.13	0.52	0.90	100.14	193	14	12	166	121	12
96PGJW010	D	K.R.	69.38	15.32	1.85	4.90	1.51	3.39	0.06	3.01	0.12	0.47	4.70	99.44	142	15	11	211	114	32
96PCMW004	D	K.R.	68.88	15.62	1.97	4.96	1.33	2.07	0.04	4.54	0.14	0.45	2.30	100.30	165	10	10	230	159	20
96PGMW007	D	K.R.	68.72	15.35	0.31	4.50	1.96	4.27	0.06	4.23	0.11	0.49	2.65	99.55	149	10	10	284	70	43
96PCMW002	D	K.R.	68.65	15.42	1.61	4.85	1.19	2.97	0.08	4.60	0.10	0.51	1.99	97.41	157	13	10	377	134	21
96PQMW036	D	K.R.	68.34	12.85	4.40	8.43	1.08	2.18	0.09	2.07	0.11	0.45	5.51	98.82	141	15	9	129	101	30
96PGJW014	D	K.R.	68.15	15.41	2.94	3.83	1.53	2.38	0.09	4.99	0.17	0.51	3.10	99.55	168	15	10	244	124	33
96PGMW003	D	K.R.	68.03	15.73	3.78	3.86	0.44	1.79	0.07	5.68	0.13	0.49	1.87	100.09	186	16	10	127	236	8
96PQMW038	D	K.R.	68.01	15.54	4.39	4.80	2.83	2.31	0.08	1.36	0.13	0.55	6.59	99.72	155	17	9	381	127	62
96PDMW005	D	K.R.	67.77	15.25	4.00	5.15	1.66	2.20	0.11	3.17	0.14	0.53	1.69	99.34	151	14	8	287	258	107
96PQMW054	D	K.R.	67.67	15.41	1.56	5.08	2.31	3.59	0.10	3.63	0.11	0.55	3.91	98.18	162	17	11	260	121	51
96PCMW001	D	K.R.	67.53	15.49	1.36	4.68	4.03	2.54	0.17	3.59	0.11	0.50	2.54	100.29	150	16	10	1033	129	63
96PCJW004	D	K.R.	67.43	14.13	2.32	6.96	2.08	2.38	0.20	3.84	0.13	0.53	1.37	99.61	147	14	8	641	163	47
96PGJW007	D	K.R.	67.35	15.15	5.23	4.92	0.63	1.49	0.10	4.51	0.13	0.48	1.88	99.84	165	16	10	133	265	16
96PQMW039	D	K.R.	67.33	16.04	3.81	4.55	2.26	1.56	0.06	3.69	0.13	0.57	5.37	99.17	182	17	9	229	100	68
96PAMW004	D	K.R.	67.26	15.50	3.83	4.98	1.01	2.04	0.08	4.64	0.12	0.54	4.32	99.10	149	13	8	232	245	32
96PDMW004	D	K.R.	66.98	16.43	3.56	4.11	1.38	2.68	0.10	4.14	0.11	0.50	1.83	99.50	147	12	8	271	305	92
96PGJW013	D	K.R.	66.82	14.98	1.48	5.51	1.35	3.79	0.08	5.22	0.14	0.61	2.94	100.05	151	16	12	325	117	16
96PGJW017	D	K.R.	65.44	18.59	4.54	3.16	2.16	1.72	0.08	3.64	0.14	0.52	3.04	99.95	142	14	8	273	256	47

Table 3.1. (continued) Major and trace element data for rocks of the HBGB.

Sample	Rock Type	Litho unit	SiO_2	Al_2O_3	CaO	Fe_2O_3	K_2O	MgO	MnO	Na_2O	P_2O_5	TiO_2	LOI	TOTAL	Zr	Y	Nb	Ba	Sr	Rb
96PAMW012	D	K.R.	65.44	17.06	3.73	4.84	1.50	1.83	0.09	4.75	0.17	0.60	3.35	98.62	145	10	8	346	302	48
96PCJW002	D	K.R.	65.35	15.49	1.28	6.30	3.96	3.01	0.18	3.69	0.15	0.59	1.89	99.98	156	16	8	703	92	69
96PCJW003	D	K.R.	65.35	15.24	1.36	6.48	4.01	3.02	0.18	3.62	0.14	0.59	1.70	99.32	163	18	8	717	92	66
96PTRW024	D	K.R.	64.68	17.26	6.74	3.97	2.11	1.45	0.13	2.91	0.18	0.57	3.18	98.94	154	10	10	308	198	42
96PQMW018	D	K.R.	64.68	16.00	4.92	6.91	1.52	2.27	0.10	2.88	0.13	0.59	4.29	99.78	151	17	8	215	209	40
96PCJW012	D	K.R.	63.61	20.57	3.61	3.19	2.02	1.11	0.08	4.92	0.20	0.69	1.31	100.81	211	18	14	462	265	26
96PAJW001	R	Win L.	74.88	15.45	1.33	0.71	4.06	0.86	0.04	2.06	0.15	0.46	3.35	99.06	169	15	10	413	102	107
96PTMW123	D	Win L.	68.26	15.94	3.03	4.13	1.62	1.75	0.04	4.36	0.30	0.57	3.88	98.74	134	11	12	429	339	36
96PNJW010	D	Win L.	66.14	17.62	2.23	5.85	2.52	0.85	0.08	3.69	0.27	0.74	3.59	98.94	179	23	10	488	266	61
97PBMW104	D	Win L.	70.24	15.05	3.10	3.23	3.14	1.68	0.06	3.00	0.16	0.35	6.01	98.84	128	9	11	670	650	71
96PAJW003	R	Win L.	77.36	12.94	1.19	0.69	1.96	0.79	0.06	4.87	0.04	0.09	2.53	99.26	81	12	17	346	101	37
96PAJW013	R	Win L.	77.21	13.64	0.15	0.27	4.82	0.07	0.01	3.74	0.03	0.05	0.62	99.18	49	10	20	588	20	114
96PAJW011	R	Win L.	77.01	13.59	0.81	0.86	2.46	0.38	0.04	4.70	0.04	0.10	2.46	99.12	84	12	14	440	116	81
96PAJW012	R	Win L.	76.92	13.60	0.81	0.89	2.45	0.35	0.04	4.78	0.04	0.12	1.84	99.55	89	18	16	614	96	51
96PAJW007	R	Win L.	76.28	13.28	1.54	1.55	2.61	0.65	0.05	3.84	0.04	0.16	3.00	99.24	134	17	15	374	104	56
96PQMW006	R	Win L.	76.05	13.35	1.02	2.19	0.71	0.43	0.04	5.96	0.06	0.18	1.02	98.61	169	10	12	118	207	16
96PAJW010	R	Win L.	76.05	14.79	0.33	0.79	5.05	0.49	0.03	2.35	0.04	0.07	2.43	99.42	56	14	19	531	31	140
96PAJW006	R	Win L.	73.82	14.18	1.73	1.90	3.22	0.62	0.06	4.18	0.06	0.23	3.62	98.64	202	17	13	489	141	63
97PQMW109	D	S.L.	68.23	16.30	1.48	0.36	3.08	3.47	0.09	2.92	0.24	0.58	2.67	99.52	148	8	6	515	188	74
96PQIW003	R	S.L.	71.81	14.82	3.11	3.57	2.45	1.23	0.07	2.17	0.23	0.54	1.56	99.17	154	16	12	1204	471	41
96PQIW004	R	S.L.	71.17	16.04	2.24	3.53	3.54	1.29	0.11	1.21	0.25	0.61	2.67	99.04	171	17	12	400	164	68
96PGJW081	R	S.L.	71.09	15.17	4.07	3.83	1.89	1.61	0.07	1.62	0.18	0.48	2.35	98.76	162	15	15	353	247	41
96PQIW014	D	S.L.	70.36	15.18	1.99	4.22	2.21	1.21	0.03	4.21	0.13	0.47	2.94	96.56	170	13	11	310	186	51
96PGJW064	D	S.L.	68.58	15.20	2.63	4.70	1.03	2.10	0.07	5.09	0.13	0.46	1.27	98.35	173	14	10	263	352	35
96PGJW074	D	S.L.	68.40	15.32	5.45	4.71	2.02	1.81	0.15	1.42	0.19	0.53	2.67	98.62	147	15	10	750	384	52
96PQIW002	D	S.L.	67.73	15.13	6.00	5.43	0.96	1.24	0.11	2.59	0.22	0.58	1.81	99.60	156	16	8	220	896	33
96PQIW016	D	S.L.	67.41	17.23	5.04	3.25	2.05	0.56	0.07	3.30	0.33	0.75	3.08	99.25	240	33	15	291	277	58
96PGJW076	D	S.L.	67.07	18.25	2.24	3.33	2.43	0.82	0.04	4.65	0.41	0.76	1.99	98.87	186	19	10	702	636	60
96PQIW009	D	S.L.	66.96	14.18	5.79	5.68	1.07	2.45	0.09	2.83	0.36	0.60	3.56	99.12	151	15	8	235	479	31

Table 3.1. (continued) Major and trace element data for rocks of the HBGB.

Sample	Rock Type	Litho unit	SiO_2	Al_2O_3	CaO	Fe_2O_3	K_2O	MgO	MnO	Na_2O	P_2O_5	TiO_2	LOI	TOTAL	Zr	Y	Nb	Ba	Sr	Rb
96PQMW113	D	S.L.	64.75	15.32	5.80	5.75	1.71	2.33	0.16	3.14	0.39	0.64	1.72	99.11	158	13	8	467	337	38
96PGJW069	D	S.L.	64.28	16.71	5.42	5.09	1.86	1.98	0.16	3.39	0.41	0.69	1.42	98.56	168	19	8	481	323	46
96PTMW119	D	Wolv L.	69.60	16.18	2.75	2.73	0.91	1.09	0.03	6.27	0.10	0.39	1.63	99.38	111	5	3	228	303	35
96PGJW093	R	F.L.	78.31	10.89	2.45	3.80	1.84	0.69	0.07	1.71	0.02	0.22	1.07	99.46	497	127	28	330	43	37
97PPQW001	R	F.L.	77.79	11.36	1.17	4.46	2.13	1.25	0.07	1.56	0.03	0.18	2.11	99.15	309	60	10	407	62	31
96PGEW008	R	F.L.	77.70	11.41	0.80	3.33	0.98	0.39	0.04	5.14	0.02	0.19	1.15	99.20	346	61	14	296	43	16
97PPTW002	R	F.L.	76.94	12.61	0.66	3.00	2.20	1.76	0.04	2.51	0.04	0.23	1.78	99.87	447	90	31	535	65	33
96PGJW062	R	F.L.	76.64	11.18	1.75	5.23	2.43	1.71	0.17	0.64	0.02	0.24	2.06	98.90	530	155	27	408	23	37
96NPW102	R	F.L.	76.19	11.65	1.19	4.94	1.11	1.27	0.12	3.23	0.03	0.27	1.64	99.59	554	153	29	174	49	16
96NPW101	R	F.L.	76.13	11.34	1.44	4.61	1.85	1.16	0.07	3.12	0.03	0.24	1.09	99.06	545	158	29	618	84	33
96NPW104	R	F.L.	75.76	11.30	2.33	5.34	1.87	2.40	0.07	0.58	0.05	0.30	2.31	98.96	559	145	27	238	50	52
96PGJW089	R	F.L.	75.74	11.71	1.34	5.99	2.33	1.89	0.15	0.47	0.05	0.32	2.18	99.46	558	149	25	606	14	41
97PGMW201	R	F.L.	75.65	11.72	2.08	5.14	1.85	2.18	0.06	0.97	0.04	0.25	2.09	99.60	443	134	27	155	37	47
96PGJW061	R	F.L.	75.56	11.46	2.07	5.42	1.36	2.10	0.07	1.61	0.04	0.31	2.57	98.33	561	162	27	172	46	40
96NPW103	R	F.L.	75.06	11.11	1.94	6.26	1.16	0.87	0.07	3.19	0.04	0.31	1.05	99.23	553	138	26	479	102	33
97PGMW101	R	F.L.	74.98	11.69	2.93	5.39	1.53	2.15	0.07	0.87	0.04	0.25	2.27	98.46	427	125	29	140	42	40
96PGJW091	R	F.L.	74.74	11.18	2.72	5.75	0.95	0.56	0.14	3.61	0.04	0.30	1.09	99.12	548	153	27	408	102	20
97PBMW102	R	C.L.	76.45	13.52	0.63	0.96	3.23	0.43	0.03	4.59	0.07	0.08	1.46	98.34	43	3	2	557	111	85
97PBMW103	R	C.L.	73.37	15.15	0.63	0.54	6.09	0.30	0.03	3.65	0.13	0.10	0.54	99.84	57	4	2	987	42	101
97PFMW004	D	S.V.	62.80	16.19	8.15	5.84	0.70	3.24	0.10	2.20	0.20	0.67	2.79	99.49	118	14	6	274	350	21
96PGMW036	A	S.V.	63.31	15.13	12.85	2.80	0.40	1.24	0.08	3.36	0.14	0.69	5.83	98.10	104	17	7	130	189	13
96PFMW003	A	S.V.	62.03	14.44	10.06	5.86	0.40	2.18	0.12	3.97	0.19	0.74	6.07	99.20	116	21	9	113	112	13
96PGCW004	A	S.V.	61.91	20.29	3.18	2.72	3.53	1.08	0.05	6.18	0.20	0.84	1.55	99.91	122	12	8	1001	228	49
97PQMW110	A	S.V.	61.57	17.49	6.83	6.06	0.42	3.11	0.07	3.55	0.14	0.75	3.34	99.91	109	17	4	83	199	10
96PQJW001	D	S.L.	66.93	12.93	8.28	5.94	1.35	3.16	0.20	0.53	0.22	0.47	2.76	99.23	124	12	8	332	243	31
96PGJW068	D	S.L.	66.58	17.54	4.10	3.52	1.00	1.27	0.10	4.47	0.42	0.98	1.41	98.23	297	37	14	170	355	23
96PQIW001	D	S.L.	66.23	15.31	5.33	5.87	0.64	1.80	0.11	3.89	0.27	0.55	2.19	99.05	158	17	10	150	824	25
96PGJW079	D	S.L.	65.29	13.88	2.98	9.93	1.11	2.87	0.30	2.83	0.30	0.53	3.10	97.88	158	15	8	375	439	34
96PFMW004	A	S.V.	60.75	16.42	7.78	0.74	0.10	3.94	0.11	2.76	0.13	0.74	3.60	99.32	121	17	2	40	270	8

Table 3.1. (continued) Major and trace element data for rocks of the HBGB.

Sample	Rock Type	Litho unit	SiO_2	Al_2O_3	CaO	Fe_2O_3	K_2O	MgO	MnO	Na_2O	P_2O_5	TiO_2	LOI	TOTAL	Zr	Y	Nb	Ba	Sr	Rb
96PUJW014	A	S.V.	60.56	15.63	6.28	8.84	1.54	3.44	0.14	2.23	0.30	1.02	6.74	98.79	156	24	9	695	302	43
97PAMW113	A	S.V.	60.27	17.39	4.35	0.63	0.17	2.62	0.13	7.86	0.22	0.87	4.16	99.35	143	17	8	70	112	6
97PUMW001	A	S.V.	60.11	15.97	4.61	8.72	0.81	4.08	0.13	4.51	0.17	0.90	4.66	99.52	130	21	6	242	105	21
96PGXW008	A	S.V.	59.94	16.99	4.27	6.15	2.26	4.08	0.13	4.83	0.21	1.14	4.37	99.15	155	17	11	401	213	55
96PGMW043	A	S.V.	59.85	14.61	7.27	10.13	0.24	2.65	0.13	3.78	0.16	1.17	1.69	99.08	157	21	10	56	94	6
96PQMW115	A	S.V.	59.58	16.56	10.42	6.17	0.46	3.65	0.14	2.33	0.14	0.57	2.87	99.03	85	12	4	96	175	16
96PUMW101	Dio	S.V.	59.31	19.66	7.51	5.99	0.66	2.53	0.08	3.57	0.13	0.55	3.68	99.13	85	16	9	167	275	20
96PGMW041	A	S.V.	58.89	16.20	6.07	7.83	1.88	5.38	0.13	2.75	0.09	0.79	7.29	98.72	105	20	7	306	90	48
96PCMW006	A	S.V.	58.47	16.07	10.19	8.05	0.31	3.41	0.15	2.41	0.15	0.80	1.18	99.21	129	20	10	71	137	12
96PFMW001	A	S.V.	58.25	16.05	7.98	9.23	0.31	4.45	0.12	2.65	0.15	0.80	2.53	99.53	121	16	6	134	315	10
96PKMW001	A	S.V.	58.17	16.36	7.54	7.40	0.60	4.89	0.11	4.24	0.11	0.57	2.31	99.35	90	14	6	139	194	14
96PGJW080	A	S.V.	57.38	16.92	6.95	9.53	1.47	3.55	0.16	2.55	0.33	1.17	3.76	98.36	165	21	8	396	412	38
97PTMW108	Dio	S.V.	56.64	20.83	7.20	6.50	0.81	3.13	0.07	4.19	0.06	0.56	4.23	99.14	90	11	2	142	254	15
96PGMW038	A	S.V.	56.37	16.46	7.31	8.89	1.29	5.60	0.13	3.04	0.15	0.78	2.60	99.04	128	19	8	202	147	46
96PQMW001	A	S.V.	56.26	17.60	9.94	7.28	1.00	4.65	0.19	2.30	0.12	0.67	3.98	99.10	98	17	2	163	137	38
97PFMW003	A	S.V.	56.17	17.29	8.59	7.90	0.42	6.36	0.15	2.23	0.14	0.75	4.23	99.79	113	19	2	110	193	10
96PGMW048	A	S.V.	55.94	17.92	9.41	8.26	0.18	3.83	0.15	3.41	0.12	0.78	4.72	99.07	99	17	6	42	318	6
96PGMW032	A	S.V.	55.82	17.46	6.70	10.15	0.72	5.55	0.15	2.38	0.17	0.89	3.62	98.68	142	21	8	373	307	21
97PFMW005	A	S.V.	55.47	15.74	9.13	10.12	0.33	6.02	0.13	2.08	0.13	0.84	0.99	99.45	107	22	2	96	177	8
96PQMW031	A	S.V.	54.86	16.94	8.09	11.98	0.49	6.03	0.22	0.62	0.12	0.66	4.78	99.30	102	15	6	106	294	17
97PFMW001	A	S.V.	54.78	19.29	3.75	9.41	1.01	5.09	0.17	5.30	0.18	1.02	4.45	99.47	148	19	4	163	177	25
97PQMW002	A	S.V.	53.58	17.46	9.88	9.62	0.62	7.27	0.19	0.60	0.10	0.68	4.46	99.70	88	17	2	126	313	17
96PQMW024	B	Hay	56.17	16.09	8.34	9.45	0.18	4.81	0.21	3.67	0.07	1.00	3.34	99.14	66	21	4	57	154	10
97PBKW076	B	Hay	53.86	16.01	12.00	10.56	0.09	4.08	0.22	2.15	0.09	0.95	5.80	99.40	51	21	2	16	122	2
96PAMW011	B	Hay	53.69	16.50	9.68	8.55	1.95	2.85	0.19	4.58	0.25	1.76	7.99	99.87	134	33	11	849	670	37
96PQMW051	B	Hay	53.38	12.61	8.79	16.11	0.33	3.93	0.26	3.17	0.13	1.31	3.72	98.72	85	25	4	89	147	8
96PQMW062	B	Hay	52.77	15.43	8.65	11.60	0.41	7.79	0.23	2.06	0.07	0.99	3.49	99.04	60	21	2	110	115	10
96PAMW003	B	Hay	52.52	14.94	8.95	12.17	0.40	4.10	0.21	3.07	0.49	3.16	4.97	99.40	222	34	15	132	402	13
96PAMW006	B	Hay	52.51	16.40	5.86	14.92	0.35	6.21	0.26	2.45	0.05	0.97	4.87	99.38	48	21	2	74	190	19

Table 3.1. (continued) Major and trace element data for rocks of the HBGB.

Sample	Rock Type	Litho unit	SiO_2	Al_2O_3	CaO	Fe_2O_3	K_2O	MgO	MnO	Na_2O	P_2O_5	TiO_2	LOI	TOTAL	Zr	Y	Nb	Ba	Sr	Rb
96PTMW002	B	Hay	52.41	13.96	11.61	12.09	0.24	6.71	0.18	1.84	0.07	0.89	5.20	99.45	64	17	4	53	123	11
96PQMW033	B	Hay	52.35	14.85	7.19	13.49	0.39	6.74	0.18	3.49	0.07	1.25	8.60	99.50	66	18	2	72	64	9
96PBMW008	B	Hay	52.35	13.06	10.69	11.72	0.16	8.29	0.16	2.67	0.06	0.83	2.06	99.23	56	14	4	46	152	12
96PQMW019	B	Hay	52.26	14.72	14.93	11.47	0.46	3.90	0.24	1.15	0.08	0.78	8.36	99.32	49	18	4	22	66	11
96PBMW012	B	Hay	52.15	13.26	12.00	12.38	0.13	7.40	0.20	1.56	0.08	0.83	2.88	99.22	53	19	2	42	137	8
96PTMW004	B	Hay	52.12	13.08	7.84	16.80	0.10	5.26	0.21	2.59	0.16	1.83	2.44	99.21	118	31	6	26	194	6
96PTMW006	B	Hay	51.80	15.33	12.93	12.42	0.13	5.43	0.21	0.89	0.08	0.79	7.97	99.16	49	18	2	22	77	9
96PBMW011	B	Hay	51.76	14.71	7.97	15.06	0.07	6.88	0.20	2.05	0.09	1.23	7.32	99.04	72	22	2	22	92	11
97PMDW025	B	Hay	51.65	13.60	10.51	12.48	0.27	8.06	0.20	2.32	0.06	0.85	3.95	98.93	55	21	3	61	103	4
96PTMW012	B	Hay	51.60	15.20	11.05	12.79	0.12	6.98	0.20	1.19	0.06	0.81	5.21	99.25	51	15	2	27	130	9
97PBKW074	B	Hay	51.60	17.28	12.98	10.53	0.06	4.88	0.21	1.67	0.05	0.73	6.41	99.85	35	17	2	21	137	2
96PQMW002	B	Hay	51.44	16.89	8.52	11.82	0.37	6.78	0.25	2.76	0.09	1.10	3.54	99.36	66	19	2	68	104	8
97PMDW028	B	Hay	51.34	13.61	11.67	12.70	0.25	7.77	0.18	1.57	0.08	0.83	5.38	99.60	59	21	3	37	81	3
96PBMW010	B	Hay	51.00	15.08	11.62	12.34	0.09	5.83	0.21	2.92	0.07	0.85	7.16	98.85	52	17	2	27	100	9
96PGMW028	B	Hay	50.83	14.54	11.99	12.53	0.32	6.70	0.20	2.02	0.07	0.80	4.30	98.74	48	17	2	111	87	11
96PTMW007	B	Hay	50.73	15.45	5.55	17.41	0.11	8.20	0.30	1.16	0.09	1.01	6.28	99.26	58	17	2	32	71	9
96PTMW013	B	Hay	50.71	13.39	12.68	12.57	0.09	7.72	0.21	1.71	0.07	0.83	3.90	99.03	57	19	2	32	181	8
96PCMW005	B	Hay	50.68	14.92	9.43	14.81	0.20	6.79	0.20	1.82	0.08	1.07	2.88	99.50	65	21	2	52	120	8
96PTMW005	B	Hay	50.65	13.92	10.88	14.76	0.18	6.57	0.22	1.69	0.08	1.05	3.16	99.19	62	19	4	42	123	10
96PGMW046	B	Hay	50.62	13.98	11.17	14.34	0.28	7.24	0.20	1.13	0.07	0.97	3.87	99.71	66	19	4	47	230	10
96PBMW019	B	Hay	50.48	16.45	11.08	12.69	0.11	5.22	0.23	2.61	0.15	0.98	4.15	99.02	63	19	2	47	198	8
96PTMW010	B	Hay	50.48	13.63	11.03	13.15	0.17	7.86	0.22	2.50	0.07	0.89	4.84	99.32	60	17	2	42	66	8
96PGMW030	B	Hay	50.39	14.60	11.39	13.55	0.08	7.35	0.22	1.44	0.08	0.90	3.45	99.45	53	17	2	31	156	8
97PMDW027	B	Hay	50.37	10.29	9.05	12.65	0.14	13.83	0.21	2.71	0.05	0.71	3.20	99.23	42	18	2	72	68	2
96PBMW001	B	Hay	50.34	14.42	9.04	13.68	0.09	8.59	0.19	2.64	0.07	0.94	4.37	99.86	60	19	2	31	126	10
96PQMW065	B	Hay	50.28	13.15	7.22	17.33	0.25	7.23	0.23	2.77	0.15	1.39	3.06	98.47	104	29	6	37	69	8
96PQMW042	B	Hay	50.26	14.33	9.33	14.71	0.34	7.34	0.21	2.34	0.09	1.04	3.19	99.22	72	23	4	36	190	10
96PBMW017	B	Hay	50.20	15.30	9.48	13.60	0.19	8.24	0.18	1.98	0.06	0.77	3.37	99.18	44	15	2	52	102	8
96PFMW006	B	Hay	50.14	12.55	11.33	16.77	0.24	5.42	0.22	1.53	0.22	1.59	2.70	98.72	109	29	2	156	150	8

Table 3.1. (continued) Major and trace element data for rocks of the HBGB.

Sample	Rock Type	Litho unit	SiO_2	Al_2O_3	CaO	Fe_2O_3	K_2O	MgO	MnO	Na_2O	P_2O_5	TiO_2	LOI	TOTAL	Zr	Y	Nb	Ba	Sr	Rb
96PAJW016	B	Hay	50.11	14.62	10.14	14.60	0.29	7.06	0.25	1.85	0.09	0.99	6.83	99.14	55	17	2	54	156	6
96PQMW055	B	Hay	50.11	13.85	11.00	16.46	0.36	3.85	0.26	2.50	0.13	1.49	5.45	98.73	90	26	4	75	116	9
96PFMW013	B	Hay	50.05	13.89	9.73	13.42	0.33	9.52	0.19	1.81	0.10	0.96	3.11	99.17	69	17	4	135	187	10
96PTMW001	B	Hay	49.99	15.61	11.61	13.70	0.19	5.75	0.21	1.80	0.13	1.01	3.86	99.10	57	19	2	47	353	8
96PQMW029	B	Hay	49.94	14.93	9.99	13.96	0.16	7.87	0.20	1.91	0.08	0.96	3.69	99.17	60	21	6	47	130	6
96PTMW014	B	Hay	49.93	14.21	8.17	13.00	0.68	10.40	0.22	1.90	0.13	1.37	3.94	99.37	88	17	8	162	344	21
96PTRW026	B	Hay	49.83	16.43	9.24	14.58	0.34	4.96	0.43	2.72	0.10	1.37	1.50	98.97	77	21	2	169	125	8
96PGMW026	B	Hay	49.77	16.72	10.67	13.06	0.12	7.17	0.23	1.25	0.08	0.92	4.66	99.66	54	17	2	37	122	6
96PBMW004	B	Hay	49.71	14.80	14.68	12.10	0.14	5.51	0.22	1.96	0.06	0.83	4.21	99.84	47	15	2	42	109	8
96PBMW015	B	Hay	49.71	14.42	11.48	13.34	0.12	7.90	0.22	1.92	0.07	0.81	2.77	99.45	47	14	2	26	89	10
96PGMW024	B	Hay	49.61	14.07	8.83	15.34	0.09	7.51	0.21	3.09	0.08	1.16	3.72	99.61	75	21	4	52	181	6
96PBMW016	B	Hay	49.56	13.91	10.91	15.20	0.16	6.29	0.21	2.53	0.09	1.14	10.01	99.23	64	16	2	56	69	11
96PGMW047	B	Hay	49.49	13.44	15.27	12.66	0.32	5.39	0.27	2.08	0.11	0.98	7.40	99.24	75	20	4	44	133	7
97PTDW018	B	Hay	49.40	14.45	10.82	14.22	0.08	7.43	0.22	2.48	0.06	0.83	2.31	98.94	37	19	2	26	168	2
97PTDW024	B	Hay	49.31	14.82	13.23	14.17	0.18	5.76	0.22	1.37	0.08	0.86	3.28	99.30	41	17	2	42	165	4
96PQMW041	B	Hay	49.20	13.78	7.45	18.12	0.56	6.40	0.23	2.56	0.15	1.55	3.54	98.83	91	25	6	68	101	15
96PGMW044	B	Hay	49.10	14.84	7.36	17.12	0.07	7.10	0.22	2.64	0.11	1.45	7.94	98.19	86	24	7	17	80	7
97PTDW056D	B	Hay	48.90	11.60	8.52	12.96	0.59	15.33	0.18	1.08	0.07	0.77	4.33	99.37	41	17	2	105	156	15
96PAMW009	B	Hay	48.67	15.65	11.77	14.23	0.45	6.50	0.23	1.64	0.06	0.80	2.57	99.33	40	19	2	129	252	14
96PGMW031	B	Hay	48.49	15.72	11.29	13.02	0.09	8.62	0.20	1.67	0.06	0.84	3.93	99.80	53	19	4	26	123	6
96PBMW014	B	Hay	48.27	14.85	13.98	12.38	0.10	7.95	0.19	1.43	0.08	0.76	2.73	99.80	46	16	2	31	97	8
96PDMW001	BA	Hay	57.39	14.73	6.45	9.20	0.32	4.07	0.19	4.71	0.48	2.44	3.91	99.41	254	38	9	99	381	10
97PGMW001	BA	Hay	56.53	17.76	7.18	8.12	2.80	3.73	0.13	2.32	0.36	1.08	7.44	99.22	111	24	4	501	142	81
96PDMW008	BA	Hay	56.44	17.39	4.78	10.15	0.30	3.93	0.15	5.29	0.19	1.38	6.23	99.11	132	26	9	81	211	17
96PDMW007	BA	Hay	55.52	17.35	9.64	7.93	0.99	1.92	0.14	5.18	0.24	1.09	8.27	99.11	114	26	9	154	229	46
96PKMW002	BA	Hay	54.79	15.29	9.73	10.03	0.16	6.32	0.19	2.57	0.10	0.81	4.79	99.28	86	17	4	42	161	8
97PFMW002	BA	Hay	54.40	16.07	10.02	9.37	0.50	5.65	0.15	2.68	0.19	0.97	6.12	98.76	97	24	2	135	378	15
96PDMW009	BA	Hay	53.01	16.92	5.09	11.49	0.12	7.47	0.15	4.51	0.21	1.02	5.12	98.78	106	21	9	85	307	11
96PAMW008	B	Hay	51.62	15.81	11.25	13.20	0.06	4.33	0.23	2.27	0.05	1.15	6.72	99.49	49	19	2	22	188	11

Table 3.1. (concluded) Major and trace element data for rocks of the HBGB.

Sample	Rock Type	Litho unit	SiO_2	Al_2O_3	CaO	Fe_2O_3	K_2O	MgO	MnO	Na_2O	P_2O_5	TiO_2	LOI	TOTAL	Zr	Y	Nb	Ba	Sr	Rb
96PQMW021	B	Hay	50.98	13.65	10.44	16.57	0.16	5.38	0.25	0.45	0.13	2.00	4.20	99.43	85	23	6	32	176	11
96PDMW003	B	Hay	50.75	16.14	7.01	15.63	0.13	4.42	0.30	4.48	0.04	1.09	2.95	99.48	37	19	2	78	234	8
96PAMW010	B	Hay	49.96	14.69	9.57	14.00	0.19	7.42	0.23	2.76	0.05	1.14	2.64	99.16	44	15	2	62	114	10
96PTJW003	B	Hay	48.13	17.45	7.60	14.42	0.87	9.04	0.20	1.17	0.04	1.06	5.02	99.06	44	17	2	223	96	17

Analytical method: X-ray flourescence. Major element analysed on glass beads. Trace elements analyses on pressed powder discs.

K.R. = Koignuk River formation, Win L. = Windy Lake formation, S.L. = Square Lake formation, Wolv L. = Wolverine Lake formation, F.L. = Flake Lake formation, C.L. = Clover Lake formation, S.V. = Son Volt formation, Hay = Hayden formation.

B = Basalt, BA = Basaltic Andesite, A = Andesite, D = Dacite, R = Rhyolite, Dio = Diorite

Table 3.2. Rare earth element data for rocks of the HBGB.

Sample	97PGMW101	96PCMW107	96PCMW108	97PBMW103	96PTMW119	97PQMW109	96PQMW113	97PBMW104	97PTMW108	96PUMW101
Litho unit	F.L.	K.R.	K.R.	C.L.	Wolv L.	S.L.	S.L.	Win L	S.V.	S.V.
V (ppm)	8	50	68	7	39	67	85	44	98	79
Cr (ppm)	119	33	27	84	39	50	55	64	51	75
Co (ppm)	4.5	13	17	1.4	10	11	18	6	19	15
Ni (ppm)	252	22	-10	-10	28	22	37	14	52	38
Cu (ppm)	-10	20	15	84	-10	15	34	11	13	60
Zn (ppm)	43	134	42	31	43	59	123	68	53	67
Ga (ppm)	25	16	18	20	21	17	17	18	18	16
Ge (ppm)	0.9	0.6	0.8	0.7	0.7	0.7	0.8	0.8	0.8	0.9
Rb (ppm)	40	55	15	102	29	74	32	74	14	17
Sr (ppm)	45.3	116	179	42.3	277	188	309	650	246	204
Y (ppm)	134	9.9	12	4.3	5.4	9.5	13	9.9	11	13
Zr (ppm)	450	141	156	57	102	131	146	154	70	125
Nb (ppm)	28	5.6	6.2	2	2.7	6.8	6.2	12	2.8	4.8
Mo (ppm)	1.4	1	1.2	0.6	0.5	2.6	0.6	0.4	0.3	0.4
Sn (ppm)	1.7	2.9	1.6	-0.5	-0.5	-0.5	-0.5	1	2.2	-0.5
Sb (ppm)	0.24	0.16	0.3	0.65	0.14	0.13	0.28	0.15	0.66	1.18
Cs (ppm)	0.4	1.3	0.3	2.4	1.5	1.3	2.1	3	1.1	0.6
Ba (ppm)	124	905	194	990	226	509	448	663	141	140
La (ppm)	46.1	18.1	17.6	16.1	10.1	23	34	63.4	9.27	11.3
Ce (ppm)	107	36.5	34.6	33.5	20	51	81.3	130	18.3	23.1
Pr (ppm)	13.8	3.905	3.608	3.52	2.203	5.857	9.894	13.73	2.019	2.571
Nd (ppm)	61.5	14.2	13.3	12.3	8.63	22	38.9	47.9	8.07	10.2
Sm (ppm)	16.3	2.7	2.64	2.58	1.84	3.63	6.29	6.67	1.87	2.19
Eu (ppm)	3.854	0.759	0.742	0.315	0.541	0.973	1.523	1.464	0.687	0.699
Gd (ppm)	18.5	2.27	2.34	1.86	1.4	2.46	4.08	3.75	1.87	2.04
Tb (ppm)	3.73	0.33	0.35	0.19	0.17	0.31	0.51	0.41	0.31	0.34
Dy (ppm)	22.3	1.75	2.09	0.93	1.06	1.77	2.51	1.9	1.99	2.19
Ho (ppm)	4.79	0.33	0.42	0.13	0.18	0.32	0.43	0.32	0.41	0.44
Er (ppm)	14.7	0.98	1.22	0.33	0.53	0.97	1.35	1.02	1.21	1.33
Tm (ppm)	2.397	0.14	0.184	0.034	0.068	0.132	0.163	0.112	0.188	0.202
Yb (ppm)	16.4	0.88	1.12	0.05	0.34	0.66	0.97	0.6	1.12	1.24
Lu (ppm)	2.34	0.152	0.183	0.025	0.071	0.13	0.175	0.126	0.185	0.215
Hf (ppm)	13	4	4.3	2.3	2.9	3.4	3.7	3.7	1.9	3.2
Ta (ppm)	1.62	1.37	2.06	0.34	1.08	0.52	1.41	0.84	0.26	1.22
W (ppm)	0.5	22	44	0.4	26	0.7	28	0.6	0.3	18
Tl (ppm)	0.19	0.48	0.22	0.37	0.18	0.48	0.21	0.41	0.07	0.1
Pb (ppm)	6	25	6	8	7	6	9	20	6	8
Bi (ppm)	0.05	-0.05	0.39	1.3	0.35	-0.05	0.13	0.93	0.32	0.09
Th (ppm)	5.04	3.49	3.04	2.86	1.98	2.8	3.05	13.9	1.53	2.35
U (ppm)	0.92	0.61	0.48	0.66	0.26	0.44	0.32	3.04	0.15	0.27

Table 3.2. (concluded) Rare earth element data for rocks of the HBGB.

Sample	96PQMW115	96PFMW004	96PAMW113	96PTMW002	96PBMW011	96PBMW015	96PDMW009	96PDMW001	96PAMW008
Litho unit	S.V.	S.V.	S.V.	Hay (BG-1)	Hay (BG-1)	Hay (BG-1)	Hay (BG-2)	Hay (BG-2)	Hay (BG-3)
V (ppm)	158	119	127	262	315	261	395	250	261
Cr (ppm)	160	75	45	288	107	296	802	190	151
Co (ppm)	22	24	21	44	41	50	70	45	49
Ni (ppm)	43	80	36	67	38	90	322	126	97
Cu (ppm)	52	64	81	105	133	110	208	93	118
Zn (ppm)	82	75	83	80	88	94	159	179	79
Ga (ppm)	17	17	20	16	15	15	20	23	15
Ge (ppm)	1.8	1.1	1	1.4	1.2	1.4	1.9	1.2	1.3
Rb (ppm)	13	1	3.4	2.4	0.5	1.6	18	6	2.7
Sr (ppm)	167	261	120	129	85.5	98.5	272	384	139
Y (ppm)	13	15	20	20	23	17	26	42	23
Zr (ppm)	82	118	132	53	56	39	128	214	66
Nb (ppm)	4.2	5.4	7.9	2.7	2.7	2	6	8	4.2
Mo (ppm)	0.5	0.6	0.7	0.3	0.1	0.4	0.6	0.6	0.2
Sn (ppm)	0.6	-0.5	0.4	-0.5	-0.5	-0.5	1.5	1.7	1.5
Sb (ppm)	0.42	0.52	0.16	0.61	0.08	0.23	0.51	0.36	0.2
Cs (ppm)	0.4	0.4	0.2	-0.1	0.1	-0.1	1.3	0.1	0.1
Ba (ppm)	89	22	54	39	8.8	9.6	126	228	71
La (ppm)	9.19	11.3	19.1	3.23	3.24	2.42	15	12.4	5.05
Ce (ppm)	20.2	24.1	41.1	8.8	9.13	6.48	41.4	39.3	13
Pr (ppm)	2.382	2.749	4.763	1.272	1.368	0.941	5.74	5.971	1.81
Nd (ppm)	9.85	11.3	19.1	6.56	7.06	4.97	27	30.3	8.94
Sm (ppm)	2.25	2.52	3.91	2.15	2.38	1.64	6.8	8.67	2.77
Eu (ppm)	0.708	0.799	1.127	0.726	0.782	0.577	1.92	2.507	0.852
Gd (ppm)	2.25	2.53	3.55	2.7	3	2.2	6.32	8.95	3.27
Tb (ppm)	0.37	0.42	0.62	0.52	0.6	0.43	1.01	1.55	0.64
Dy (ppm)	2.37	2.54	3.5	3.4	3.95	2.84	5.34	8.22	3.98
Ho (ppm)	0.48	0.51	0.69	0.72	0.85	0.61	0.97	1.5	0.84
Er (ppm)	1.41	1.52	2.08	2.15	2.6	1.86	2.7	4.19	2.51
Tm (ppm)	0.218	0.236	0.3	0.332	0.416	0.288	0.36	0.586	0.39
Yb (ppm)	1.32	1.43	1.92	2.18	2.76	1.85	2.04	3.71	2.5
Lu (ppm)	0.22	0.232	0.287	0.33	0.425	0.294	0.324	0.52	0.387
Hf (ppm)	2.2	3.1	3.5	1.6	1.7	1.2	3.5	5.8	2
Ta (ppm)	1.3	0.66	0.55	0.34	0.33	0.65	1.17	1.04	0.79
W (ppm)	20	4.9	0.3	4.3	5.3	15	5.2	2.4	8.5
Tl (ppm)	-0.05	-0.05	-0.05	0.1	-0.05	-0.05	0.2	0.07	-0.05
Pb (ppm)	8	7	9	5	-5	5	6	6	5
Bi (ppm)	0.25	0.23	0.1	-0.05	-0.05	-0.05	-0.05	-0.05	-0.05
Th (ppm)	1.44	1.66	2.45	0.34	0.52	0.32	0.86	1.2	0.64
U (ppm)	-0.05	0.15	0.42	-0.05	-0.05	-0.05	0.07	-0.05	-0.05

Analytical method: ICP-MS

K.R. = Koignuk River formation, Win L. = Windy Lake formation, S.L. = Square Lake formation, Wolv L. = Wolverine Lake formation, F.L. = Flake Lake formation, C.L. = Clover Lake formation, S.V. = Son Volt formation, Hay = Hayden formation.

Major and Trace Elements

Uncertainties about the nature of plate tectonic and petrochemical processes that operated in the Late Archean hinder detailed interpretation of the lithogeochemistry of greenstone belts. Many workers believe the Archean mantle may have been significantly different from the Phanerozoic and Proterozoic mantle, precluding direct comparison of major and trace element characteristics of Archean rocks with those from various modern tectonic settings. This qualification should be kept in mind for the following discussion, in which geochemical signatures established from the recent rock record will be used to suggest possible paleotectonic settings for rocks from the HBGB.

Rocks in ancient greenstone belts have experienced alteration and metasomatism of variable intensity that may modify primary igneous chemical compositions. Therefore, caution must be exercised attempting to interpret first order geochemical characteristics. Large ion lithophile elements (LILE), K, Na, Rb, Sr, and Ba may all be mobile during low-grade metamorphism, therefore little reliance can be placed on them. However, many workers are in general agreement that high field strength elements (HFSE), Al, Y, P, MREE, and HREE are relatively insensitive to the secondary alteration processes in greenstone belts (e.g. Rollinson, 1993; Kerrich and Wyman, 1997). Thus, greater reliance will be placed on the HFSE, Ti, Zr, Y, Al, Nb, and the REE.

Although, greenschist facies metamorphic conditions affected the entire HBGB, primary igneous textures such as pillows and flow banding are commonly well preserved, therefore the prefix "meta" has been abandoned and igneous nomenclature is used to describe the HBGB volcanic rocks.

Variation diagrams were constructed (Figure 3.4) to test the relative mobility and incompatibility of Al_2O_3, TiO_2, P_2O_5, and assess the utility of the HFSE as discriminants in identifying and characterising magmatic suites within the HBGB. The near constant ratios of

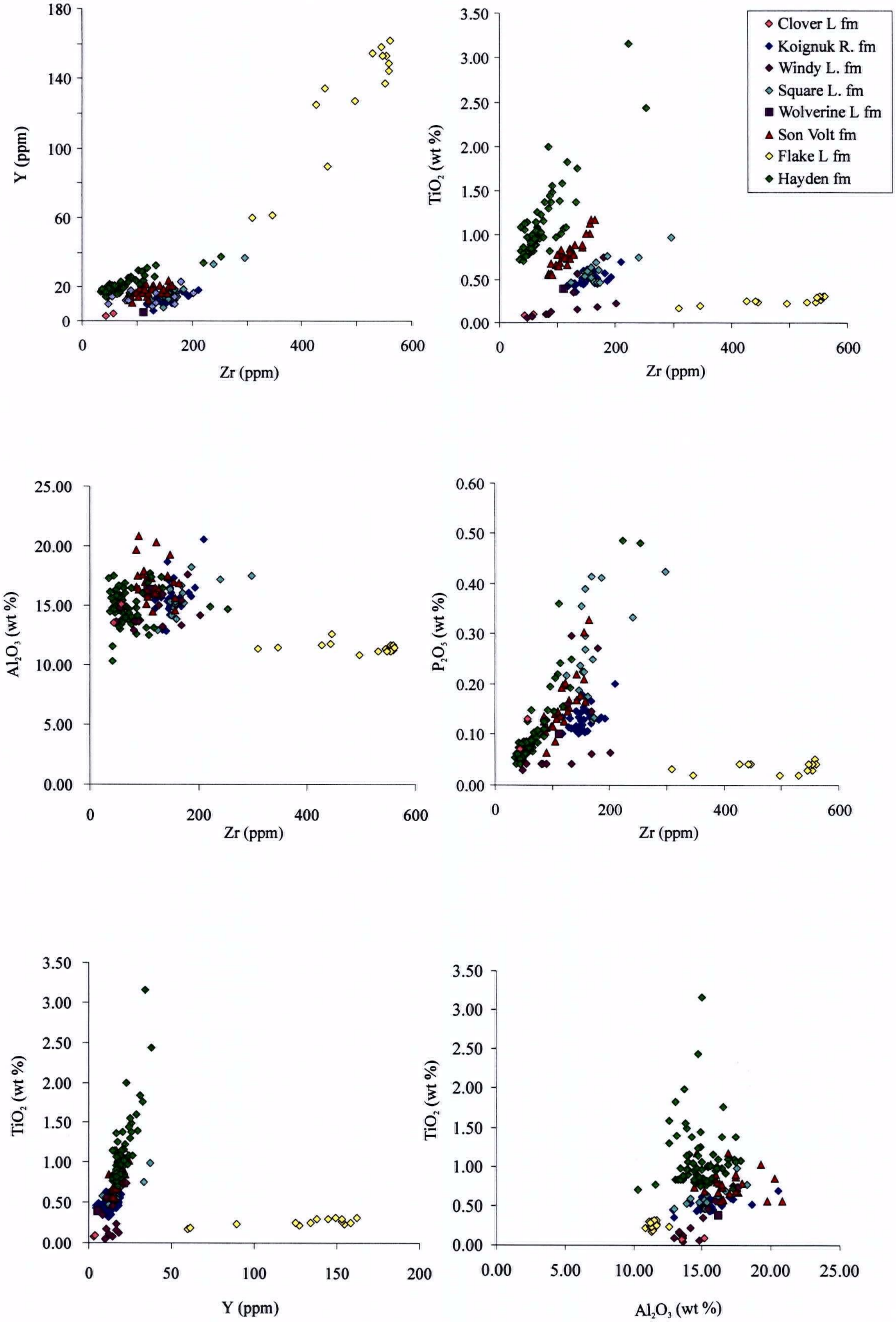

Figure 3.3a. Inter-element variation plots. Element pairs exhibiting strong linear relationships are thought to be incompatible in melts and immobile during metasomatism.

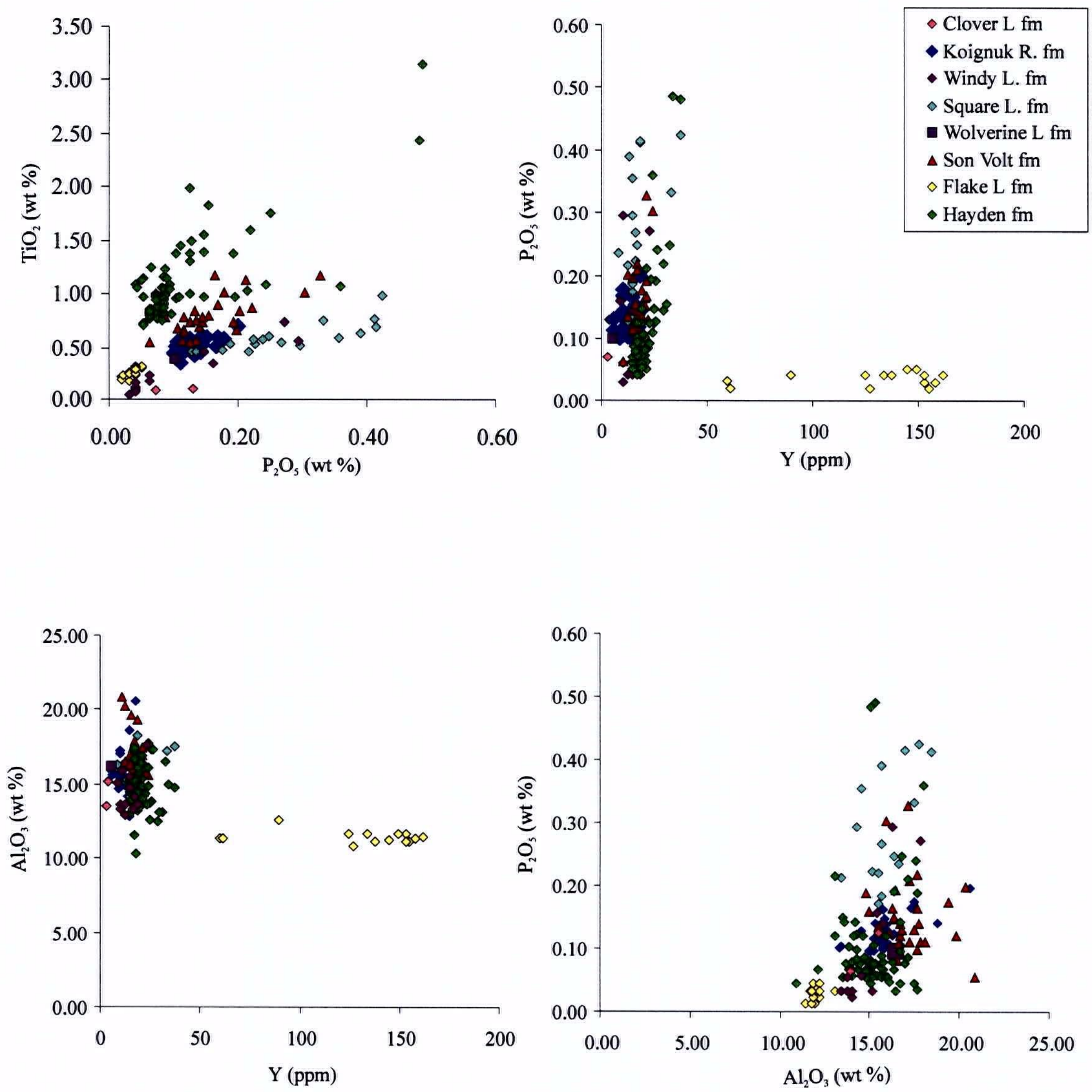

Figure 3.3b. Inter-element variation plots. Element pairs exhibiting strong linear relationships are thought to be incompatible in melts and immobile during metasomatism.

TiO_2, Zr, and Y suggest these elements behaved incompatibly and hence, did not partition into the phenocryst phases in rocks of all compositions. In addition, P_2O_5 and Al_2O_3 appear to behave incompatibly in rocks of mafic compositions. It should be noted that non-linear scatter within some element pairs is not only caused by mobility and compatibility but may also arise from: 1) the presence of mixed rock suites, 2) difficulty in sampling true liquid compositions (particularly problematical with calc-alkaline felsic rocks), 3) variable fractionating assemblages during fractional crystallisation, 4) sampling bias and 5) a combination of the above (Rollison, 1993). In the following discussion less reliance will be placed on elements which display random scatter.

Chemical classification of rocks from the HBGB

Rocks within the HBGB data set span basalt to rhyolite compositions based on a SiO_2 versus Zr/TiO_2 plot (3.5a) after Winchester and Floyd (1977). A SiO_2 frequency diagram (Figure 3.5b) indicates a tri-modal rock distribution for the HBGB corresponding to peaks between 48-54 %, 66-70 % and 74-78 % weight percent SiO_2

Magmatic affinities for supracrustal rocks within the HBGB was determined through immobile and incompatible elements Zr and Y (Figure 3.6) using the guidelines of MacLean and Barret (1993). Mafic (Hayden formation) and intermediate composition rocks (Son Volt formation) are dominantly of tholeiitic and transitional affinities, respectively, with calc-alkaline rocks dominating the main felsic successions in the HBGB (Wolverine Lake, Square Lake, Windy Lake, Koignuk River, and Clover Lake formations). However, a rare spatially- restricted tholeiitic rhyolite unit (Flake Lake formation) is an exception to the felsic trend.

a)

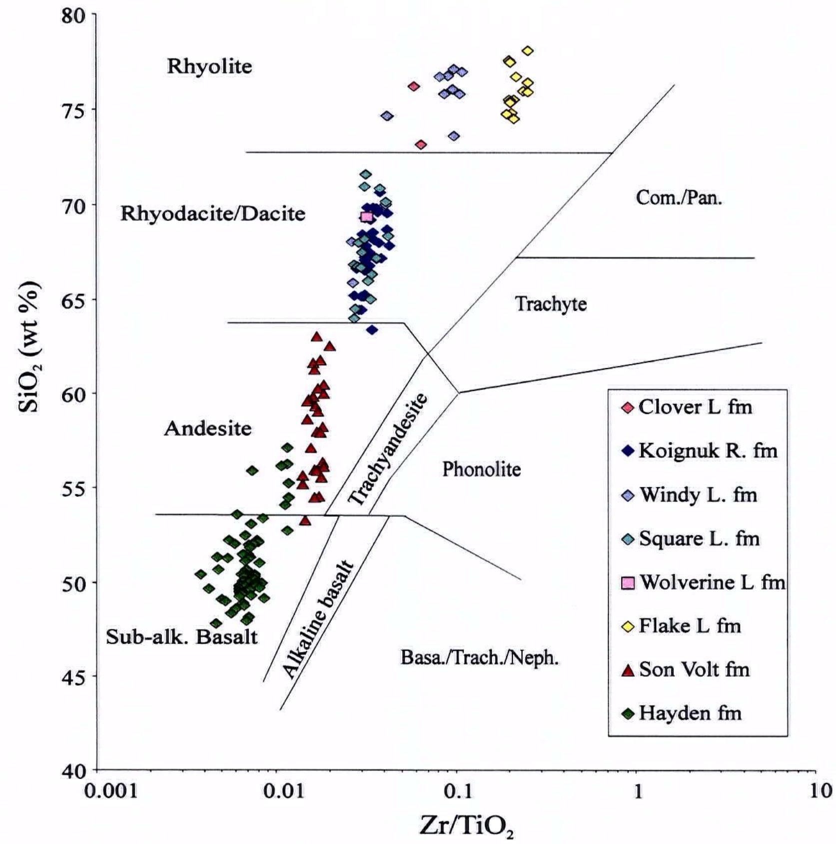

b)

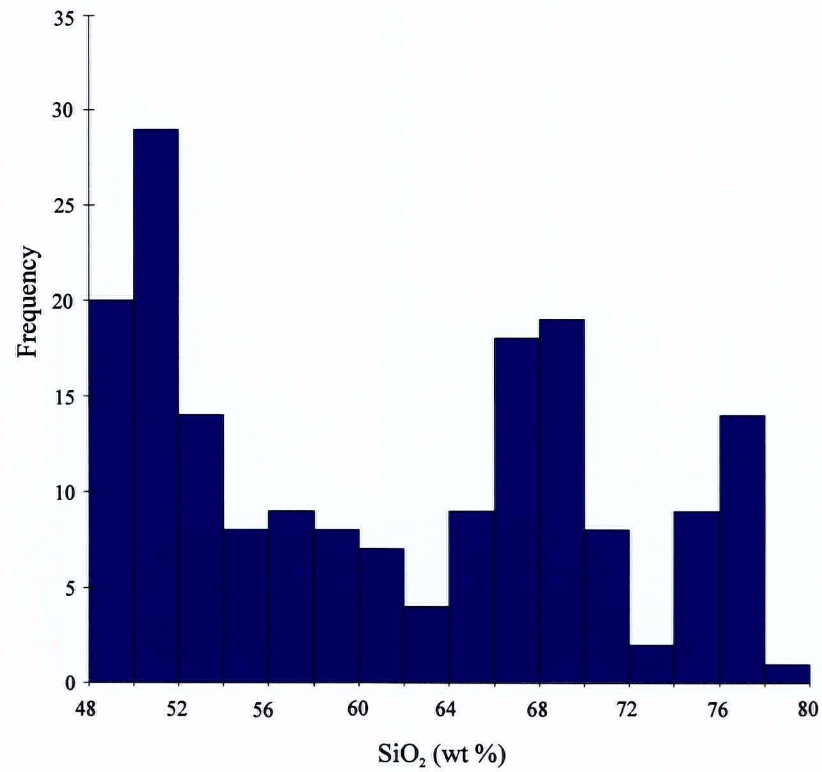

Figure 3.5. a) SiO_2 (wt %) versus Zr/TiO_2 discrimination plot after Winchester and Floyd (1977). The plot illustrates the compositional range of the data set from the HBGB. b) Histogram of SiO_2 frequency distribution for rocks of the HBGB.

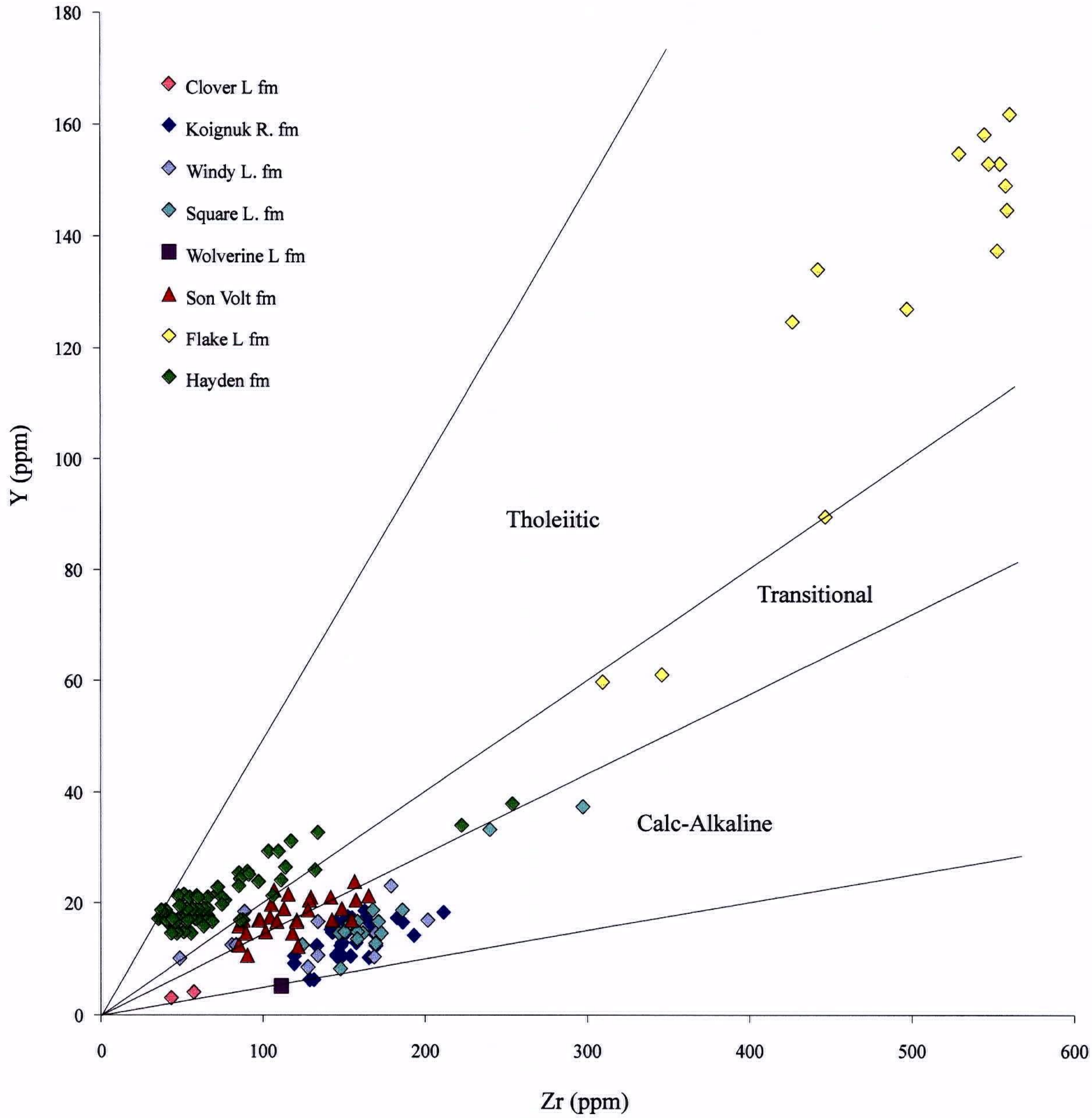

Figure 3.6. Y-Zr magmatic affinity plot after Barrett and MacLean (1993). Zr/Y values of 2-4.5, 4.5-7, and >7 correspond to tholeiitic, transitional, and calc-alkaline affinities, respectively.

Lithogeochemistry

Mafic rocks

Mafic rocks are the most abundant preserved volcanic lithology in the HBGB. All mafic volcanic rocks within the HBGB are collectively grouped together, forming the Hayden formation (Figure 3.2 and 3.3). Based on HFS inter-element ratios, primarily TiO_2/Zr (Figure 3.7) and REE patterns (Figure 3.8) (Table 3.3) the Hayden formation may contain up to three distinct mafic suites: BG-1, BG-2, and BG-3.

The regionally extensive BG-1 suite forms the dominant lithology in the HBGB. BG-1 flows are tholeiites characterised by mean HFSE ratios: $Ti0_2/Zr = 161$, $Zr/Y = 3$, $TiO_2/Y = 53$, $Al_2O_3/TiO_2 = 14$, $P_2O_5/Zr = 15$, $P_2O_5/Y = 50$, $TiO_2/ P_2O_5 = 11$, and Mg# of 49. On a chondrite normalised diagram (Figure 3.8) selected (n=3) BG-1 rocks plot as a relatively flat coherent group at around 10 times chondrite with $[La/Yb]_N = 0.8\text{-}1.0$, $[La/Sm]_N = 0.9$, $[Gd/Yb]_N = 0.9\text{-}1.0$, with a slight negative Eu anomaly (Eu/Eu* = 0.9). Primitive mantle normalised REE (Figure 3.8) are relatively flat with marked troughs in Nb and P, likely resulting from the presence of titanite and apatite, respectively or alternately the troughs suggests a sialic contribution (Barley, 1986) to this suite. The low abundances of elements with high ionic potential (Nb, Zr, Y, Ti) and REE profiles on chondrite and primitive mantled normalised plots are consistent with a MORB, island arc or back-arc setting. The low Zr/Nb ratio (19.5-20.7), relatively flat REE profile, and lack of strongly depleted LREE is more typical of basalts erupted in a back-arc basin setting (Wilson, 1989, Kerrich and Wyman, 1997).

Dominantly situated in the northern HBGB in the upper portion of the Hayden formation mafic pile, a rare commonly pillowed mafic suite of tholeiitic to transitional basaltic andesite composition comprises BG-2 rocks. This suite is characterised by relatively higher abundances of HFSE and REE with mean HFSE inter-element ratios of $Ti0_2/Zr = 98$, $TiO_2/Y =$

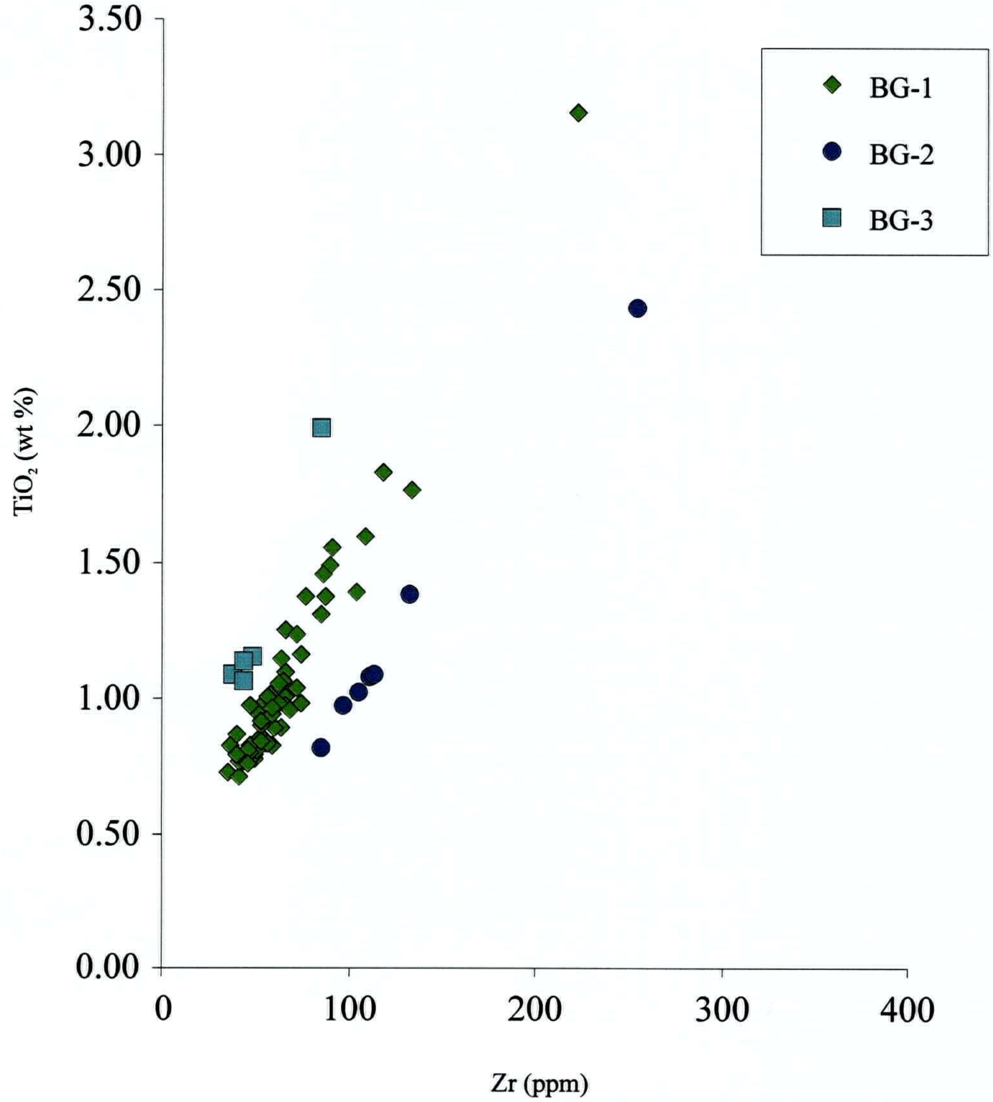

Figure 3.7. Binary immobile element plot of TiO_2 vs. Zr suggesting the presence of three distinct mafic magmatic suites.

a)

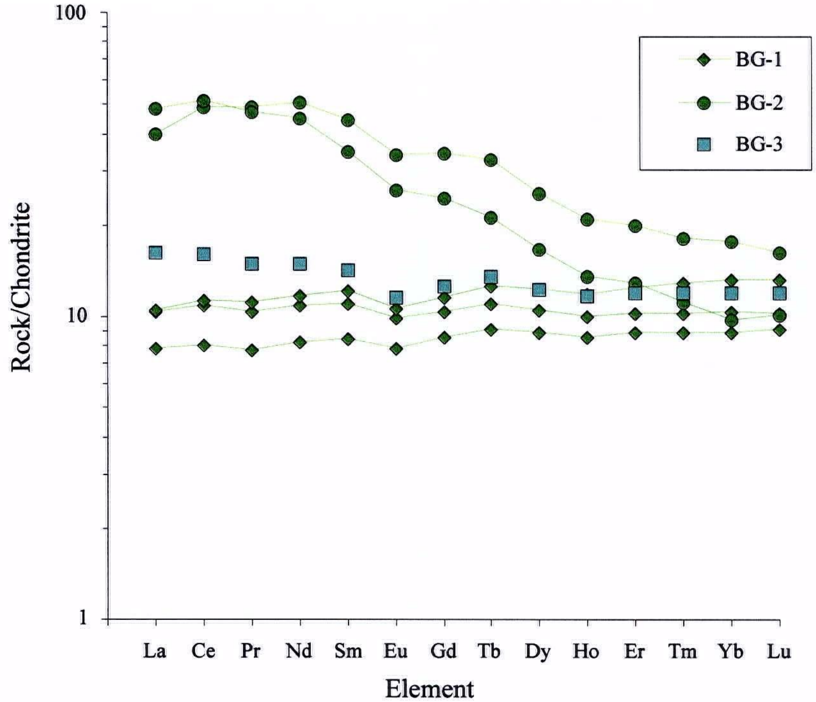

b)

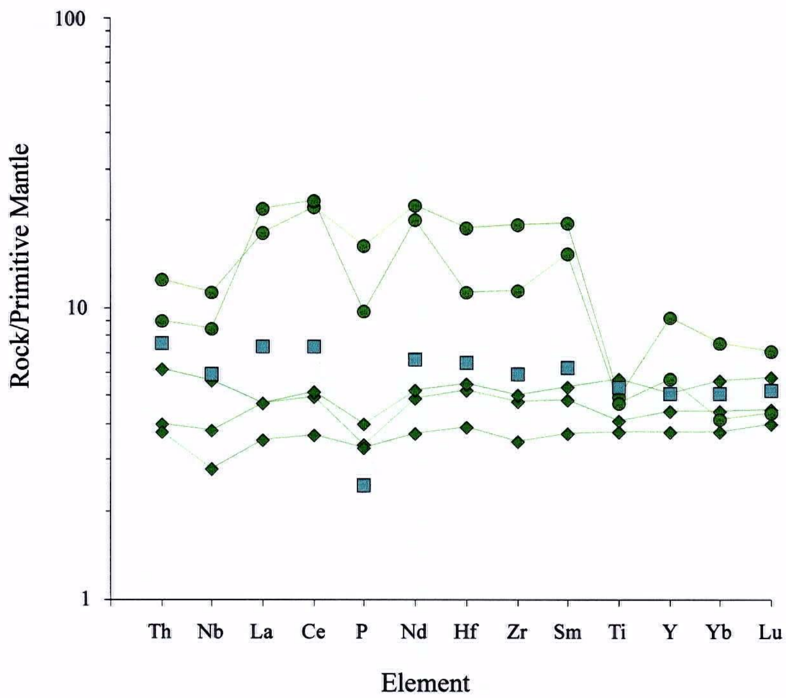

Figure 3.8. a) Chondrite normalised rare earth element plot for mafic rocks of the Hayden formation. Normalising values from Boynton (1984). b) Primitive mantle normalised rare earth element plot for mafic rocks from the Hayden formation. Normalising values from Sun and McDonough (1989).

Table 3.3. Inter-element ratios for rock formations within the HBGB.

	Hayden formation						Son Volt formation		Flake Lake formation		Wolverine Lake formation		Square Lake formation		Windy Lake formation				Koignuk River formation		Clover Lake formation	
	BG-1 (n=57)		BG-2 (n=7)		BG-3 (n=5)		(n=28)		(n=14)		(n=1)		(n=17)		FG-1 (n=4)		FG-2 (n=8)		(n=35)		(n=2)	
	mean	s.d	mean	s.d	mean	s.d	mean	s.d	mean	s.d	mean	s.d	mean	s.d	mean	s.d	mean	s.d	mean	s.d	mean	s.d
TiO_2/Zr	165	20	98	3	249	24	67	6	5	0	35	-	35	5	35	9	12	1	33	4	18	-
TiO_2/Y	530	98	488	83	690	127	451	84	21	5	763	-	374	101	396	106	91	44	393	107	263	-
Zr/Y	3	1	5	1	3	1	7	1	4	1	22	-	11	2	12	3	8	4	12	3	14	-
Al_2O_3/TiO_2	15	4	15	4	13	4	22	6	45	9	41	-	27	4	32	8	108	71	31	3	156	-
P_2O_5/Zr	15	3	20	7	12	2	14	3	0.7	0.2	9	-	16	5	15	6	4	2	8	1	20	-
P_2O_5/Y	48	16	98	32	33	13	90	30	3	1	200	-	170	64	171	82	32	12	101	36	289	-
TiO_2/P_2O_5	12	2	5	2	22	4	5	1	7	2	4	-	2	0.6	2	1	3	1	4	1	1	-
Mg #	49	7	48	9	44	9	-	-	-	-	-	-	-	-	-	-	-	-	-	-	-	-
	n=3		n=2		n=1		n=5		n=1		n=1		n=2		n=1				n=2		n=1	
La_n/Yb_n	0.8-1.0	-	2.3-5.0	-	1.4	-	4.7-6.7	-	1.9	-	20.0	-	23.5-23.6	-	71.2	-	-	-	10.6-13.9		217.1	-
La_n/Sm_n	0.9-1.0	-	0.9-1.4	-	1.1	-	2.6-3.1	-	1.8	-	3.5	-	3.4-4.0	-	6.0	-	-	-	4.2		3.9	-
Gd_n/Yb_n	0.9-1.0	-	2.0-2.5	-	1.1	-	1.3-1.5	-	0.9	-	3.3	-	3.0-3.4	-	5.0	-	-	-	1.7-2.1		30.0	-

49, $Zr/Y = 5$, $Al_2O_3/TiO_2 = 13$, $P_2O_5/Zr = 20$, $P_2O_5/Y = 101$, $TiO_2/ P_2O_5 = 5$ and a Mg# = 48 (Table 3.3). REE patterns (Figure 3.8) for BG-2 are typified by fractionated LREE and HREE over relatively flat MREE ($[La/Yb]_N = 2.3\text{-}5.0$, $[La/Sm]_N = 0.9\text{-}1.4$, $[Gd/Yb]_N = 1.9\text{-}2.5$) and a slight negative Eu anomaly (Eu/Eu* = 0.9). Primitive mantle normalised REE patterns (Figure 3.8) are variably spiked with deep troughs at Th, Nb, P, and Ti and peaks at Ce, Nd, and Sm. REE patterns and trace element signatures are suggestive of an ocean island, E-MORB, or back-arc basin setting for this rock suite (Wilson, 1989, Kerrich and Wyman, 1997).

As with the previous rock suite, basalts of BG-3 rarely crop out within the HBGB and could not be distinguished from BG-1 in the field. This Fe-tholeiitic suite is represented by 5 samples and is characterised by HFSE ratios of $Ti0_2/Zr = 249$, $Zr/Y = 3$, $TiO_2/Y = 69$, $Al_2O_3/TiO_2 = 12$, $P_2O_5/Zr = 12$, $P_2O_5/Y = 34$, $TiO_2/ P_2O_5 = 20$, and a Mg# = 44 (Table 3.3). The REE pattern (Figure 3.8) for a sole representative of this suite displays slight fractionation of the LREE ($[La/Yb]_N$ =1.4), and relatively flat MREE and HREE ($[La/Sm_N$ = 1.1 and $[Gd/Yb]_N$) at approximately 10 times chondrite with a negative Eu anomaly (Eu/Eu* = 0.9). On a primitive mantle normalised (Figure 3.8) REE diagram BG-3 is characterised by a relatively flat profile with major troughs at Nb and P. The trace element and REE geochemistry is consistent with either an E-MORB, back-arc, or island arc setting. The low Zr/Nb ratio (15.7) and slight LREE enrichment are consistent with either a back-arc basin or an E-MORB setting. The similar REE patterns (Figure 3.8), slight overlap of most HFSE ratios (Table 3.3) with BG-1 rocks and the random distribution of this suite among BG-1 flows suggest that this unit is comprised of metasomatized BG-1 rocks rather than a distinct rock suite.

Intermediate rocks

Although normally considered rare in greenstone belts, andesitic flows and associated pyroclastic units comprise a significant proportion (~ 10-15 %) of exposed supracrustal rocks in the HBGB. All intermediate extrusive and hypabyssal rocks within the HBGB are assigned to the Son Volt formation (Figure 3.2 and Figure 3.3). Son Volt lithologies are dominantly comprised of epiclastic rocks, although massive and pillowed units occur locally. Plagioclase occurs as the primary phenocryst phase with rare subordinate hornblende phenocrysts present. The formation is characterised by mean HFSE ratios of $Ti0_2/Zr = 68$, $Zr/Y = 7$, $TiO_2/Y = 45$, $P_2O_5/Zr = 14$, $P_2O_5/Y = 90$, $TiO_2/ P_2O_5 = 5$ (Table 3.3) and is of transitional magmatic affinity. A subset of samples, including an intrusive phase thought to be a subvolcanic feeder to the volcanic suite, display similar REE patterns (Figure 3.9). LREE are enriched over the MREE and HREE, resulting with moderate $[La/Yb]_N = 4.7\text{-}6.7$, $[La/Sm_N = 2.6\text{-}3.2$, and $[Gd/Yb]_N = 1.3\text{-}1.5$ ratios. The Eu anomaly ($Eu/Eu^* = 0.9\text{-}1.1$) when it occurs is minor and varies from positive to negative in the suite. Primitive mantle normalised REE patterns display pronounced troughs at Nb, P, and Ti and peaks at Th, La-Ce, and Nd-Sm. The deep troughs indicate this suite has experienced crustal contamination (Kerrich and Wyman. 1997; Poliat et al., 1998). The fractionated REE patterns and marked troughs at Th, Nb and Ti are consistent with a magmatic arc setting for this suite (Poliat et al., 1998, Wilson, 1989).

Felsic Rocks

Felsic volcanic and associated reworked pyroclastic rocks comprise approximately 30 % of the exposed supracrustal rocks in the HBGB. These rocks are divided into six formations (Flake Lake, Wolverine Lake, Square Lake, Windy Lake, Koignuk River, and Clover Lake formations; Figure 3.2 and 3.3) based on field relationships and age constraints.

Structural data (pillow tops) suggest the Flake Lake formation locally overlies the volumous mafic pile northwest of Spyder Lake (Figure 3.2b) and age constraints (Chapter 2) indicate that it is the oldest felsic volcanic package in the HBGB. Rocks of this formation occur as massive quartz-eye rhyolitic volcanic flows of tholeiitic affinity characterised by mean HFSE

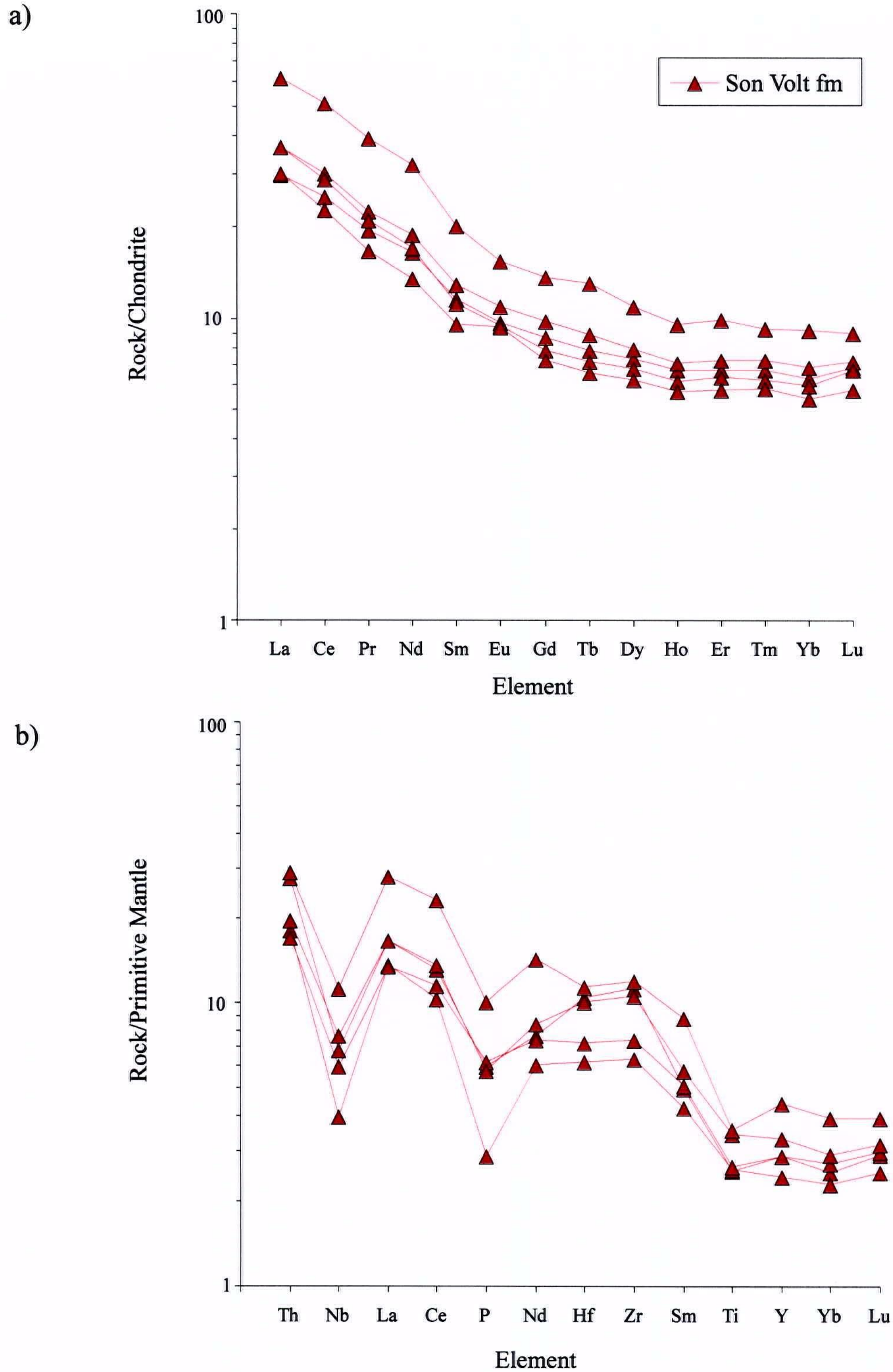

Figure 3.9. a) Chondrite normalised rare earth element plot for intermediate rocks from the Son Volt formation. Normalising values from Boynton (1984). b) Primitive mantle normalised rare earth element plot for intermediate rocks from the Son Volt formation. Normalising values from Sun and McDonough (1989).

ratios of: TiO_2/Zr = 5, TiO_2/Y = 2, and Zr/Y = 4, P_2O_5/Zr = 1, P_2O_5/Y = 3, and TiO_2/P_2O_5 = 7 (Table 3.3). Chondrite normalised REE patterns (Figure 3.10) are mildly fractionated ($[La/Yb]_N$ =1.9) at around 100 times chondrite, LREE enriched ($[La/Gd]_N$ = 1.8), with relatively flat HREE's ($[Gd/Yb]_N$ = 0.9 and a pronounced negative Eu anomaly (Eu/Eu* =0.7) consistent with a highly evolved melt. Primitive mantle normalised REE patterns (Figure 3.10) are nearly flat with pronounced troughs at P and Ti and a minor trough at Nb. This type of felsic rock has not previously been recognised in the SSP and is absent in most Archean cratons except in the Superior Province (Thurston and Fryer 1983; Lesher et al., 1986; Barrie et al., 1993; Jackson et al., 1994), where it commonly forms the major host for volcanogenic massive sulphide deposits (Barrie et al., 1993;Thurston 1981; Lesher et al., 1986). The REE patterns, high abundance of HFSE, and inter-element ratios are suggestive of a back-arc basin or MORB setting for this suite (Pearce et al., 1984; Lentz, 1998; Barrie et al., 1993).

The Wolverine formation, comprising a series of hypabyssal rhyodacite intrusions, crops out in the northern portion of the HBGB southwest of Patch Lake (Figure 3.2a). This formation is represented by a single sample of calc-alkaline affinity with inter-element ratios of TiO_2/Zr = 35, Zr/Y = 22, TiO_2/Y = 42, P_2O_5/Zr = 9, P_2O_5/Y = 200, TiO_2/P_2O_5 = 3.81 (Table 3.3). Chondrite normalised REE pattern's (Figure 3.10) are moderately fractionated ([La/Yb] = 20.0, [La/Sm] = 3.5, and [Gd/Yb] = 3.3) with distinct troughs at Nb and P on a primitive mantle normalised REE plot (Figure 3.10).

Spatially restricted highly fragmental calc-alkaline felsic suites located in the west central HBGB comprise the Square Lake formation (Figure 3.2). Rocks of this formation are characterised by variable inter-element ratios (Table 3.3) with moderately fractionated chondrite normalised REE patterns ([La/Yb] = 23.5-23.6, [La/Sm] = 3.4-4.0, and [Gd/Yb] = 3.0-3.4; Figure 3.10) and troughs at Nb, P, and Ti on a primitive mantle normalised plot (Figure 3.10).

a)

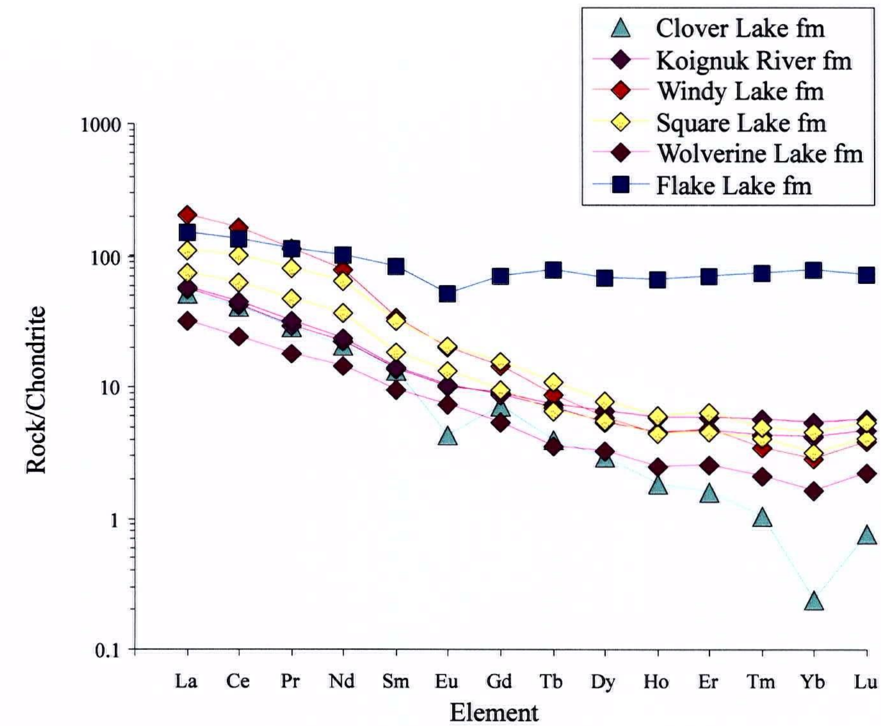

b)

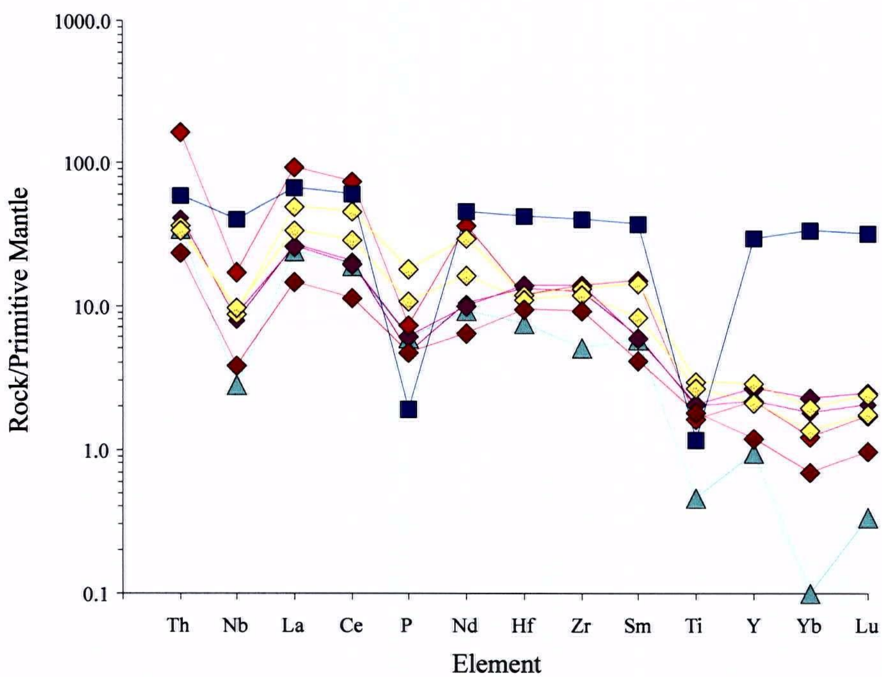

Figure 3.10. a) Chondrite normalised rare earth element plot for felsic rock formations from the HBGB. Normalising values from Boynton (1984). b) Primitive mantle normalised rare earth element plot for felsic rock formations from the HBGB. Normalising values from Sun and McDonough (1989).

Felsic volcanic and associated volcaniclastic rocks of the Windy Lake formation span the length of the HBGB (Figure 3.2), and form one of two regionally extensive felsic formations. Element ratios (Table 3.3) suggest this formation is comprised of at least two distinct calc-alkaline magma suites. FG-1 (Table 3.3) rocks are distinguished from FG-2 rocks by mean HFSE ratios of TiO_2/Zr = 35 and P_2O_5/Zr = 15. REE patterns (Figure 3.10) for this suite are strongly fractionated ($[La/Yb]_N$ = 71.2) with LREE and HREE enrichment ($[La/Sm]_N$ =6.0, and $[Gd/Yb]_N$ = 5.0) and a minor negative Eu anomaly (Eu/Eu* = 0.9). Primitive mantle normalised REE patterns display marked embayments at Nb, Ti, and P (Figure 3.10). A strongly altered, spatially restricted pyroclastic unit characterised by constant TiO_2/Zr = 12 and P_2O_5/Zr = 4 comprise FG-2 rocks (Table 3.3).

The regionally extensive Koignuk formation includes a series of calc-alkaline felsic units that crop out along the western margin of the HBGB (Figure 3.2). REE patterns (Figure 3.10) are characterised by shallow sloping fractionated REE patterns ($[La/Yb]_N$ = 10.6-13.9) with LREE enrichment ($[La/Sm]_N$ =4.2) and relatively flat HREE ($[Gd/Yb]_N$ = 1.7-2.1) and a minor negative Eu anomaly (Eu/Eu* =0.9) on a chondrite normalised plot. Primitive mantle normalised REE patterns (Figure 3.10) display marked troughs at Nb, Ti, and P. Inter-element ratios (Table 3.3) are fairly uniform given the porphyritic nature typical of calc-alkaline rocks and are characterised by mean values of TiO_2/Zr = 33, Zr/Y = 12, Al_2O_3/TiO_2 = 31, P_2O_5/Zr = 8, TiO_2/P_2O_5 = 4.

Rocks comprising the Clover Lake formation crop out as a massive quartz-poor calc-alkaline rhyolite flow. The unit is thus far spatially restricted to a sole occurrence in the southern portion of the HBGB (Figure 3.2b). HFSE ratios (TiO_2/Zr = 18, Zr/Y = 14, TiO_2/Y = 16, P_2O_5/Zr = 20, P_2O_5/Y = 289, TiO_2/P_2O_5 = 1; Table 3.3), highly fractionated REE patterns ($[La/Yb]_N$ = 217.1, $[La/Sm]_N$ =3.9, and $[Gd/Yb]_N$ = 30.0; Figure 3.10), and pronounced negative Eu and Yb distinguish the suite from other felsic suites in the HBGB. A significant negative Eu anomaly (Eu/Eu* = 0.4) is present as well as is a strongly pronounced negative Yb anomaly. The Eu anomaly is believed to result from the weak alteration of feldspars or the result of the magmatic fractionation of plagioclase while the Yb anomaly likely reflects analytical measurement difficulties. Primitive mantle normalised REE patterns (Figure 3.10) demonstrate pronounced troughs at Nb, P, Ti, and Yb.

Primitive mantle normalised REE patterns (Figure 3.10) for all calc-alkaline formations are typified by deep embayments at Nb, P, and Ti consistent with melts that have experience crustal contamination. Inter-element ratio's and fractionated REE patterns coupled with Nb, P, and Ti depletions suggest a magmatic arc setting for calc-alkaline rocks in the HBGB (Wilson, 1989, Pearce and Peate, 1995; McCulloch and Gamble, 1991).

Discussion and Conclusions

Determining an evolutionary model for the HBGB is fraught with difficulties ranging from our poor understanding of Archean systems to the "grungy" and often poorly preserved rock record in the HBGB and other Archean greenstone belts. Any one model must explain the tholeiitic to calc-alkaline progression of the volcanic pile and the presence of two geochemically distinct mafic suites (BG-1 and BG-2) within the Hayden formation documented in this study. Given the protracted evolution of the HBGB (>116 m.y.) and diverse geochemical signatures of the volcanic sequences, the present stratigraphy of the HBGB is thought to reflect episodic magmatism formed in an arc/back-arc geodynamic setting analogous to the present Mariana or the Tonga-Kermadec arc.

The evolution of the HBGB began with the deposition of the >2716 Ma Hayden formation, comprised of the dominant BG-1 suite and the subordinate BG-2 suite. However, BG-1 and BG-2 rocks appear to have evolved in different geodynamic settings. HFSE ratios, flat REE patterns and a lack of strongly depleted LREE patterns for BG-1 rocks is consistent with deposition in a back-arc basin, whereas the enriched LREE patterns of the subordinate BG-2 suite suggest this suite is likely to of evolved in an ocean island or enriched MORB settings. However, geochemical diversity of basalts in a back-arc settings is seen in the Mariana and Lau Basins (Stern et al., 1990; Ewart et al., 1998; and Gribble et al., 1998) where basalts of MORB and ocean island affinities coexist. Often the MORB basalts grade into ocean island basalts if slab roll back has occurred allowing OIB enriched melts to enter the back-arc source region. This appears to be the case with the Hayden formation. BG-2 rocks are crudely restricted to the upper mafic pile of the Hayden formation above the ubiquitous BG-1 suite. Given the position of the BG-2 rocks at the top of the mafic pile below the transitional and calc-alkaline rock formations coupled with the low Nb values for this suite it is likely this suite was also deposited in a back-arc setting.

During the waning stages of mafic volcanism the deposition of the tholeiitic 2716 Ma Flake Lake formation occurred. The flat REE pattern, the HFSE abundances, and position near the top of the Hayden formation are consistent with this unit forming in the same back-arc basin as the mafic rocks (BG-1 and BG-2) of the Hayden formation. The Flake formation possibly representing the differentiated product of a high level Hayden mafic magma or the partial melting of mafic or felsic rocks (Barrie et al., 1993).

Overlying the Hayden and Flake Lake formation, are intermediate rocks of the Son Volt formation. Fractionated REE patterns and marked Nb, P, and Ti depletions signify an evolution from back-arc spreading to an arc building phase for the HBGB. This formation is in turn overlaid by a series of temporally distinct felsic formations (2690 Ma Square Lake, 2685 Ma Windy Lake, and 2677 Ma Koignuk River formations). The calc-alkaline affinities of these rocks and similar trace element depletions as rocks from the Son Volt formation are typical of modern arc rocks and signify intense arc development. In addition the temporal distribution of these formations indicates arc magmatism occurred episodically. Finally, the Wilco and Hope

Bay formation are thought to record the uplift and erosion of the HBGB and mark the cessation of evolution for the HBGB.

References

Barley, M.E. (1986). Incompatible-element enrichment in Archean basalts: A consequence of contamination by older sialic crust rather than mantle heterogeneity. Geology v. 14, p 947-950.

Barrie, C.T., Ludden, J.N., and Green, T.H. (1993). Geochemistry of volcanic rocks associated with Cu-Zn and Ni-Cu deposits in the Abitibi subprovince. Economic Geology v.88, p 1341-1358.

Bevier, M.L., and Gebert, J.S. (1991) U-Pb geochronology of the Hope Bay-Elu Inlet area, Bathurst Block, Northeastern Slave Structural Province, N.W.T. Canadian Journal of Earth Sciences, v 28, p 1925-1930.

Bowring, S.A., Housh, T.B., and Isachsen, C.R. (1990). The Acasta Gneisses: Remnant of the Earth's early crust. In H.Newsom and J.Jones (eds), Origin of the Earth. Oxford University Press, p. 319-343).

Boynton, W.V. (1984). Geochemistry of the rare earth elements: meteorite studies. In Henderson P. (ed.), Rare earth element geochemistry. Elsevier, p 63-114.

Davis, W.J., and Hegner, E. (1992). Neodymium isotopic evidence for the tectonic assembly of Late Archean crust in the Slave Province, Northwest Canada. Contributions to Mineralogy and Petrology, 111: p 493-504.

Ewart, A, Collerson, K.D., Regelous, M, Wendt, J.I., and Niu, Y. (1998). Geochemical evolution within the Tonga-Kermadec-Lau Arc-back-arc systems; the role of varying mantle wedge composition in space and time. Journal of Petrology, v 39, p 331-368.

Fraser, J.A. (1964). Geological notes on the northeastern District of Mackenzie, Nortwest Territories; Geological Survey of Canada, Paper 63-40 (Map 45-1963, Scale 1:506 800) p 20.

Fyson, W.K. (1997). Chronological charts and Archean Stratigraphy of the Slave Province. Northwest Territories Geology Division EGS paper 1997-13, p 18.

Gebert, J.S., 1993. Geology and mineral potential of the Archean Hope Bay and Elu Inlet volcanic belts, Northeastern Slave Structural Province, District of Mackenzie, NWT. Northern affairs program Northwest Territories Geology Division EGS paper 1993-1, p 103.

Gibbons, W.A., (1987). Preliminary geology of the central Hope Bay volcanic Belt, northern portions of NTS 77 A/3,6 (map with marginal notes, 1:50 000 scale) DIAND, EGS 1987-12.

Gribble, R.F, Stern, R.J., Newman, S., Bloomer, S.H., and O'Hearn, T. (1998). Chemical and isotopic composition of lavas from the northern Mariana trough; implications for magmagenesis in back-arc basins. Journal of Petrology, v 39, p 125-154.

Henderson. J.B. (1970). Stratigraphy of the Yellowknife Supergroup, Yellowknife Bay-Prosperous Lake area, District of Mackenzie,Geological Survey of Canada, Paper 70-26.

Isachsen, C.E., and Bowring, S.A. 1994. Evolution of the Slave: Geology, v.22, p 917-920.

Jackson, S.L., Fyon. J.A., and Corfu, F. (1994). Review of Archean supracrustal assemblages of the southern Abitibi greeenstone belt in Ontario, Canada; products of microplate interaction with large-scale plate tectonic setting. Precambrain research. 65, 183-205.

King, J.E., and Helmstaedt, H. (1997). The Slave Province, North-West Territories, Canada. In M.J. De Wit, and L.D. Ashwal. (eds), Greenstone Belts. Oxford Monographs on Geology and Geophysics; no. 35. p 459-479.

Kerrich, R. and Wyman, D.A. (1997). Review of developments in trace-element fingerprinting of geodynamic settings and their implications for mineral exploratrion. Australian Journal of Earth Sciences, v. 44, p 465-487.

Lambert, M.B., Burbidge, G., Jefferson, C.W., Beaumont-Smith, C., and Lustwerk (1990). Stratigraphy, facies and structure in volcanic and sedimentary rocks of the Archean Back River volcanic complex, N.W.T. Current Research, Part C, Geological Survey of Canada, Paper 90-1C, p 151-165.

Lesher, C.M., Goodwin, A.M., Campbell, I.H., and Gorton M.P. (1986). Trace element geochemistry of ore-associated and barren, felsic metavolcanic rocks in the Superior Province, Canada. Can. J. Earth Sci. 23, 222-237.

Lentz, D.R. (1998). Petrogenic evolution of felsic volcanic sequences associated with Phanerozoic volcanic-hosted massive sulphide systems: the role of extensional geodynamics.

Lindsey, D. (1998) Geochemical and Petrographic Study of the Mafic-Ultramafic Suite in the Hope Bay Volcanic Belt, Slave Structural Province, NWT. B.Sc. thesis, University of British Columbia 55 p

MacLean, W.H. and Barrett, T.J. (1993). Lithogeochemical techniques using immobile elements. Journal of Geochemical Exploration, v. 48, p 109-133.

McCulloch, M.T., and Gamble, J.A. (1991). Geochemical and geodynamical constraints on subduction zone magmatism. Earth and Planetary Science Letters, v. 102, p 358-374.

McLennan, S.M. and Taylor, S.R.(1984). Archean sedimentary rocks and their to the composition of the Archean continental crust. In A. Kroner, G. Hanson, and A. Goodwin (eds), Archean Geochemistry, Springer-Verlag, Berlin, p 47-72.

Mortensen., J.K., Relf, C., Davis, W.J., and King, J.E. (1992). U-Pb zircon ages from the Shallow Bay volcaniclastic belt, Contwoyto Lake area, NWT: Age constraints for Lupin-type iron formation. Radiogenic Age and Isotope Studies: Report 5, Geological Survey of Canada, Paper 91-2, p 9-15.

Padgham, W.A. (1985). Observations and speculations on supracrustal successions in the Slave Structural Province. In L.D. Ayres, P.C Thurston, K.D. Card, and W. Weber (eds), Evolution of Archaean Sequences. Geological Association of Canada. Special Paper 28, p 133-151.

Padgham, W.A. (1991). The Slave Province, an overview; Geological Survey of Canada, Open File 2168, pp.1-40.

Pearce, J.A., Harris, N.B.W., and Tindle, A.G. (1984). Trace element discrimination diagrams for tectonic interpretation of granitic rocks. Journal of Petrology, v. 25, p 956-983.

Pearce, J.A., and Peate, D.W. (1995). Tectonic implications of the composition of volcanic arc magmas. Annual Review of Earth and Planetary Sciences, v. 23, p 251-285.

Poliat, A., Kerrich, R., and Wyman, D.A. (1998). The late Archean Schreiber-Hemlo and White River-Dayohessarah greenstone belts, Superior Province: collages of ocean plateaus, oceanic arcs, and subduction accretion complexes. Tectonphysics, v 289, p 295-326.

Rollison, H. (1993). Using geochemical data: evaluation, presentation, interpretation. Longman, Harlow, p 352.

Stern, R.J., Lin, P.N., Morris, J.D., Jackson, M.C., Fryer, F., Bloomer, S.H., and Ito, E. (1990). Enriched back-arc basin basalts from the northern Mariana Trough: implications for the magmatic evolution of back-arc basalts. Earth and Planetary Science Letters, v 100, p 210-225.

Stern, R. and Bleeker, W. (1997). Geology and SHRIMP zircon geochronology of the Acasta gneisses; initial results. Geological Survey of Canada, Program with Abstracts, p 4.

Sun, S.S. and McDonough, W.F. (1989). Chemical and isotopic systematics of oceanic basalts; implications for mantle composition and processes. In Saunders A.D. and Norry M.J. (eds.), Magmatism in Ocean basins. Geolical Society of London, Special Publication, v 42, p313-345.

Thorpe, R.I., Cumming, G.I., and Mortensen, J.K. (1992). A significant Pb isotope boundary in the Slave Province and its probable relation to ancient basement in the western Slave Province. In Project summaries: Canada-Northwest Territories Mineral Development Subsidiary Agreement Geological Survey of Canada, Open File 2484, p 179-164.

Thurston, P.C. (1981). Economic evaluation of Archean felsic volcanic rocks using REE geochemistry. In Archean geology (ed J.E Glover and D.I. Groves), Special publication No.7, geological Society of Australia, p 439-450.

Thurston, P.C. and Fryer, B.J. (1983). The geochemistry of repetitive cyclical volcanism from basalt through rhyolite in the Uchi-Confederation greenstone belt, Canada. Contribut. Mineral. Petrol. 83, 204-226.

van Breemen, O., Davis, W.J., and King, J.E. (1992). Temporal distribution of granitoid plutonic rocks in the Slave Province, Northwest Canadian Shield, Canadian Journal of Earth Sciences v.29, p 2186-2199.

Wilson, M. (1989). Igneous Petrogenesis: A global tectonic approach. Chapman and Hall, New York, 466p.

Winchester, J.A. and Floyd, P.A. (1977). Geochemical discriminants of different magma series and their differentiation producsts using immobile elements. Chemical Geology, v. 20, p 325-343.

Yamashita, K., Jensen, J.E., Creaser, R.A., and Gebert, J.S. (1995). Geology, geochemistry, and Nd isotopic study of the Hanikahimajuk Lake area (NTS 86 I/2, 86 H/14,15), northern Point lake belt, Slave Stuctural Province, NWT; Geological Association of Canada, Program with Abstracts, v.20, p A-112.

Chapter 4

Conclusion

Twenty-one U-Pb zircon and titanite ages, one hundred and seventy four major and trace element analyses, and nineteen rare earth element analyses were produced in this study. The U-Pb geochronology together with the lithogeochemistry and geological mapping provides a relatively detailed tectonic evolutionary framework for the formation of supracrustal successions within the Late Archean HBGB.

The HBGB is characterised by a basal series of mafic dominated tholeiitic volcanic flows (Young Group) overlain by a sequence of calc-alkaline volcanic rocks (Westerberg Group) that are in turn overlain by sedimentary rocks of the Tweedy and Farrar group. These successions were deposited over a period in excess of 116 m.y. from ca. 2716 to ca. 2600 Ma. Chemical compositions of volcanic rocks are typified by low abundances of HFSE and depletions in Nb, Ti, Eu, and P relative to REE. The striking similarity between the overall lithologic assemblages and the geochemical signature of volcanic rocks in the HBGB with modern arc and back-arc systems (e.g. Mariana and Tonga-Kermadec regions) suggest the HBGB evolved in an arc geodynamic setting.

The Young Group, a series of primarily mafic flows, was deposited in a back-arc basin, the bulk of which was deposited before ca. 2716 Ma. Detrital zircon ages (ca. 3.3 and 2.8 Ga) from a turbidite within the HBGB may provide evidence for the existence of ancient crystalline basement in the vicinity. This was followed by deposition of the Westerberg Group, which comprises arc magmatism that occurred between ca. 2699-ca. 2677 Ma. Age constraints suggest that this arc magmatism was episodic. Following the main stage of arc formation the deposition of ca. 2663 Ma Tweedy and ca. 2600 Ma Farrar Group, thought to record the erosion and subsequent uplift of the HBGB, respectively, mark the end of the depositional history of the HBGB.

Results from this study raise several questions. The most pressing questions are:

1) Although, the bulk of mafic volcanism in the HBGB is assumed to have occurred prior to ca. 2716 Ma, minor basalt flows are distributed sporadically throughout the stratigraphy. Are there any younger mafic flows, or is the distribution of mafic rocks throughout the stratigraphy a function of structural repetition? Did mafic volcanism occur contemporaneously with arc magmatism?

2) Chronological constraints suggest the presence of thrust faults within the HBGB. Are they Archean structures or the result of the Proterozoic Thelon and/or Wopmay orogen?

3) What age is the Son Volt formation? It is at present loosely bracketed between 2716 Ma (age of the Flake Lake formation) and 2699 Ma (age of the overlying Wolverine Lake formation). The Son Volt formation represents the earliest phase of arc magmatism within the HBGB and an age for this unit would better constrain the total evolution of arc activity in the HBGB.

4) Does crystalline basement exist within the eastern SSP? No basement has been documented in the eastern SSP thus far. However, detrital zircon ages (ca. 2.8 and 3.3 Ga) with little evidence of prolonged transport indicate an ancient basement source. Did these zircon crystals originate from the western SSP where basement is known to exist or were they derived from a basement block within the Bathurst Block or just east, outboard of the present eastern boundary of the SSP?

Appendix 1

Analytical Precision

Three duplicate Mineral Deposit Research Unit in-house standards and seven field duplicate sample pairs were submitted with batches of samples analysed, to examine the precision of the data (XRF and ICP-MS).

XRF

Analytical errors (Table 5.1) for major element data were often better than 5 % with rare exceptions exceeding this value. Trace elements exhibited a larger range of values, typical relative errors were below 10 % in most cases except for Nb which displayed larger errors likely in response to values in close proximity to the detection limit.

ICP-MS

Analytical errors (Table 5.2) for rare earth and transition element data rarely exceed 10 %. Errors associated with the rare earth elements and high field strength elements most commonly used in this study, rarely exceeded 5 %.

Table 5.1 Duplicate analyses for XRF data

	96PDMW120 n=2		96PTMW119 n=2		96PUMW110 n=2		97PBMW105 n=2		97PGMW101 n=2		MBX1 n=2		WP1 n=2		ALB1 n=2	
Element	Mean	% Error	Mean	% Error	Mean	% Error	Mean	% Error	Mean	% Error	Mean	% Error	Mean	% Error	Mean	% Error
SiO2 %	62.96	0.03	68.22	0.23	58.71	0.26	68.68	0.36	72.72	0.82	57.84	0.21	64.12	0.08	55.20	0.43
Al2O3 %	15.58	0.74	15.76	0.38	16.62	0.30	15.40	0.29	11.30	0.53	17.42	0.26	16.22	0.12	18.76	0.43
CaO %	4.58	3.17	2.61	3.26	4.05	5.07	3.52	1.42	2.42	16.53	3.61	0.83	4.87	0.21	10.32	0.48
Fe2O3 %	5.04	0.79	2.51	6.59	7.33	0.61	3.12	0.48	5.08	1.97	3.91	0.13	4.50	0.56	1.61	0.93
K2O %	1.40	0.71	0.89	0.56	0.14	11.11	1.30	13.08	1.63	9.82	4.95	0.81	1.72	0.58	0.88	1.14
MgO %	2.57	0.19	1.04	2.88	3.20	2.50	0.85	21.89	2.09	0.96	1.94	0.78	2.54	0.20	2.83	2.12
MnO %	0.09	5.88	0.03	0.00	0.11	0.00	0.07	7.69	0.07	7.69	0.08	6.67	0.09	0.00	0.04	0.00
Na2O %	3.62	2.35	6.22	1.37	5.67	2.03	4.63	2.49	0.89	5.62	5.00	0.60	4.22	0.83	5.72	0.35
P2O5 %	0.18	5.56	0.10	5.26	0.13	7.69	0.12	8.33	0.04	0.00	0.24	2.13	0.19	2.70	0.29	0.00
TiO2 %	0.56	0.90	0.32	3.13	0.69	0.73	0.43	2.33	0.32	6.25	0.49	2.04	0.51	0.99	0.61	0.83
Ba	159.50	0.94	221.50	0.68	93.50	6.95	327.50	5.34	142.50	5.26	677.50	0.37	630.00	3.17	245.00	4.08
Rb	35.00	0.00	31.00	9.68	1.50	33.33	25.00	12.00	42.00	9.52	84.00	0.00	25.00	4.00	23.00	4.35
Sr	972.50	5.40	298.50	0.84	166.50	5.11	327.00	10.09	38.00	5.26	482.00	0.00	704.00	0.57	702.00	0.00
Nb	5.00	20.00	5.00	20.00	9.00	5.26	4.00	14.29	27.00	3.70	12.00	9.10	5.00	20.00	6.00	20.00
Zr	78.00	3.85	103.00	3.88	126.50	2.77	127.50	1.18	420.00	2.14	97.50	1.54	126.00	0.00	69.00	0.00
Y	11.50	4.35	5.00	0.00	20.50	2.44	6.00	0.00	125.00	4.00	18.00	0.00	16.50	3.03	18.08	4.76

Figure 5.2. Duplicate analyses for ICP-MS data

	97PQMW109		96PFMW004	
	n=2		n=2	
Element	Mean	% Error	Mean	% Error
V (ppm)	68.50	2.19	120.00	0.83
Cr (ppm)	52.50	4.76	76.50	1.96
Co (ppm)	10.50	4.76	24.00	0.00
Ni (ppm)	20.50	7.32	80.50	0.62
Cu (ppm)	14.50	3.45	65.00	1.54
Zn (ppm)	53.00	11.32	76.50	1.96
Ga (ppm)	17.00	0.00	17.00	0.00
Ge (ppm)	0.65	7.69	1.10	0.00
Rb (ppm)	74.00	0.00	1.30	23.08
Sr (ppm)	185.00	1.62	263.50	0.95
Y (ppm)	9.75	2.56	15.00	0.00
Zr (ppm)	134.00	2.24	119.00	0.84
Nb (ppm)	6.65	2.26	5.40	0.00
Mo (ppm)	2.80	7.14	0.65	7.69
Sb (ppm)	0.14	3.70	0.55	4.59
Cs (ppm)	1.30	0.00	0.40	0.00
Ba (ppm)	501.50	1.50	22.50	2.22
La (ppm)	24.85	7.44	11.60	2.59
Ce (ppm)	54.30	6.08	24.65	2.23
Pr (ppm)	6.21	5.69	2.82	2.36
Nd (ppm)	23.65	6.98	11.55	2.16
Sm (ppm)	3.82	4.85	2.61	3.26
Eu (ppm)	1.03	5.12	0.81	0.81
Gd (ppm)	2.47	0.20	2.57	1.56
Tb (ppm)	0.33	4.62	0.44	3.45
Dy (ppm)	1.85	4.07	2.60	2.31
Ho (ppm)	0.33	3.03	0.52	1.92
Er (ppm)	1.01	3.96	1.54	1.30
Tm (ppm)	0.14	7.37	0.24	3.28
Yb (ppm)	0.69	3.65	1.44	0.69
Lu (ppm)	0.14	6.47	0.24	2.11
Hf (ppm)	3.65	6.85	3.15	1.59
Ta (ppm)	0.51	1.96	0.66	0.00
W (ppm)	0.75	6.67	5.05	2.97
Tl (ppm)	0.46	4.35	0.02	56.50
Pb (ppm)	0.50	38.75	7.00	0.00
Bi (ppm)	-0.05	0.00	0.25	6.12
Th (ppm)	3.01	6.98	1.68	1.19
U (ppm)	0.45	1.12	0.16	6.25